



CRANFIELD UNIVERSITY

Amaan Ghole

**Design and Analysis of Robust Controllers for
Directional Drilling Tools**

School of Water, Energy and Environment

MSc By Research Thesis

CRANFIELD UNIVERSITY

SCHOOL OF WATER, ENERGY AND ENVIRONMENT

MSc by Research Thesis

AMAAN GHOLE

Design and Analysis of Robust Controllers for Directional Drilling
Tools

Supervisor: Dr James Whidborne

Associate Supervisor: Dr Yi Cao

August 2016

©Cranfield University 2016. All rights reserved. No part of this publication may be reproduced without the written permission of the copyright owner.

Abstract

Directional drilling is a very important tool for the development of oil and gas deposits. Attitude control which enables directional drilling for the efficient placement of the directional drilling tools in petroleum producing zones is reviewed along with the various engineering requirements or constraints. This thesis explores a multivariable attitude governing plant model as formulated in [Panchal et al. \(2010\)](#) which is used for developing robust control techniques. An inherent input and measurement delay which accounts for the plant's dead-time is included in the design of the controllers. A Smith Predictor controller is developed for reducing the effect of this dead-time. The developed controllers are compared for performance and robustness using structured singular value analysis and also for their performance indicated by the transient response of the closed loop models. Results for the transient non-linear simulation of the proposed controllers are also presented. The results obtained indicate that the objectives are satisfactorily achieved.

Keywords : Attitude, Multivariable Control, Robust Control, Deadtime, Smith Predictor, μ analysis

Acknowledgements

Foremost, I would like to express my sincere gratitude to my advisor Dr. James Whidborne for the continuous support of my MSc study and research, for his patience, motivation, enthusiasm, and immense knowledge. His guidance helped me throughout my research. I could not have imagined having a better advisor and mentor for my MSc by Research. I would also like to thank Dr Yi Cao for his helpful insight and inputs which helped in the realization of this thesis.

I would also like to express my gratitude to my parents and grand parents for their unconditional love and prayers and also for supporting me in all times thick and thin.

Also, I thank my friends Mohammed Alieh and Emmanuelle Maillot. In particular, I am grateful to my friend Ananias Medina who was always available to clarify my doubts related to the subject.

Lastly, but most importantly I'd like to thank Almighty God for allowing my presence on earth.

List of Figures

1	Directional Drilling (Downton et al.; 2000)	5
2	Applications of Directional Drilling (Downton et al.; 2000)	7
3	Rotary Steerable System (Panchal et al.; 2012)	9
4	Conventional Measurement Scheme (Panchal et al.; 2012)	12
5	Control Algorithm for Trajectory Control (Pirovolou et al.; 2011)	15
6	S/T Mixed Sensitivity Standard Form	22
7	Design 1: Nominal Closed Loop Responses	27
8	Design 1: Loop-shape	28
9	Design 2 : Closed Loop Responses	29
10	Design 2 : Loop Shape	30
11	Nominal Closed Loop Response Comparison	31
12	PI Controller Scheme	32
13	Nominal Closed Loop Step Response PI Pole Placement	33
14	Simulink Closed Loop Interconnection	34
15	Tuning Goals	35
16	Unstable Plant: Step Tracking Response	36
17	Tuning Report	37
18	Robust PI Controller Transient Response	38
19	Robust PI Controller Loop Shapes	38
20	Structure of the Smith Predictor	39
21	Unstable MIMO Stabilization	42
22	PI-SP Closed Loop Simulink Interconnection	46

23	PI-SP Closed Loop Transient Responses	47
24	PI-SP Pole Zero Plot	47
25	H_∞ -SP Closed Loop Transient Responses	48
26	H_∞ -SP Pole Zero Plot	48
27	Standard $M - \Delta$ configuration	50
28	Robust Stability $N\Delta$ structure	52
29	Robust Stability $M\Delta$ Structure	54
30	Robust Stability $M\Delta$ Structure-SP	55
31	Robust Performance $N\Delta$ Structure	56
32	Robust Performance $N\Delta$ Structure-SP	57
33	NP,RS,RP for Pole Placement Design	57
34	Robust Performance Report	58
35	NP,RS,RP for Robust PI Controller Design	58
36	NP,RS,RP for H_∞ Design 1	59
37	NP,RS,RP for H_∞ Design 2	59
38	NP,RS,RP for $H_\infty - SP$ Design	60
39	NP,RS,RP for $PI - SP$ Design	60
40	H_∞ Design 2 vs Robust PI Transient Response	62
41	PI-SP vs H_∞ -SP Transient Response	63
42	PI vs PI-SP Transient Response	64
43	H_∞ vs H_∞ -SP Transient Response	65
44	Nominal Performance Analysis	66
45	Robust Stability μ_M Comparison	66
46	Robust Performance μ_N Analysis	67
47	Drill Cycle Definition	69
48	Simulink Block Diagram PI controller	70
49	Simulink Block Diagram H_∞ -SP controller	70
50	θ_{inc} Reference Tracking	72
51	θ_{azi} Reference Tracking	72

52	Attitude-Tracking Transient Attitude Response, H_∞ Design, Zoomed View	73
53	Effect of saturation on Controller Output- H_∞	75
54	Effect of saturation on Controller Output- PI	76
55	Attitude-Tracking Transient Attitude Response, H_∞ Design, Zoomed View for Saturated and Unsaturated Signals	76
56	Different saturation level and their effect on performance	77
57	Control System Tuner Application	97
58	Select Blocks to Tune	98
59	Step Tracking Goal	99
60	Step Tracking Goal Graphical Illustration	100
61	Sensitivity Goal	101
62	Sensitivity Goal Graphical Illustration	102
63	Robustness goal	103
64	Robustness Goal Graphical Illustration	104
65	Overshoot Goal	105
66	Overshoot Goal Graphical Illustration	106
67	Achieved Step Tracking Goal	106
68	Achieved Sensitivity Tracking Goal	107
69	Achieved Robustness Goal	107
70	Overshoot Goal	108
71	Report Performance PI pole placement	109
72	Report Performance Robust PI	109
73	Report Performance H_∞ Design 1	109
74	Report Performance H_∞ Design 2	110
75	Report Performance PI-SP	110
76	Report Performance H_∞ SP	110
77	Report stability PI Pole placement	110
78	Report stability Robust PI	110
79	Report stability H_∞ Design 1	111

80	Report stability H_∞ Design 2	111
81	Report stability PI-SP	111
82	Report stability H_∞ -SP	111
83	Attitude-tracking Transient Attitude Response, PI-SP design, Zoomed View	112
84	Attitude-tracking Transient Attitude Response, Robust PI design, Zoomed View	113
85	Attitude-tracking Transient Attitude Response, H_∞ -SP Design, Zoomed View	114
86	Effect of saturation on Controller Output- PI	115
87	Effect of saturation on Controller Output- H_∞ -SP	115
88	Effect of saturation on Controller Output- PISP	116
89	Effect of saturation on Controller Output- Nonlinear PI simulation	116
90	Effect of saturation on Controller Output- Nonlinear H_∞ SP Simulation . .	117
91	Effect of saturation on Controller Output- Nonlinear PISP simulation . . .	117
92	Sub-system Directional Drilling Plant	118
93	Sub-system Virtual Control Transformation	119
94	Sub-system Drill Cycle	120
95	Sub-system Drill Kinematics	120

List of Tables

1	Nominal Parameters	25
2	Design 1: Controller Specifications H_∞	25
3	Uncertain Parameters	26
4	H_∞ Design 2: Controller Specifications	27
5	Rise Time Comparison	62
6	Robust Performance and Robust Stability Trade-off	64
7	Transient Simulation Parameters	69

Nomenclature

Δ	Uncertainty Block or Matrix
Δ_{τ_d}	Uncertainty Range for the Parameter τ_d
Δ_{α_1}	Uncertainty Range for the Parameter α_1
Δ_{α_2}	Uncertainty Range for the Parameter α_2
Δ_{τ_1}	Uncertainty Range for the Parameter τ_2
Δ_{τ_2}	Uncertainty Range for the Parameter τ_2
$\Delta_{V_{rop}}$	Uncertainty Range for the Parameter V_{rop}
$\Delta_{K_{dls}}$	Uncertainty Range for the Parameter K_{dls}
$\mu(X)$	Structured Singular Value of X
ω_c	Bandwidths for S_{nom} and T_{nom}
ω_a	Closed Loop Azimuth Natural Frequency
ω_i	Closed Loop Inclination Natural Frequency
ω_l	Lower Bound of the Study Frequency Range
ω_n	Upper Bound of the Study Frequency Range
ω_u	Study Frequency Upper Limit
Φ	MIMO Smith Predictor Pre-filter
ϕ_{ij}	Terms of the MIMO Smith Predictor Pre-filter Φ
ρ	Spectral Radius
σ_X	Singular Values of X
τ	Time Constant Associated with the Delay
τ_1	Actuation Delay Time Constant
τ_2	Measurement delay time constant
τ_c	Time Constant

τ_d	Actuator dynamics time constant
θ_{azi}	Azimuth Angle
θ_{inc}	Inclination Angle
A_0	Open Loop Characteristic State Space Matrix for G_0
A_{cl}	Closed Loop Characteristic State Space Matrix for PI pole Placement Design
A	High/Low Frequency Gain
B_0	Open Loop Input State Space Matrix for G_0
B_{cl}	Closed Loop Input State Space Matrix for PI Pole Placement Design
b_j	Column Vector With Elements in B
C_0	Open Loop Output State Space Matrix for G_0
c_i	Row Vector With Elements in C
$c2d$	MATLAB Function to Convert a System from Continuous Time Domain to Discrete Time Domain
d_{ij}	Delay in Discrete time in the Positions i, j
Δ_P	Fictitious Uncertain Block or Matrix
$\dot{x}(t)$	Rate of the States in the State Space System
e	Control System Error Defined like $e = r - y$
e_{azi}	Control System Error in the Azimuth Channel
e_{inc}	Control System Error in the Inclination Channel
$F_L(X, Y)$	Lower Linear Fractional Transformation of X and Y
$F_U(X, Y)$: Upper Linear Fractional Transformation of X and Y
G	Auxiliary System for represent H_∞ Mixed Connection
g_{ij}	Terms of the Matrix $G(z)$
G_{unc}	Linear System with parametric uncertain
G_{wd}	Nominal Linear System
G_0	Nominal Linear System Without Delay and Without Lag
$G_0(z)$	System Without Delay in Discrete Time Domain
$G_T(z)$	Resultant Free Delay System in MIMO Smith Predictor Creation
gt_{ij}	Terms of the Matrix $Gt(z)$
H_∞	Mixed Sensitivity Controller
h_{lag}	First order transfer function that modelling the actuator dynamics

h_1	Input delay associated to Actuation dynamics
h_2	Output delay associated to Measurement dynamics
$hankelmr$	Model Order reduction by hankel method function
$hinfsyn$	H_∞ Controller MATLAB function
I	Identity Matrix
J	Quadratic cost function
K	Generic Controller (PI, H_∞ or PI, H_∞ for the System with SP)
K_{dls}	Maximum Dog Leg Severity or Curvature Response
k_{ia}	Azimuth Integral Gain for PI Controller
k_{ii}	Inclination Integral Gain for PI Controller
k_{pa}	Azimuth Proportional Gain for PI Controller
k_{pi}	Inclination Proportional Gain for PI Controller
K_I	Integral Gain Matrix for PI Controller
K_P	Proportional Gain Matrix for PI Controller
L	Open Loop System
M	Partitioned Interconnection Transfer Function Matrix for Robust Stability Analysis
M_{ij}	Terms of the Matrix M
N	Partitioned Interconnection Transfer Function Matrix for Robust Performance Analysis
$P(s)$	Delayed System without lag in Continuous Time Domain
$P(z)$	Delayed System without lag in Discrete Time Domain
r	Reference Signal
r_{azi}	Reference for Azimuth Angle
r_{inc}	Reference for Inclination Angle
$robustperf$	Robust Performance Analysis Function
$robuststab$	Robust Stability Analysis function
S	Sensitivity Functions with Uncertainty
S_{nom}	Nominal Sensitivity functions
T	Closed Loop functions with Uncertainty
T_{nom}	Nominal Closed Loop functions

T_s	Sample Time
u	System Input
u_{azi}	Virtual Control Input for Azimuth Channel
U_{dls}	Dog log severity or Curvature
u_{inc}	Virtual Control Input for Inclination Channel
U_{tf}	Tool face Angle Control Input
V_{dr}	Drop Rate Disturbance
V_{rop}	Rate of Penetration
V_{tr}	Turn rate Disturbance
W_1	Diagonal matrix of weights w_1
w_1	Weight Function for Sensitivity Response
W_2	Diagonal Matrix of Weights w_2
w_2	Weight Function for Closed Loop Response
x	Model States
y	Model Outputs
y_a	Azimuth Channel Output
$y_i(z)$	Inclination Channel Output
z	Weights Functions Outputs

Abbreviations

BHA	Bottom Hole Assembly
DTC	Dead Time Compensator
HSV	Hankel Singular Values
LFT	Linear fractional transformations
LQR	Linear Quadratic Regulator
MD	Measured Depth
MIMO	Multi Input Multi Output
MWD	Measurements While Drilling
NP	Nominal Performance
PDM	Positive Displacement Motors
PI	Proportional Plus Integral
PID	Proportional Integral Derivative
RP	Robust Performance
RS	Robust Stability
RSS	Rotary Steerable System
SISO	Single Input Single Output
SP	Smith Predictor
TVD	True Vertical Depth
ZOH	Zero Order Hold

Contents

List of Figures	ix
List of Tables	xiii
Nomenclature	xiv
Abbreviations	xviii
1 Introduction	1
1.1 Background	1
1.2 Objective	1
1.3 Contributions	2
1.4 Structure of Thesis	2
2 Review	4
2.1 Directional Drilling	4
2.1.1 Applications of Directional Drilling	6
2.2 Engineering	7
2.2.1 Deflecting Tools and Techniques	7
2.2.2 Rotary Steerable Systems	8
2.2.3 Actuation	11
2.2.4 Measurements	12
2.3 The Control Problem	14
2.3.1 Specific Control Problem	14

3	Plant Modeling	17
3.1	Tool Kinematics	17
3.1.1	Virtual Control Transformation	17
3.1.2	Unmodelled Dynamics	18
3.2	Linearization	19
3.3	Plant including Lag and Delays	20
3.4	Open-loop Plant Analysis	20
3.5	Conclusion	21
4	Controller Design	22
4.1	H_∞ Control	22
4.1.1	Hankel Norm Approximation	24
4.1.2	Design 1	24
4.1.3	Design 2	26
4.2	PI Controller	29
4.2.1	Pole Placement Design	30
4.2.2	Robust PI Controller Design	33
4.3	Conclusion	37
5	Smith Predictor Controller	39
5.1	Generalized Smith Predictor	39
5.2	Modifications and extensions	40
5.3	MIMO Smith Predictor(Albertos et al.; 2015)	41
5.3.1	Application to Drilling Plant	43
5.4	Conclusion	46
6	Controller Robustness Analysis	49
6.1	Theoretical Background: Measures of Robustness	49
6.1.1	Uncertainty	49
6.1.2	Linear Fractional Transformation	49

6.1.3	Structured Singular Value	50
6.1.4	Nominal Performance	51
6.1.5	Robust Stability	51
6.1.6	Robust Performance	52
6.2	Plant Specific Uncertainty	53
6.2.1	Uncertainty Modelling	53
6.3	Robustness Analysis Plant interconnection	53
6.3.1	Robust Stability	53
6.3.2	Robust Performance	54
6.4	μ -analysis Results	54
6.4.1	PI Controllers	54
6.4.2	H_∞ Controllers	55
6.4.3	Smith Predictor	56
6.5	Conclusion	56
7	Comparison of Designed Controllers	61
7.1	Transient Response Comparison	61
7.2	Nominal and Robustness Comparison	62
7.3	Conclusion	65
8	High Fidelity Simulations	68
8.1	Drill Cycle	68
8.2	Transient Simulation Description	69
8.3	Transient simulation results	71
8.4	Conclusion	71
9	Controller Action	74
9.1	Effect of Saturation	74
9.2	Conclusion	75
10	Conclusion	78

10.1 Summary of contributions	78
10.2 Recommendations	79
A MATLAB Code	81
A.1 Uncertain Parameters	81
A.2 H_∞ Controller	81
A.3 Smith Predictor Controller	86
A.4 PI controller	90
A.5 Comparisons	95
B Control System Tuner Graphical Representation	97
C Reports	109
D Transient simulations results	112
E Simulink	118

Chapter 1

Introduction

1.1 Background

Directional Drilling has become widely used in the demanding oil and gas industry in recent times. It enables cost effective reservoir exploitation by aiding increased recovery from existing wells. It also aids the exploration of difficult to commercialize reserves. Rotary steerable tools, which enable the direction of well propagation, are being widely developed which opens up the area of research in applying control engineering techniques to automate this process. Directional drilling is essentially an ‘attitude control’ problem and concerns the control of the drills dynamics in terms of inclination and azimuth. A model of borehole propagation has been developed in [Panchal et al. \(2010\)](#) and the present work extends the techniques of previous developments as seen in [Bayliss and Whidborne \(2015\)](#) and ([Bayliss et al.; 2014](#)). Attitude control of directional drilling tools is considered, with respect to a dynamic system formulated by directly related parameters. It is well known that drilling in general is a complex operation and a lot of variables dictate such an operation. The dynamic model is controllable but nevertheless, has a great amount of parametric uncertainty and external unmodelled dynamics. These uncertainties and unmodelled dynamics should be accommodated in the design of controllers which allow better and robust designs.

1.2 Objective

Although there are many different control design methods there is a need for a unifying method and tools for comparing the designs. Hence, the aim of this project is to provide such a method. In order to successfully meet this aim the following objectives are outlined:

1. Validate existing designs and facilitate improvements by considering the unmodelled plant dynamics in the design of the multivariable controllers.
2. Design a controller to counter the effect of the system dominant delay characteristics associated with the measurement feedback delay.
3. Use structured singular value analysis μ for the robustness analysis of the designed

controllers and finally use high-fidelity non-linear simulations in order to test that the system is indeed improved using the designed controllers.

1.3 Contributions

Apart from the objectives listed above, this work includes the following original contributions:

1. A multivariable Smith predictor based deadtime compensator is proposed to control the plant dynamics dominated by temporal delays associated with the plant's input and output dynamics. This predictive technique facilitates robustness and better performance in terms of improved rise time of the closed loop systems.
2. The 'Control System Tuner' application is proposed to auto tune the closed loop dynamics. This is a good approach if the performance and robustness requirements are well known and thus a better control design is achieved.

1.4 Structure of Thesis

The background of this work, the aims and objectives of this thesis, and the contributions made are described in this introductory chapter.

In chapter 2, directional drilling is introduced, followed by its applications. The necessary engineering systems related to the directional drilling tool are described. Lastly, the attitude control problem is described, previous work is reviewed and the chosen system model is justified.

In chapter 3, the selected plant model as in [Panchal et al. \(2010\)](#) is described for its dynamics related to the the attitude of the drilling tool. The unmodelled dynamics are also presented. A control transformation for the plant model is explained and the plant is linearized for subsequent controller design.

In chapter 4, PI and H_∞ controllers are designed for two plant models. The first model excludes the effects of lag and delays, and the second includes these effects.

In chapter 5, the Smith predictor controller is proposed along with its modifications and extensions to multivariable systems. A modified multivariable smith predictor scheme is designed and applied to the drilling tool and two stabilizing controllers are designed.

In chapter 6, robust control analysis preliminaries are presented and a structured singular value μ analysis is performed to assess the developed control systems for robust stability and robust performance.

In chapter 7, the designed controllers are compared for their transient response and structured singular value analysis.

In chapter 8, the designed controllers are applied to a non-linear plant model created in Simulink.

In chapter 9, the whole process is critically evaluated and with the benefit of hindsight, some improvements are suggested for future related works.

Note that the relevant mathematical control problems are briefed before their application to the concerned drilling plant in this work. The problem formulations and the necessary control system techniques are presented when deemed required.

Chapter 2

Review

The purpose of this chapter is to introduce the readers to directional drilling and its applications. It identifies the important engineering aspects of actuation and measurement related to the directional drilling process. The specific control problem is identified and a literature review is presented and analysed, explaining various bottom-hole trajectory and attitude estimating models and related control techniques.

2.1 Directional Drilling

‘Directional Drilling is used when a well is intentionally deviated to reach a bottomhole location that is different from the surface location.’ ([Bommer; 2008](#)). It can also be described as the process of directing the well bore along some trajectory to a predetermined target. In simpler words, it is the practice of drilling non vertical wells. It is identified as a technique to reach otherwise inaccessible petroleum reserves.

Directional drilling emerged in the 1920’s when basic well bore surveying methods were first introduced. It was observed that while drilling vertical sections, the wells would tend to deflect in unwanted directions ([Felczak et al.; 2012](#)). The verticality and smooth well bore requirements for effectively producing an oil reservoir led to drillers combating this deviation from vertical in order to maintain a vertical hole. These techniques were later utilized to deliberately deflect the well path to access abstractly located petroleum reserves.

The process of drilling is highly uncertain in terms of reservoir rock formations and other geological aspects, which can be avoided with a comprehensive geological analysis and controlled directional drilling. Deviation control is the process of keeping the well bore contained within some prescribed limits relative to inclination angle and horizontal excursion from the vertical or both. Directional drilling has become an integral part of the oil and gas industry today. The technology used to deviate vertical wells has improved over the years and automated directional control has been proposed and field tested in [Sun et al. \(2012\)](#), [Brakel and Azar \(1989\)](#), [Downton et al. \(2000\)](#) and [Panchal et al. \(2010\)](#).

Directional drillers must follow a well path designed by the well planner and geologist. Periodic surveys are taken during drilling to provide inclination and azimuth measurements

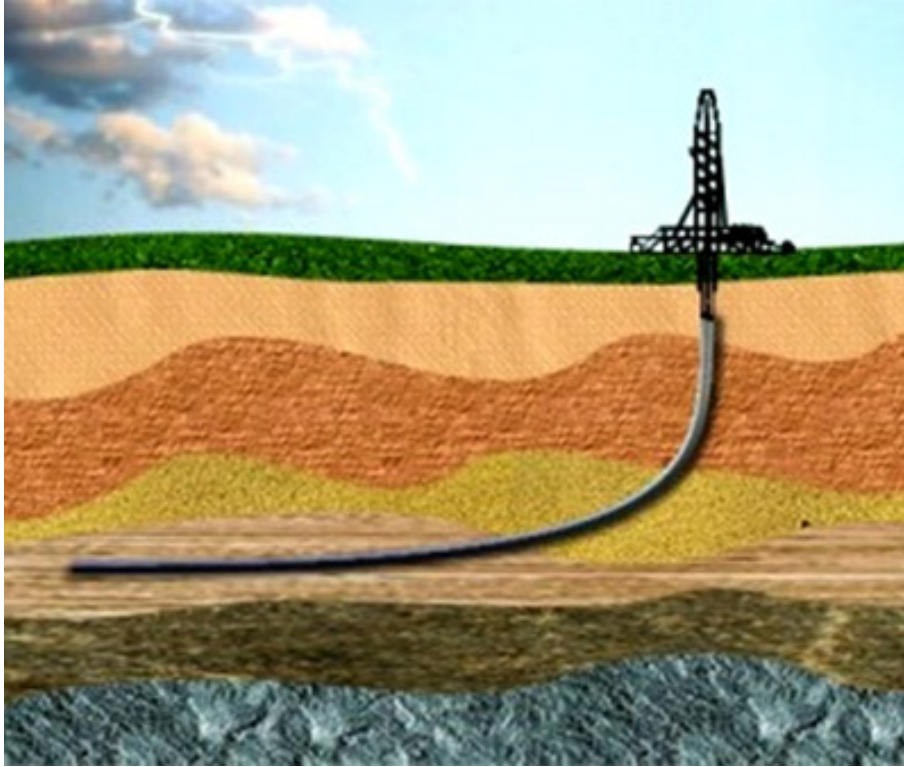


Figure 1: Directional Drilling ([Downton et al.; 2000](#))

of the well-bore. If the current path deviates from the planned path, corrections can be made through various available techniques. The control action depends upon the severity of the deviation from the prescribed plan.

The acclaimed application of the Rotary Steerable System (RSS) was noticed when an extended reach well was drilled, in the Wythch Farm oilfield with a departure of more than 10 km ([Genevois et al.; 2003](#)). Directional drilling using rotary steerable provided better solutions to obstacles such as slide drilling, improved hole cleaning, penetration rates and differential sticking. These benefits of directional drilling will be highlighted in subsequent sections.

Technique

Directionally drilled wells normally begin with a vertical well-bore. At a pre-designed depth the directional driller deflects the well path by increasing inclination. This point is known as the *kick-off point*. The kick-off point leads into the build section. The position of kick-off depends on several parameters including geological considerations, proximity of other wells and geometry of the wells. The *rate of build* which is the rate of change of the increasing angle in the hole, depends upon the total depth of the well, torque and drag limitations, mechanical limitations of the drill string and the logging tools. The optimum rate of build is 1.5° to 3° per 100 ft. Higher build up rates are required for horizontal wells. Weight on bit (drilling mud weight controlled by the directional driller to turn the bit), rotary speed, Bottom Hole Assembly (BHA) stiffness, hole diameter, hole angle and formation characteristics all affect the capability and efficiency of a directional drilling

tool.

2.1.1 Applications of Directional Drilling

There are numerous applications to directional drilling which aid the drilling contractor ([Downton et al.; 2000](#)). These are the following:

Side-tracking existing wells: Wells are side-tracked, i.e. at a point in the well bore, if the present hole is not producing effectively or due to loss of equipment (fish) in the well-bore. The present hole is cemented shut to avoid pressure challenges and a new side-track is achieved with the help of directional drilling. A window is cut through the casing using a whip-stock to regain productivity of a crushed or obstructed well. Side tracking may also be carried for a re-drill or re-completion. [Shengzong et al. \(1999\)](#) described a novel method for sidetracking horizontal wells.

Restricted surface locations: Oil deposits may lie in locations below towns, rivers, mountains. If a drilling rig cannot be set up over the producing formation, horizontal displacement can be achieved to reach the formation with the help of directional drilling. When permission to drill over sensitive area is denied, directional drilling is used as a medium to exploit oil and gas resources. In the case of a blow-out, directional drilling facilitates the construction of relief wells with greater accessibility and simplicity. Extended reach wells are drilled for such applications.

To reduce the number of offshore platforms: A number of wells can be drilled from a single drilling platform, hence reducing drilling cost substantially.

To drill relief wells: If a blow out occurs and the well is no longer accessible a relief well is drilled to intersect the uncontrolled well and mud and water are pumped into it, to stabilize bottom hole pressure.

Controlling vertical wells: The wells have a tendency to drift from vertical due to rock formations and gravity. Other reasons for wanting a straight bore-hole is to simplify cementing operations and also to stay within specifications of lease lines.

Fault drilling: Geological faults sometimes are very steeply dipping and it is difficult to maintain a vertical well-bore as the bit has a tendency to follow the direction of the fault. Directional drilling helps to avoid the fault, by either drilling on the up-thrown or down-thrown side of the fault.

Salt dome drilling: Directional drilling helps us to avoid salt dome regions since they have a tendency to collapse and cause serious problems while drilling.

Directional drilling has become an integral part of the oil and gas industry. The concept of directional drilling remains the same, even with the intense advances in technology. The oil and gas industry has witnessed the emergence of the rotary steerable systems which enable faster drilling, smoother well bores and extended-reach drilling. These systems have many advantages over conventional mud motors.

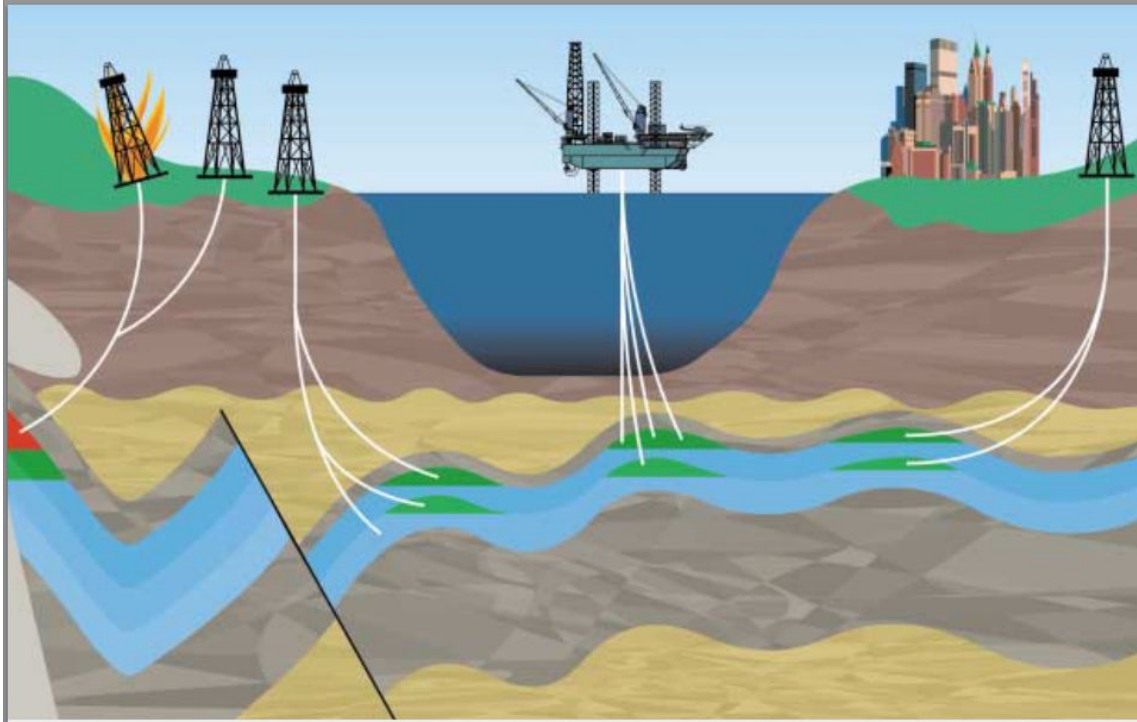


Figure 2: Applications of Directional Drilling ([Downton et al.; 2000](#))

2.2 Engineering

2.2.1 Deflecting Tools and Techniques

Various types of directional drilling tools have been used over the years. With the advancement of technology and modern inventions, there has been a considerable improvement in meeting desired targets while drilling. A sophisticated rise in technology and its successful applications in the overburdened oil and gas industry hence needs to be documented and studied. Below are different techniques that directional drillers have used over the past years and a comparative improvement is noticed. The structure and primary deflection techniques are highlighted for familiarity.

Whip-stocks: The whip-stock was the first deflecting tool at the advent of directional drilling. A standard whip-stock is seldom used nowadays. Whip-stocks have not totally disappeared from the market and are used to accomplish casing exits, open hole sidetracking, through tubing sidetracking, section milling and multilateral completion systems ([Downton et al.; 2000](#)). A whip-stock is a wedged steel tool which is used to mechanically alter a well path down-hole. The whip-stock is oriented to deflect the bit from the borehole and in the direction of the azimuth of the well.

The use of whip-stock offers limited attitude control and would frequently result in missed targets, due to the absence of accuracy of measurements and feedback control. The modern directional deflection tools offer better and extended attitude control.

Jetting: Jetting is a technique used to deflect well-bores in soft formations. This tech-

nique outmoded the use of whip-stocks as the primary deflection technique.

A special jet bit may be used to facilitate deflection, but it is also common practice to use standard soft-formation tri-cone bit, with a large nozzle and two other smaller ones. The formation needs to be a soft one with high penetration rates. The formations tend to get more compact as the depth increases and if the rate of penetration cannot be maintained above 80 feet/hour, they are not suitable for jetting. The jetting is powered by hydraulic horsepower in order to erode the formation. The jetting method sprays water in the desired direction to devitrify the ground, then excavate the dull part out of the ground. (Kim et al.; 2014)

Positive Displacement Motors: Positive displacement motors (PDM) have been critical advancements in trajectory control of directional drilling. Positive displacement motors are steerable assemblies capable of various operations, such as kicking off and building angle in a directional well to drilling tangent sections while maintaining accurate attitude and trajectory.

The design of the tool includes a dump sub, a power unit, a transmission bent-housing unit and a bearing section. The power unit uses a rotor/stator pair which converts hydraulic energy of the circulating mud to mechanical energy of a rotating shaft, in this case, the drill bit. The power section has direct control over the torque of the bit and its rotary speed. Various types of positive displacement tools have been seen in the industry with the bent housing motor having the widest applications. The bent housing is widely used due to its short bit to bend distance which allows the tool to drill at greater build rates and reduces bit offset. This kind of PDM allows easier orientation and long rotation periods.

The basic technique to make the required deflection from the drill-string axis is made by using the PDM which helps align the bend in the motor in the desired direction. Directional Drilling with a PDM is accomplished in two modes, namely the rotating and the sliding mode. The drill string is held stationary and drill bit makes the necessary indentation, with the drill string following in sliding mode. This essentially creates a reasonable level of tortuosity, which tends to increase friction while drilling and running casing. (Downton et al.; 2000) Another shortcoming of PDMs is they can instigate stuck pipe situations. While drilling, the drill-string is positioned on the lower end of the borehole, and drilling fluids flowing unevenly around the drillpipe, impairs the capacity of the mud to remove cuttings (Felczak et al.; 2012).

Although mud motors have certain shortcomings, they are still widely used for directional drilling operations. Some noteworthy advantages are that all types of rock formations can be drilled with positive displacement motors and they are versatile in the use of different cutting mechanisms. Also, moderate flow rates are required for the efficient functioning of the motor and hence most surface pumps can be used to operate these down-hole motors.

2.2.2 Rotary Steerable Systems

RSS are the latest advancement in directional drilling technology and facilitate intelligent systems for greater and more efficient exploitation of oil and gas. Hence, an entire section is devoted to understanding their characteristics and productive applications. Figure 3 shows the main components of the directional drilling tool. RSS have led to achievements

previously not possible with the use of conventional directional drilling systems like mud motors. Rotary steerable systems enable faster drilling, smoother well bores and extended reach drilling (Pirovolou et al.; 2011). These systems were developed initially to drill extended reach wells. In conventional drilling operations, which constitute the major expenditure in oil and gas exploration and production, RSS help in reducing drilling time significantly which makes it cost effective. Rotary steerable systems, uses the top drive of the drilling rig to rotate the entire drill string, which is the primary characteristics of a rotary steerable system. It further comprises of the bottom hole assembly which include the drill bit, the steering unit, the control and sensor unit and lastly the power generation unit.

The aim of directional drilling to meet all or one of its possible applications leads to developing complex well bore trajectories. Rotary steerable system enable us to achieve these complex geometries, including horizontally deviated wells and extend reach wells. Rotary steerable systems enable continuous rotating of the drill string while steering, which disqualify the sliding mode of conventional mud motors. Rotary steerable systems have proved their efficiency at directional drilling to ascertain smoother well bores and better economic capability.

Drilling technology has been improved greatly in the past years with the development and application of modern technologies. Ongoing research in the oil and gas industry only aims at further improving the process of oil and gas procurement keeping in mind cost efficiency, health and safety. This however pushes the industry to get eminently autonomous in times to come.

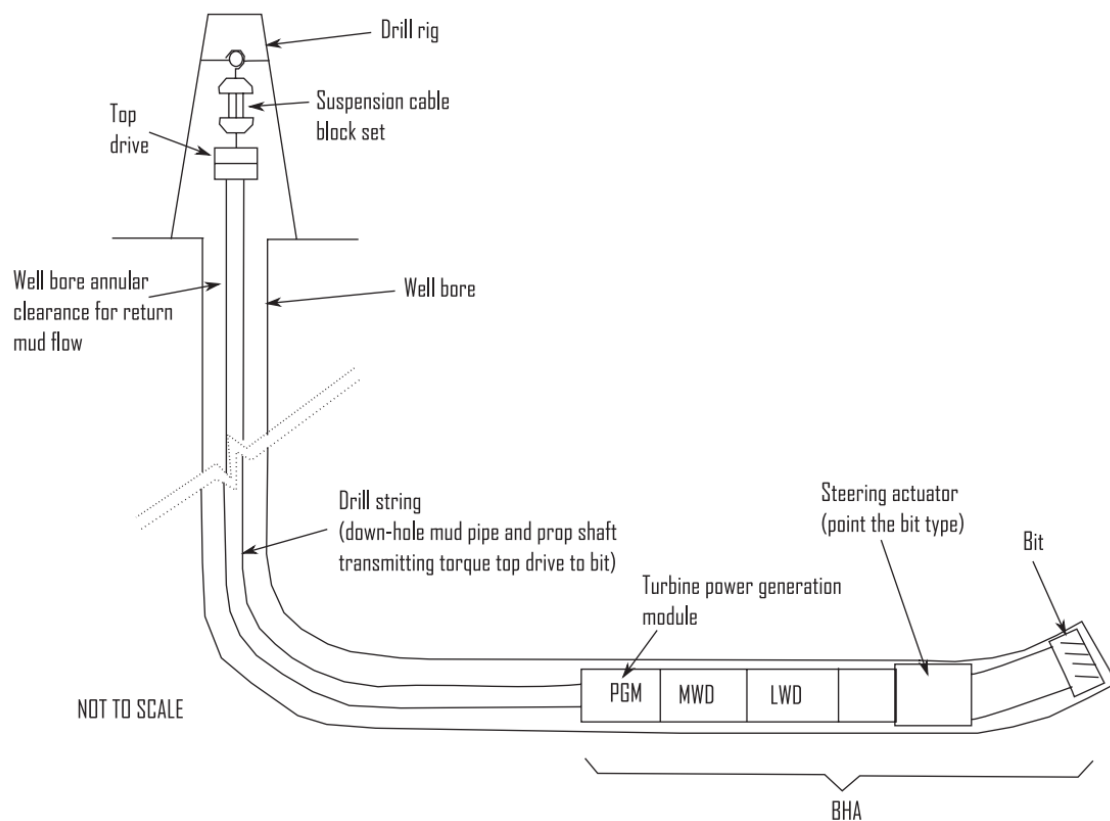


Figure 3: Rotary Steerable System (Panchal et al.; 2012)

The area of concern in this research area is the control unit. Due to various advances in the technology of sensors and measurements while drilling, it is possible to obtain comprehensive information in regards to the drills' attitude. These measurements are then fed back into our feedback controller loop which correct any change in the trajectory, to point towards the desired target.

The main advantage of steerable tools is to guide our bottom hole assembly down-hole to predetermined targets in the earth's frame. The continuous rotation of the drill string further helps in an improved transportation of the drill cuttings to the surface, which helps in maintaining a smoother well bore. The full rotation of the drill string helps to reduce drag, stick slip and also improves the rate of penetration as compared to conventional mud motor systems. The rate of penetration depends upon the weight of bit and friction that arises in case of a stationary drill, full rotation however increases the efficiency and anchors the bottom hole assembly in the hole. The sliding mode used in conventional mud motors, requires the drill string to be stationary and the drilling is carried out with the help of a positive displacement motor, housed in the BHA, with the drill string sliding behind it, The sliding mode causes well bore tortuosity. The importance of tortuosity has been pointed in [Gaynor et al. \(2001\)](#), where the tortuosity has been redefined as to having two components, macro- and micro-tortuosity. The use of RSS reduces well bore tortuosity as it helps with better weight transfer and hydraulic performance which enables us to drill much complex well bores.

Rotary steerable systems are being widely used to access tight and difficult to access formations. Rotary steerable systems, more importantly rotary closed-loop systems have achieved a higher system reliability and a reduction in maintenance requirements as pointed out in [Gruenhagen et al. \(2002\)](#). Rotary steerable systems are further seen to be able to drill more complex formations and this was tested in the Janice field overcoming conventional directional drilling techniques for proper reservoir navigation ([Johnstone and Stevenson; 2001](#)).

[Johnstone and Stevenson \(2001\)](#) describe the use of the rotary closed drilling technology for horizontal field development. It was seen that the use of this technology was able to mitigate various problems, like poor directional control, sliding issues, ledging, well-bore stability and differential sticking previously observed in the targeted field in the North Sea. The application and benefits of the rotary steerable systems are pointed out and tested in various field applications, only to prove their ideal nature and feasibility in achieving the best possible results in oil and gas production.

Rotary steerable systems have been developed by various companies. The Power drive rotary tool by Schlumberger is a good example to point out the positives of this system. The power drive tool has various variations depending upon formation requirements. An example is the world record set by a well that reached 40,329 ft of measured depth with a horizontal section of 35,770 ft in length using Schlumberger's PowerDrive Xceed tool in Qatar's Al-Shaheen field ([Downton et al.; 2000](#)).

The other companies that have developed RSS technology are: Baker Hughes, Weatherford, Sperry drilling services and TerraVici Drilling solutions.

2.2.3 Actuation

The way the bottom hole is propagated depends on the type of actuation used, with each individual type having its advantages and disadvantages. Among several types of RSS developed so far, the '*push the bit*' and '*point the bit*' are the most commonly used ones (Kim et al.; 2014).

This research deals with the more advanced RSS system. For most early RSSs, the steering mechanism belongs to the push the bit type. The two following mechanisms are explained in greater detail in the following sections.

The *push the bit* system is the older of the two mechanisms. A simple push the bit system steers the drilling assembly by applying a side load to the bit. In this mechanism, an input shaft connects the rotary valve to the control unit, to regulate the position of the push point. The direction of the BHA is changed with a number of pads or blades to push the drill away from the wellbore (Kim et al.; 2014). The push point is the point opposite the desired trajectory. A lateral load is applied to the shaft which pushes against the well bore and in turn creates a deflection in the opposite direction. This deflection of the input shaft is made with the help of a hydraulic mechanism. Precise positioning of the actuator pads is possible to achieve the geometrical target with respect to the borehole and its centreline.

The advantages of this actuation technique as mentioned in Hahne et al. (2004) are that the system is agile to change trajectory and can respond rapidly to well bore changes. The disadvantage would be that since very short gauge bits are used, this may in turn result in hole-spiraling.

A pure *point the bit* system steers by precisely tilting the bit in exactly the same direction in which the well path needs to be steered (Hahne et al.; 2004). The point the bit type actuation has a steering unit inside of the RSS (Yonezawa et al.; 2002).

The point the bit system uses the same principle as a bent housing, uses a steering actuator to align the bit in the direction of propagation. The internal mechanism of the actuator controls the angular orientation of the bit. This mechanism is independent of the drill string rotation. The point the bit system consists of a drill collar and a drill bit shaft, which rotates in the opposite direction as the drill string. The steering actuator and a control mechanism are held in the drill collar.

The push the bit system can use long gauge bits and hence eliminate the problem of a spiraling. The disadvantage is that overall dogleg severity capability is lower than that in push the bit tools and they are slower to respond to trajectory changes (Hahne et al.; 2004).

More recently, hybrid mechanisms have been used which include both push the bit and point the bit principles in alternate sections. This is known as a duty cycle. Depending on the requirement of the well bore, the drilling assembly alternates between push the bit and point the bit modes. These systems are more agile than push the bit systems and provide better well bore quality than point the bit systems. A hybrid model of actuation has been developed, in which a universal steering unit combines the advantages of both push the bit and point the bit systems (Kim et al.; 2014). It is proposed, to build a greater build angle as compared to conventional single mode RSS systems.

2.2.4 Measurements

Measurement while drilling is a technique which provides us with real time data to help with steering the drill-bit. MWD tools are enclosed in the BHA well behind the bit. MWD uses magnetometers and accelerometers to determine borehole inclination and azimuth during actual drilling. These are the main two parameters which help steer the well according to a specified plan or trajectory which is defined by a team of reservoir engineers, drilling engineers, geologists among others. This data which is obtained down-hole is then transmitted to the surface using pulses, like electromagnetic telemetry, mud pulse telemetry or wireline. The communication and control architecture is limited to having low bandwidth communication links as pointed out in [Downton \(2012\)](#). The unified model proposed in [Downton \(2012\)](#) allows high frequency communication and allows cross domain models such as a drilled wired drill pipe, which however can be disruptive. A short-distance telemetry system is used in the PowerDrive RSS developed by Schlumberger ([Downton et al.; 2000](#)). This telemetry system uses magnetic pulses and does not require hard wiring which can prove to be disruptive. The PowerPulse MWD system is used in conjunction with the PowerDrive tool and facilitates real-time upward communication. This MWD tool is a part of the BHA which also includes the bit, the steering actuator and the power generation unit. In Figure 5, as seen in [Panchal et al. \(2012\)](#), shows the conventional inclination and azimuth of drill string while also considering the steering direction.

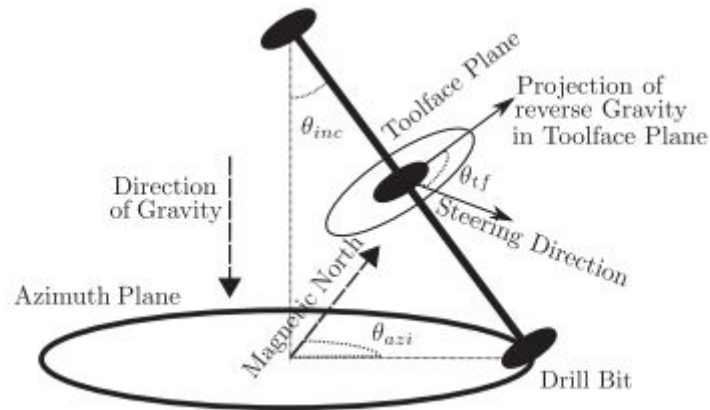


Figure 4: Conventional Measurement Scheme ([Panchal et al.; 2012](#))

MWD sensor pack is used to make attitude measurements both continuously and statically when the tool is not propagating. Owing to accelerometers, the static surveys are always much more accurate and are used to measure other quantities such as magnetic and gravitational field dip angle ([Panchal et al.; 2012](#)). These quantities are then used in subsequent continuous surveys where just by using the continuous axial accelerometer and magnetometer combined with these static surveys the continuous survey azimuth and inclination measurements can be made as discussed in [Panchal et al. \(2011\)](#). Strapdown sensors are mounted on the drill collar and rotate along with the drill, while roll stabilized sensors are mounted in a platform aligned with the axis of the bit but allowed to rotate relative to itself at the axis ([Barr et al.; 1995](#)). [Barr et al. \(1995\)](#) in their work compare the relative importance of strapdown and roll stabilized sensors. There has been comprehensive research in improving the measurement capabilities of these sensors. [Sugiura et al. \(2014\)](#) in their work describe the use of three-axis inclination and six-axis azimuth equations as an industry standard for attitude measurements. Azimuth measurements

are near vertical as pointed out by [Sugiura et al. \(2014\)](#). [Genevois et al. \(2003\)](#) studied the various scenarios for azimuth errors on rotary assemblies. Poor stabilizer positioning types of bits were recognized to cause azimuth walk. [Yiyong et al. \(2009\)](#) used a tri-axial micro accelerometer and a micromechanical gyroscope to measure inclination pitch, roll and azimuth angle.

Of relevant importance is the ability of the mechanism to maintain a certain attitude which is possible due to advancement in measurement while using drilling systems. These will be explained in detail in the following section.

The basic directional drilling terminologies are:

- **Inclination Angle:** The inclination angle of a well is the angle the well-bore forms between its axis and the vertical.
- **Azimuth:** The azimuth of the well bore at a point is defined as the direction of the well bore on a horizontal plane measured clockwise from a north reference. Azimuths are expressed in angles and are measured from zero to north. They are more conventionally expressed in quadrant from north in the northern quadrants and from the south in the southern quadrants.
- **Measured Depth (MD):** It is the distance measured along the well path from one reference point to another.
- **True Vertical Depth (TVD):** It is the vertical distance measured from the reference point to the survey point.

Accelerometers: The earth's gravitational field is described by a force vector which points directly to the earth's core. The altitude or the depth of the body below the earth's surface dictates the intensity and direction of the gravitational field. This acceleration which is experienced due to gravity can be measured by specific instruments known as accelerometers. An accelerometer is an electromechanical device which can measure static and continuous acceleration forces. Three axis gravity accelerometers are used to measure inclination. These measure the earth's gravitational field in the x , y and z planes. The inclination is calculated using only accelerometers and azimuth is calculated based on both accelerometer and magnetometers ([Matheus et al.; 2014](#)). A micro-electro-mechanical accelerometer system is described in [Ranger Survey Systems \(2016\)](#) which is a miniature version of this surveying tool.

[Thorogood et al. \(2010\)](#) discuss the possibility of using a combination of surface and downhole accelerometers which enable measuring drillstring vibration and stress.

Magnetometers: The earth's inherent magnetic field allows for various measurements of magnetic inclination and direction which in conjunction with measurements from the earth's gravitational field can help predict the azimuth of the concerned body. Tri-axial magnetometers are used to measure the magnetic field vector in a 3-D space. Typically, it consists of three fluxgate coils, oriented at right angles from each other. The magnetic north is determined by the direction in which the magnetic field is the strongest. The azimuth reading is calculated as the horizontal angle between the axis of the tool and the direction of the magnetic north ([Ranger Survey Systems \(2016\)](#)). Since continuous surveys have become more trustworthy, the number of static surveys required to deviate the well bore have reduced, thus decreasing drilling cost considerably ([Felczak et al.; 2012](#)).

For attitude control the two main measurements are direction and inclination, which provide the controller bottom hole with measurements to make necessary steering action for borehole propagation.

2.3 The Control Problem

2.3.1 Specific Control Problem

The attitude of an object is the orientation of the tool with respect to the earth's frame (inertial frame of reference). In simpler words, it is the angular position of an object in the space it is placed in. The attitude is measurable across three dimensions, confirmed by the Euler rotation theorem. Euler's Rotation theorem states that any orientation can be reached with a single rotation around a fixed axis. Amongst the various methods used to describe the attitude of a body quaternions, Euler angles and rotation matrices are largely the most accurate descriptions. Other attitude specifics in the oil and gas industry pertaining to geology would be strike and dip measurements. [Panchal et al. \(2012\)](#) describes the approach of transformation from Euler to quaternion, which allows to convert a set point attitude in terms of azimuth and inclination into a quaternion and eventually a vector in the earth's frame. 'The orientation control of a rigged body has important applications from pointing and slewing of aircraft, helicopter, space craft, and satellites , to the orientation of a rigid object held by a single or multiple robot arms.'

Drilling automation is a rapidly developing area within the oil and gas industry. Attitude control is the foundation of this fast developing application. Various trajectory control systems and algorithms have been designed and developed only to be field tested to further elaborate their benefits. [Pirovolou et al. \(2011\)](#) presented a trajectory control system predicting the behaviour for RSS systems.

These models are used in control algorithms to achieve automatic closed-loop control. The measurements of inclination and azimuth are used to generate a desired tool face which is the subsequent output of closed loop system to achieve desired trajectory. Various algorithms for achieving closed loop control of directional systems are proposed by [Pirovolou et al. \(2011\)](#) and [Maidla and Haci \(2004\)](#) in their respective works. Downlinking steering commands help in creating well paths that meet the required trajectory. A proposed control algorithm is shown in Figure 5([Wen and Kreutz-Delgado; 1991](#)).

Similar control applicable to directional drilling is described in [Yonezawa et al. \(2002\)](#) and [Urayama et al. \(1999\)](#). In the latter, the attitude actuation system was developed to dynamically control the bending angle and bit tool-face.

In order to be able to apply attitude control within the aforementioned trajectory control algorithm, it is essential to have a feasible dynamic and kinematic systems describing the behavior of the drill. The complexity involved in the well-bore dynamics along with the kinematics of the drill make the mathematical modeling of the drill rather tedious. Many variables interact causing the bit to follow a certain trajectory. Most of the system attitude models used for the RSS are rather complex. They are designed to capture the dynamics of attitude response of the rotary steerable tools in high fidelity. Various works have described the process of borehole propagation considering different mathematical

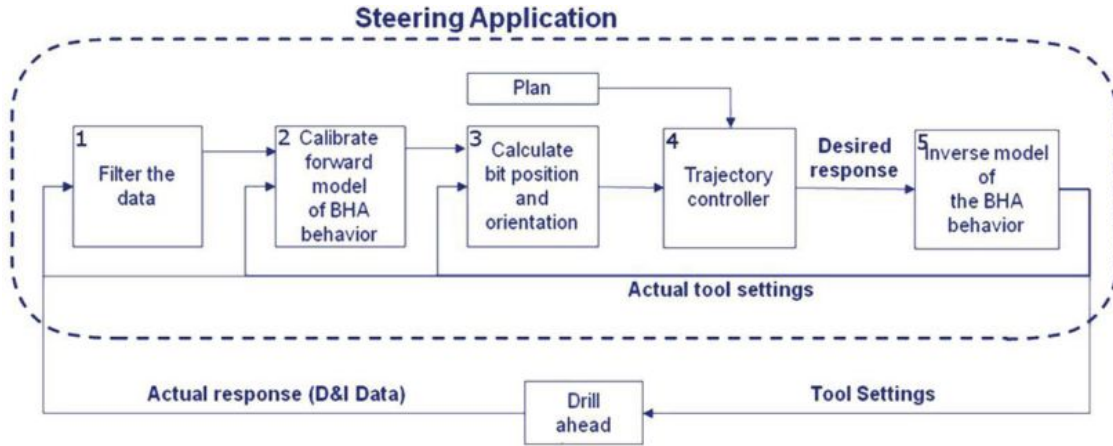


Figure 5: Control Algorithm for Trajectory Control (Pirovolou et al.; 2011)

techniques. The recent advancements in the technology of directional drilling tool enables us to maintain a desired trajectory with the help of continuous inclination and azimuth measurement sensors, compared with the reference azimuth and inclination, in a typical multi-variable control feedback system (Panchal et al.; 2012).

Li et al. (2008) and Shengzong et al. (1999) in their works consider trajectory control using piece-wise mathematics and optimal control. Piece-wise mathematics enables to identify any-point on the trajectory by ordinary equations in terms of independent parameters such tool-face and curvature. The former describes an open loop optimal control problem. Shengzong et al. (1999) considers various factors such as, geological requirements, BHA, drill string dynamics, formation etc in a constrained optimization problem for sidetracking horizontal wells. The mathematical model developed enables 3D modelling of the well trajectory.

A rock bit interaction model to predict drilling trajectory in directional wells is presented in Ho (1987), the model is trained to work in three different modes to generate logs as well as primarily predict direction. Similarly, the model as described in Downton (2007) considers a three point steering propagating system, which considers three points of borehole contact. It is proposed that the boreholes radius of curvature is the function of these three parameters, namely the distances between the stabilizers and eccentricity. It can be seen that a change in eccentricity would result in the system drilling a new radius of curvature, which is a consequence of simple geometry. The study is carried out comparing different scenarios of dynamics of flex shafts. Downton and Ignova (2011) consider the the same model and a delay-differential equation is developed describing borehole propagation. Borehole propagation function is a complex one and is said to be more accurate if more dynamics of the drill string are known. Further work considered the design of an \mathcal{L}_1 adaptive controller, which also considered inherent uncertainties and disturbances (Sun et al.; 2012). The method in itself is a novel technique for propagating the borehole and points out that even in the absence of full dynamics of drilling, there exists a complex set of behaviors resulting entirely from the manner in which the borehole is propagated according to the dictates of spatially delayed touch points, the flexibility of the system and the forces applied to the bit and its borehole propagation behavior.

Also from a physical point of view, Millheim et al. (1978) used an approximation technique

known as the finite element method to analyze bottom hole assembly configurations. This technique used parameters such as reaction forces on the bit, deviation from the center-line and collar stresses to find the dropping and turning tendencies of the various assemblies. The assemblies used were a straight beam and a curved beam element. Finite element analysis depends heavily on the design and configuration of the drilling assembly taking into various details of the drilling dynamics and well bore interaction. It is seen that a very detailed sophisticated model can be developed to achieve attitude control which however would be difficult to use and control in reality. The dynamics of the drill underground is complicated in nature and assumptions are made to avoid certain parameters and different authors prefer certain variations as compared to others. Furthermore, these models need to be trained in real time to achieve the desired response, and to be further corrected and redeveloped based on field tests. Assembly configuration and dimensions, lithology, dip, bit type, hole curvature, magnitude of inclination, bit weight and rotary speed are some of the important parameters that control the inclination and azimuth of the bit (Millheim et al.; 1978).

In Panchal et al. (2010), a generic approach to map borehole propagation in terms of inclination and azimuth is used. A simple kinematic model dictating the process of directional drilling is derived and control techniques are used to ascertain reference inclination and azimuth tracking and stability of the developed closed loop system.

The kinematic model is highly uncertain and encompasses various parametric variations. The robust stability and performance requirements are highlighted in Bayliss et al. (2014) and Bayliss and Whidborne (2015).

Three control laws have been proposed in Panchal et al. (2012). The attitude is represented as a unit vector, which helps to avoid the non-linearities that the Euler angle approximations induce. The model used to implement these controllers is a simple kinematic model which assumes the BHA to be a rigid rod hinged at one end. The three control laws proposed are variable build-rate controller, constant build-rate controller and discrete time controller. These control laws are fairly simple, however they require certain co-ordinate transformations.

The desired attitude is calculated as a unit vector from the desired Euler angles, and the required tool face is generated. The advantages of using quaternions is that while drilling parallel to the earth's magnetic or gravitational field the radial magnetometer and accelerometer readings are not disturbed (Panchal et al.; 2012).

The mathematical model proposed in Panchal et al. (2010) is comparatively simple and does not consider the lateral forces on bit. The model simply puts together the essentials required for maintaining trajectory control. This model will be studied in detail in this research.

From the study of these models, we can see that if a small number of parameters is to be identified then we can design control schemes easily. A simple model as in Panchal et al. (2010) might not touch all the dynamics of bottom hole assemblies. In case of a complex model, it may capture all the dynamics but will require more data and time to identify all the parameters and produce useful outputs and recommendations.

This research aims to study the mathematical models in Panchal et al. (2010) which are then implemented in automatic control algorithms to achieve a desired trajectory.

Chapter 3

Plant Modeling

3.1 Tool Kinematics

The specified system is modeled in terms of the tool's inclination and azimuth angles, θ_{inc} and θ_{azi} . Only the attitude dynamics of the tool are considered. The proof of the kinematic modelling is described in [Panchal et al. \(2010\)](#).

The system model is as follows,

$$\dot{\theta}_{\text{inc}} = V_{\text{rop}} (U_{\text{dls}} \cos(U_{\text{tf}}) - V_{\text{dr}}) \quad (3.1)$$

$$\dot{\theta}_{\text{azi}} = \frac{V_{\text{rop}}}{\sin(\theta_{\text{inc}})} (U_{\text{dls}} \sin(U_{\text{tf}}) - V_{\text{tr}}) \quad (3.2)$$

where θ_{inc} is the inclination angle, θ_{azi} is the azimuth angle, U_{tf} is the tool face angle control input, U_{dls} is the dog log severity or curvature, V_{rop} is the rate of penetration, V_{dr} is the drop the rate disturbance and V_{tr} is the turn rate disturbance.

The azimuth response is coupled with the inclination response by the sine of the inclination term present in the denominator of the equation governing the azimuth.

3.1.1 Virtual Control Transformation

The virtual control transformation as proposed in [Panchal et al. \(2010\)](#) gives the two inputs U_{tf} and U_{dls} in terms of the virtual inputs U_{inc} and U_{azi} as follows

$$U_{\text{tf}} = \text{ATAN2}(U_{\text{azi}}, U_{\text{inc}}) \quad (3.3)$$

$$U_{\text{dls}} = K_{\text{dls}} \sqrt{U_{\text{inc}}^2 + U_{\text{azi}}^2} \quad (3.4)$$

$$\frac{U_{\text{dls}}}{K_{\text{dls}}} = \sqrt{U_{\text{inc}}^2 + U_{\text{azi}}^2} \quad (3.5)$$

This transformation allows the partial linearization of Equations (3.1) and (3.2). The partially linearized and decoupled equations governing borehole propagation are given as

follows

$$\dot{\theta}_{\text{inc}} = V_{\text{rop}} K_{\text{dls}} U_{\text{inc}} \quad (3.6)$$

$$\dot{\theta}_{\text{azi}} = \frac{V_{\text{rop}}}{\sin(\theta_{\text{inc}})} K_{\text{dls}} U_{\text{azi}} \quad (3.7)$$

3.1.2 Unmodelled Dynamics

It is of significant importance to point out the unmodelled dynamics and their effects on the robustness and performance capabilities of control system. In this work, the unmodelled dynamics are included in the design of the controllers and later for a frequency domain robustness analysis.

U_{tf} Toolface Angle

Specifically, point the bit type actuation systems exhibit a lag in the actual tool face response, U_{tf} (Panchal et al.; 2010). The lag is modeled as a first order lag with a unity gain and time constant of τ_d . The actual tool face angle θ_{tf} is

$$\theta_{\text{tf}} = h_{\text{lag}}(s) U_{\text{tf}}(s) \quad (3.8)$$

where h_{lag} is given by the Laplace transform

$$h_{\text{lag}}(s) = \frac{1}{1 + s\tau_d} \quad (3.9)$$

Actuation Delay

The drill cycle operation also induces an actuation delay. The demand toolface U_{tf} is applied over a drilling cycle and the delay τ_2 is a function of the drill cycle. More about the drill cycle in Section 8.1. This delay is modeled using a first order Pade approximant. Pade approximants are the most used rational descriptions of a time delay which is otherwise expressed as the Laplace transform $e^{-s\tau}$, where τ is the associated time delay. The delay τ_1 is assumed to be half the drilling cycle in the Laplace transform,

$$h_1(s) = \frac{1 - s\frac{\tau_1}{2}}{1 + s\frac{\tau_1}{2}} \quad (3.10)$$

Measurement Delays

Lastly, there is a measurement delay on both feedback channels, as the attitude sensors are at a fixed distance behind the bit. The delay exists because there is a delay between the drilling of the new hole and its actual measurement. This delay time is dependent on V_{rop} . For a nominal V_{rop} , the delay in seconds is calculated assuming the sensor is at a fixed distance, D , behind the bit as

$$\tau_2 = \frac{D}{V_{\text{rop}}} \quad (3.11)$$

It is modeled as a first order Pade approximant,

$$h_2(s) = \frac{1 - s\frac{\tau_2}{2}}{1 + s\frac{\tau_2}{2}} \quad (3.12)$$

3.2 Linearization

The design and analysis of controllers for linear systems is generally a far easier problem than for non-linear systems. Hence, it is common practice to approximate a non-linear system by a linear one. The process through which a non-linear system is converted to a simple linear system is known as linearisation. Mathematically it consists of three stages

1. Choose a relevant operating point of the system for linear approximation. The two options available to choose as the operating points are
 - (a) Steady state points.
 - (b) Current location.
2. Calculate the Jacobian matrix at that point (Ogata; 2005). The Jacobian matrix is basically a truncated Taylor series expansion.
3. Use algebraic methods to solve for unknown constants, if any.

Control of a non-linear system is achieved by obtaining a linear system about a nominal point and then designing a controller using linear feedback control methods. Gain scheduling is often used, control parameters are varied according to selected system variables in a way that pieces together linear controllers.

The partially linearised equations as derived in Panchal et al. (2010) and given by Equations (3.6) and (3.7) are linearized at a nominal inclination angle, $\theta_{\text{inc}} = \hat{\theta}_{\text{inc}}$.

Now, assume that $a = V_{\text{rop}} K_{\text{dls}}$ is constant, giving the state space representation,

$$\dot{\theta}_{\text{inc}} = a U_{\text{inc}} \quad (3.13)$$

$$\dot{\theta}_{\text{azi}} = \frac{a}{\sin(\theta_{\text{inc}})} U_{\text{azi}} \quad (3.14)$$

Linearization using Jacobean matrices yields at a nominal inclination, the generalized linear form

$$\begin{aligned} \dot{x} &= A_0 x + B_0 u \\ y &= C_0 x \end{aligned} \quad (3.15)$$

where

$$A_0 = \begin{bmatrix} 0 & 0 \\ -a \csc(\theta_{\text{inc}}) \cot(\theta_{\text{inc}}) & 0 \end{bmatrix} \quad (3.16)$$

$$B_0 = \begin{bmatrix} a & 0 \\ 0 & \frac{a}{\sin(\theta_{\text{inc}})} \end{bmatrix} \quad (3.17)$$

$$C_0 = \begin{bmatrix} 1 & 0 \\ 0 & 1 \end{bmatrix} \quad (3.18)$$

The transfer function of the system is thus calculated using

$$G(s) = C_0(sI - A_0)^{-1}B_0$$

Hence, the nominal transfer function is

$$G_0(s) = \begin{bmatrix} \frac{a}{s} & 0 \\ \frac{a\alpha_1\alpha_2}{s^2} & \frac{\alpha_1}{s} \end{bmatrix} \quad (3.19)$$

where, $\alpha_1 = \csc(\theta_{\text{inc}})$ and $\alpha_2 = \cot(\theta_{\text{inc}})$.

3.3 Plant including Lag and Delays

When the lag and the dynamics associated with the system are considered and combined with the linear tool dynamics, the open loop plant becomes (Bayliss and Whidborne; 2015)

$$L(s) = K(s)G_{\text{wd}}(s) \quad (3.20)$$

where, the actual model of the plant is given by

$$G_{\text{wd}}(s) = H_2(s)G_0(s)H_1(s)H_{\text{lag}}(s) \quad (3.21)$$

$$H_i(s) = h_i(s) \begin{bmatrix} 1 & 0 \\ 0 & 1 \end{bmatrix} \quad (3.22)$$

where $i = 1, 2, \text{lag}$, h_1 and h_2 are the delays associated with the input and measurements and are described by first order Pade approximants as given in Equations (3.10) and (3.12).

3.4 Open-loop Plant Analysis

Given the general linear system given by Equation (3.15), applying the Laplace transform, we get

$$\begin{aligned} sX(s) &= A_0X(s) + B_0U(s) \\ Y(s) &= C_0X(s) \end{aligned} \quad (3.23)$$

Rearranging the Equation (3.23),

$$\begin{aligned} \frac{X(s)}{U(s)} &= (sI - A_0)^{-1}B_0 \\ \frac{Y(s)}{X(s)} &= C_0 \end{aligned} \quad (3.24)$$

Multiplying the two equations given in Equation (3.24),

$$\frac{Y(s)}{U(s)} = C_0(sI - A_0)^{-1}B_0 \quad (3.25)$$

Now,

$$(sI - A_0)^{-1} = \frac{\text{Adj}(sI - A_0)}{\det(sI - A_0)} \quad (3.26)$$

$\det(sI - A_0)$ is called the characteristic equation of the system. The eigenvalues or poles of the system can be obtained by finding the roots of the characteristic equation.

$$\begin{aligned} s &= \lambda \\ \det(\lambda I - A_0) &= 0 \end{aligned} \quad (3.27)$$

Now, from the eigenvalue analysis of the linearized state space matrix A_0 , for the plant G_0 given by Equation (3.16), the eigenvalue set for the open loop plant is obtained. The eigenvalue set is

$$\lambda = \{0; 0\} \quad (3.28)$$

The plant is unstable, as indicated by the presence of poles at the origin. Hence, it can be confirmed that the open-loop dynamics are marginally unstable and hence require further control action.

3.5 Conclusion

This chapter introduced the mathematical modeling of the drill-bits dynamics in terms of its attitude. The non-linear kinematic model is linearized around a nominal operating point for linear controller development. The original kinematic model does not include the effects of the engineering constraints namely the actuator and measurement delays and the actuator lag, however they are accommodated in the linearized model for controller design in further sections. The open-loop analysis of the linearized plant model confirmed the marginal unstable dynamics of the attitude describing model.

Chapter 4

Controller Design

4.1 H_∞ Control

The H_∞ robust control theory deals with both the robustness and the performance standards of an acceptable control system. It provides high disturbance rejection and guarantees high stability for any operating conditions (Bansal and Sharma; 2013). H_∞ controller can be designed using various techniques, but H_∞ loop shaping finds wide acceptance since the performance requisites can be incorporated in the design stage as performance weights (Skogestad and Postlethwaite; 2001). Here, the H_∞ problem is described as a *mixed sensitivity* problem which is a loop shaping technique. The H_∞ controller design is

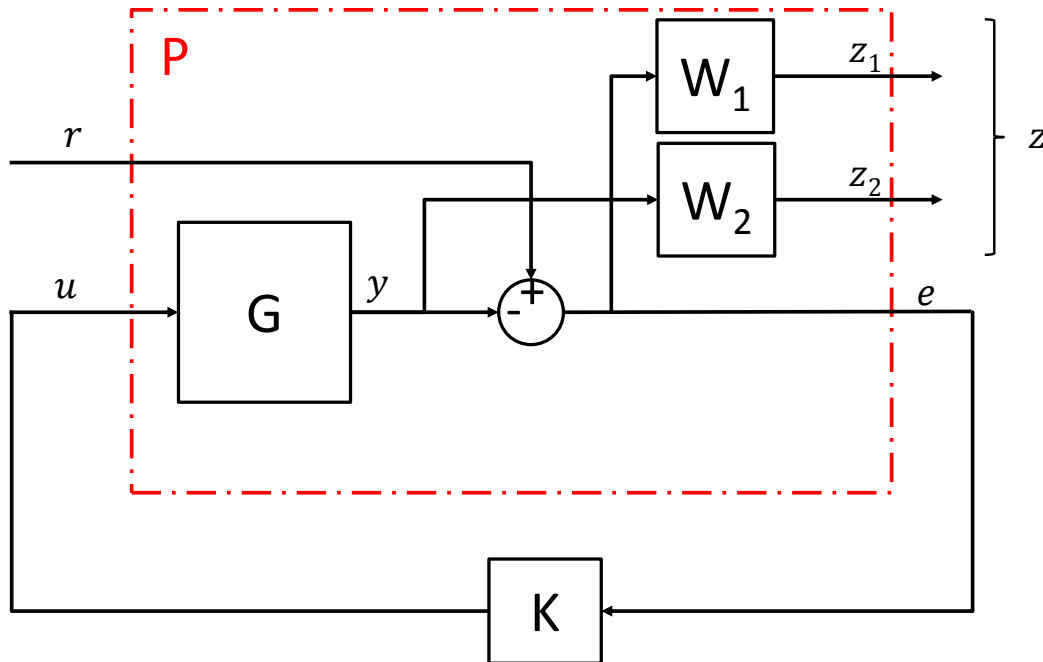


Figure 6: S/T Mixed Sensitivity Standard Form

formulated in a standard way as described in Skogestad and Postlethwaite (2001) and as

shown in Figure 6, where the standard form description is realized as

$$\begin{bmatrix} z \\ v \end{bmatrix} = \begin{bmatrix} P_{11} & P_{12} \\ P_{21} & P_{22} \end{bmatrix} \begin{bmatrix} w \\ u \end{bmatrix} \quad (4.1)$$

where,

$$P_{11} = \begin{bmatrix} W_1 \\ 0 \end{bmatrix}, \quad P_{12} = \begin{bmatrix} -W_1 G \\ W_2 G \end{bmatrix} \quad (4.2)$$

$$P_{21} = I, \quad P_{22} = -G \quad (4.3)$$

where, G is G_0 for the design 1 and G_{wd} for design 2. G_0 is the plant model without delays and lag and G_{wd} is the plant model with delays and lag.

This can be now posed as an H_∞ optimal control problem and the objective is to find an optimal controller K . Minimizing the norm

$$\min_K \| N(K) \| \quad (4.4)$$

where,

$$N = \begin{bmatrix} W_1 S_{\text{nom}} \\ W_2 T_{\text{nom}} \end{bmatrix} \quad (4.5)$$

where $S_{\text{nom}} = (I + GK)^{-1}$ is the nominal sensitivity function and $T_{\text{nom}} = GKS$ is the nominal closed loop transfer function. W_1 and W_2 are weighting functions which factor S_{nom} and T_{nom} , and are of the form

$$W_1(s) = \begin{bmatrix} w_1(s) & 0 \\ 0 & w_1(s) \end{bmatrix} \quad (4.6)$$

$$W_2(s) = \begin{bmatrix} w_2(s) & 0 \\ 0 & w_2(s) \end{bmatrix}, \quad (4.7)$$

where w_1 and w_2 can be defined as

$$w_1 = \frac{s/M + \omega_c}{s + \omega_c A} \quad (4.8)$$

$$w_2 = \frac{s + \omega_c A}{s/M + \omega_c} \quad (4.9)$$

where A is the low/high-frequency gain, M is the high/low-frequency gain and ω_c is the bandwidth for S_{nom} and T_{nom} , respectively. The parameters A , M , and ω_c need not be the same for both performance weightings. Performance weightings w_1 and w_2 and their parameters are used to tune the competing systems nominal sensitivity and closed loop transfer function also known as the complimentary sensitivity function to trade-off performance with robustness. This can be done by bounding the values of $\sigma(S_{\text{nom}})$ for performance and $\sigma(T_{\text{nom}})$ for robustness. $\sigma(S_{\text{nom}})$ and $\sigma(T_{\text{nom}})$ are the maximum singular values of the two previously defined transfer functions. Maximum singular values provides a generalization of the magnitude of a transfer function. The singular values are plotted as functions of frequency.

This can be achieved by making

$$\sigma(S_{nom}(j\omega)) < \frac{1}{|W_1(j\omega)|} \forall \omega \quad (4.10)$$

$$\sigma(T_{nom}(j\omega)) < \frac{1}{|W_2(j\omega)|} \forall \omega \quad (4.11)$$

in a standard loop shaping configuration. More detailed information about the singular value decomposition and norms on systems which leads to the definition of the maximum singular value and its application for performance and robustness is available in [Skogestad and Postlethwaite \(2001\)](#).

4.1.1 Hankel Norm Approximation

Lower-order models simplify analysis and control design, relative to higher order models. Model order reduction is used in situations when the order of a model obtained from linearizing a Simulink model is relatively high, while performing finite element calculation etc. A reduced order model helps improve the speed of simulation. During the implementation of controllers, high-order controllers lead to high cost, difficult commissioning, poor re-liability and potential problems in maintenance ([Gu et al.; 2005](#)). Hence, it is more practical to use reduced order controllers which are closed to the order of the plant to be controlled. There are various techniques to achieve controller order reduction, namely, *balanced truncation*, *singular perturbation approximation* and *Hankel-norm approximation* ([Balas et al.; 1991](#)). [Bayliss et al. \(2014\)](#) use the *Hankel Singular Values (HSV)* for the order reduction of their proposed H_∞ controller.

For a stable system, Hankel singular values indicate the state energy of the system. This enables one to obtain a reduced order model which can be determined directly by examining the systems HSV's, σ_i .

Assume that the HSV's of the system are decreasingly ordered so that

$$\Sigma = \text{diag}(\sigma_1 I_{s1}, \sigma_2 I_{s2}, \dots, \sigma_n I_{sn}) \quad \text{with} \quad \sigma_1 > \sigma_2 > \dots > \sigma_N \quad (4.12)$$

and suppose that $\sigma_r \gg \sigma_{r+1}$ for some r . The order reduction implies that the states corresponding to the singular values of $\sigma_{r+1}, \dots, \sigma_N$ are less controllable and less observable than those corresponding to $\sigma_1, \dots, \sigma_r$. Therefore, truncating the less controllable and less observable states will not lead to a loss of information about the system ([Zhou and Doyle; 1998](#)).

The Hankel model reduction function available in MATLAB *hankelmr* is considered to be better than its counter-techniques mentioned previously and produces a more reliable reduction and the algorithm enables the automatic selection of an optimal reduced system. More information about the HSV's and their application to model reduction is available in [Glover \(1984\)](#).

4.1.2 Design 1

The nominal plant G_0 , considered for preliminary H_∞ controller formulation is the same as described by Equation (3.19). In this design, the two delays and lag as described in

Section 3.1.2 are not included in the controller formulation. The controller design is made for the nominal plant parameters as described in Table 1.

The plant is augmented with weights W_1 and W_2 given by Equations (4.6) and (4.7) and w_1 and w_2 are as in Equations (4.8) and (4.9). The weighting functions are formulated using the gain values and bandwidth requirements specified in Table 2, (Bayliss et al.; 2014).

Nominal Parameter	Value	Units
V_{rop}	100	ft/hr
K_{dls}	8	deg/100 ft
τ_d	10	s
τ_1	180	s
τ_2	360	s
α_1	1	-
α_2	0	-

Table 1: Nominal Parameters

Specification	Value
$H_\infty W_1 M$ high frequency gain	5
$H_\infty W_1 A$ low frequency gain	2.5×10^{-3}
$H_\infty W_1 \omega_c$ bandwidth	$2 \times 10^{-5} \text{rad/s}$
$H_\infty W_2 M$ low frequency gain	0.9×10^{-1}
$H_\infty W_2 A$ high frequency gain	0.3×10^{-1}
$H_\infty W_2 \omega_c$ bandwidth	$0.1 \times 10^{-4} \text{rad/s}$

Table 2: Design 1: Controller Specifications H_∞

The code for the H_∞ design available in Section A.2 of Appendix A helps determine a (sub)optimal H_∞ control law, based on the prescribed open loop connection P , given by Equation (4.1). The controller obtained is of 12th order and the closed loop achieves an H_∞ norm equal to 0.4119. The higher order controllers tend to be more complex while simpler controllers are easier to implement and are more reliable since there are fewer things which can go wrong in terms of hardware fixes and software bugs (Zhou and Doyle; 1998). Model order reduction is applied using HSV decomposition and the order is reduced to 4. The MATLAB function *hankelmr* facilitates an automatic order reduction.

Design 1: Closed Loop Analysis

Now the designed controller is tested with G_{wd} , the plant model with lag and delays and the nominal closed loop is constructed. Using eigenvalue analysis as generally described in Section 3.4, the eigenvalue set of the nominal closed loop is obtained as

$$\begin{aligned} \lambda_{T_{\text{nom}}} = \{ & -0.27053; -0.26931; -0.065738 \pm 0.062984j; -0.065697 \pm 0.063061j; \\ & -0.00080105 \pm 0.0066982j; -0.00080692 \pm 0.0067186j; \\ & -4.0007 \times 10^{-5}; -2.0567 \times 10^{-5} \} \end{aligned} \quad (4.13)$$

The nominal plant is stable. It is chosen to include the uncertainties associated with the system parameters for the closed loop analysis to primarily indicate a robust design. The uncertain open loop plant, G_{unc} is formulated using a MATLAB routine given in Section A.1 in Appendix A. The uncertainty associated with the respective nominal parameters is given in Table 3. More on parametric uncertainty and uncertainty modeling is given in Section 6.1.1. The worst case is selected using trial and error from the set of 12150 uncertain plants and a similar eigenvalue assessment is made

$$\begin{aligned} \lambda_{T_{wc}} = \{ & -0.2695; -0.26747; -0.05549 \pm 0.065542j; -0.055755 \pm 0.06409j; \\ & 0.00013894 \pm 0.0052109j; -1.6102 \times 10^{-7} \pm 0.0052305j; \\ & -4.7005 \times 10^{-5}; -2.3485 \times 10^{-5} \} \quad (4.14) \end{aligned}$$

The eigenvalue analysis clearly indicates that the designed controller is not stable for the selected worst case. This is an indicator of poor robust stability of the controller.

Uncertain Parameter	Percentage/Real Uncertainty	Units
ΔV_{rop}	50%	ft/hr
ΔK_{dls}	10%	deg /100 ft
$\Delta \tau_d$	10%	s
$\Delta \tau_1$	25%	s
$\Delta \tau_2$	50%	s
$\Delta \alpha_1$	1	-
$\Delta \alpha_2$	0.0175	-

Table 3: Uncertain Parameters

The uncertain sensitivity function is $S = (I + G_{\text{unc}}K)^{-1}$ and closed loop transfer function is $T = G_{\text{unc}}KS$. In theory all the singular values associated with the uncertain sensitivity and complimentary sensitivity functions should be bounded by the inverse of the weights W_1 and W_2 . This indicates robust stability and performance for the presented case.

The stabilizing H_∞ controller for this nominal plant is tested for a set of neighboring plants, G_{unc} to assess the singular value bounds imposed on the controller. The singular values σ_S , σ_T , $\sigma_{S_{\text{nom}}}$, $\sigma_{T_{\text{nom}}}$, $\sigma_{\text{inv}(W_1)}$, $\sigma_{\text{inv}(W_2)}$ are shown in Figure 8. The nominal plant meets the bound requirements as imposed by Equations (4.10) and (4.11). However, the perturbed closed loop T and perturbed sensitivity transfer function S are seen to surpass the bound requirement for some perturbed cases for the designed controller. This indicates that the designed controller is not robust given that the lag and delays associated with the drilling tools attitude dynamics are considered in the closed loop analysis. The robust stability and robust performance requirements of the designed controller are confirmed in Section 6.4.

4.1.3 Design 2

In the previous section it was seen that a controller design for the drill model which neglects the effect of the lag and delays is conservative and gives poor response in their presence. Hence, it is chosen to include the effect of the lag and the delay in this controller design. The plant nominal model G_{wd} as given by Equation (3.21) is used to design the

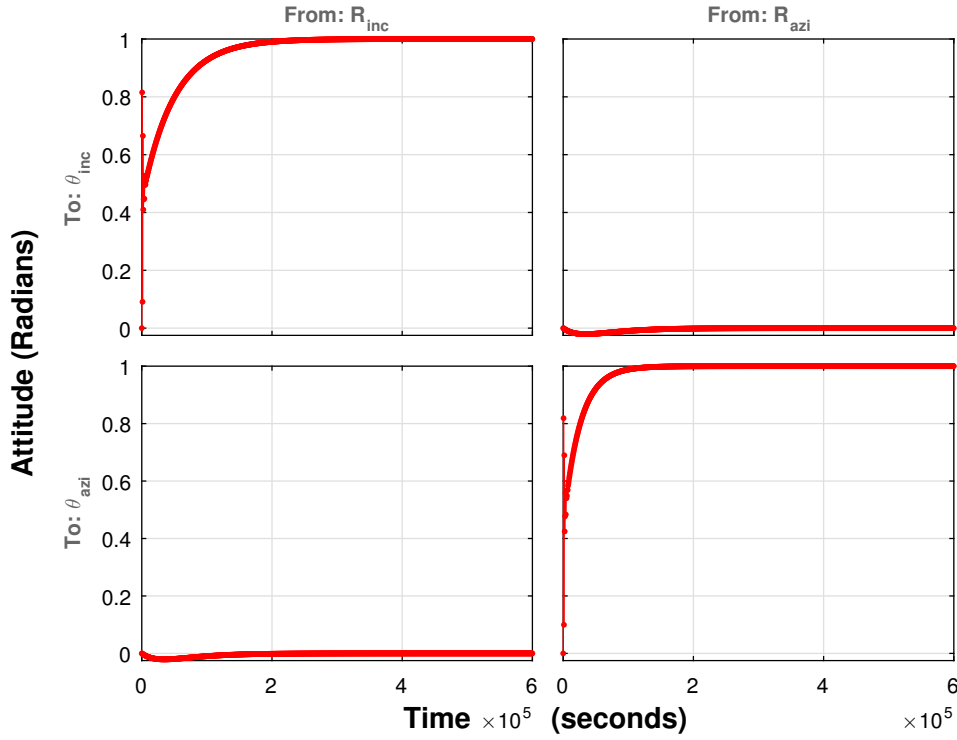


Figure 7: Design 1: Nominal Closed Loop Responses

controller. The uncertainty cannot be included in the controller design since the MATLAB function *hinfsyn* which facilitates the controller design ignores the presence of uncertain parameters. The robustness and performance weighting functions W_1 and W_2 and w_1 and w_2 are of the same form as in design 1. The weighting function tuning parameter selection requires some trial and error and the tuning parameters used in Bayliss et al. (2014) and Section 4.1.2 are used as an indicator towards the selection of suitable tuning values. The tuning parameters are given in Table 4 and the plant parameters are the same as in Table 1.

Specification	Value
$H_\infty W_1$ high frequency gain	5
$H_\infty W_1 A$ low frequency gain	2.5×10^{-3}
$H_\infty : W_1 \omega_c$ bandwidth	2×10^{-5} rad/s
$H_\infty W_2 M$ low frequency gain	0.9
$H_\infty W_2 A$ high frequency gain	2.5×10^{-1}
$H_\infty W_2 \omega_c$ bandwidth	0.8×10^{-2} rad/s

Table 4: H_∞ Design 2: Controller Specifications

Similar approach as in design 1 yields again a controller of 12th order and the closed loop achieves an H_∞ norm equal to 0.2571. Similar model order reduction as described in Section 4.1.1 is applied and a 4th order controller is obtained.

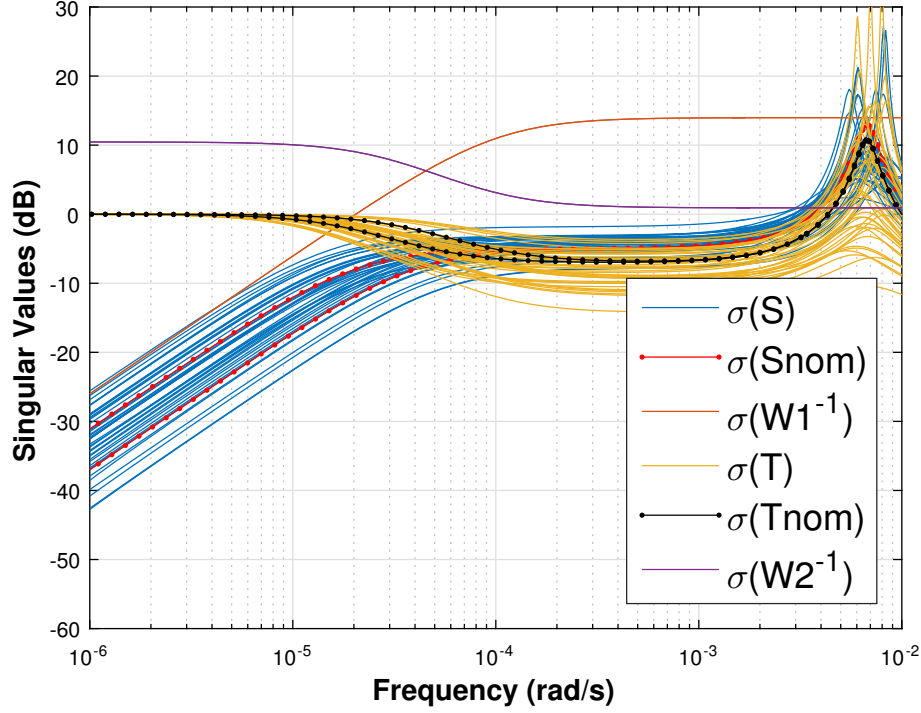


Figure 8: Design 1: Loop-shape

Design 2: Closed Loop Analysis

The stabilizing H_∞ controller for the nominal plant G_{wd} with lag and delays is tested for a set of neighboring plants G_{unc} , to assess the singular value bounds imposed on the controller. The uncertainty plant is obtained using Table 3. The singular value plots for this design are shown in Figure 10. The nominal plant meets the bound requirements as imposed by Equations (4.10) and (4.11). Unlike the previous H_∞ design, the perturbed plants, T and S meets the bound requirements for all the perturbed cases. This indicates successful robust stability and robust performance.

The closed loop transient responses for the feedback connection of the plant, G_{wd} and the stabilizing controller of this design and also for a set of perturbed plants, G_{unc} for the developed controllers can be seen in Figure 9. It is seen that the controller obtains good transient response for both the nominal plant and the parametric perturbations. The uncertain system response helps indicate the worst case combination. The worst case is chosen as the system with maximum overshoot and the eigenvalue sets for the nominal and worst case are obtained as follows

$$\begin{aligned} \lambda_{T_{nom}} = \{ & -0.3027 \pm 1.3912e - 12j; -0.099075 \pm 5.9074e - 16j; \\ & -0.013448 \pm 2.6809e - 15j; -0.0032809 \pm 3.5348e - 15j; \\ & -0.00062038 \pm 1.8498e - 15j; -2.805 \times 10^{-8}; -2.805 \times 10^{-8} \} \quad (4.15) \end{aligned}$$

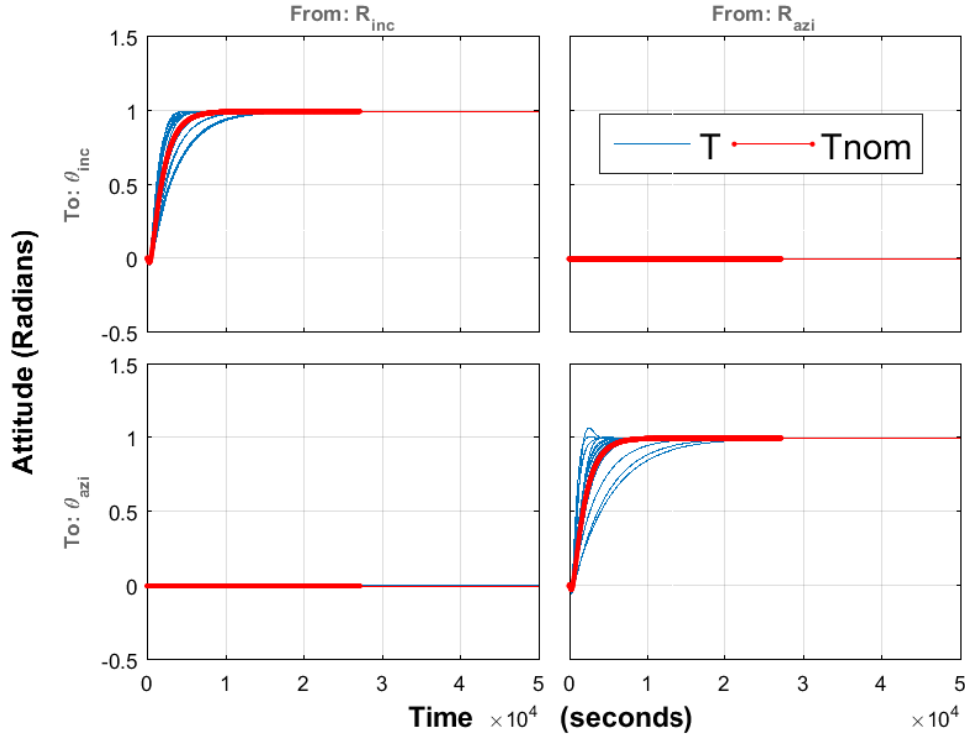


Figure 9: Design 2 : Closed Loop Responses

$$\begin{aligned}
 \lambda_{T_{wc}} = \{ & -0.30274; -0.30288; -0.078625; -0.077919 \\
 & ; -0.01185; -0.012997; -0.0009175 \pm 0.0010986j; \\
 & - 0.00062668 \pm 0.0015599j; -2.8052 \times 10^{-8}; -2.8053 \times 10^{-8} \} \quad (4.16)
 \end{aligned}$$

The eigenvalues are clearly stable and indicate robust stability. Figure 11 compares the nominal transient response for the two designs achieved. It can be seen that the H_∞ design for the plant with the lag and delays yields a better controller. The robust stability and robust performance requirements of the designed controller are confirmed in Section 6.4.

4.2 PI Controller

The PI (proportional plus integral) controller is the most commonly used controller in the industry. The PI controller is simple in its application and includes integral action which is required in control applications for set-point command tracking, implying zero steady state error. Multivariable PI controllers can be designed using the classical pole placement technique, can be formulated as a Linear Quadratic Regulator(LQR) problem (Lin and Gundes; 2000), or using control system design and tuning applications in Simulink. Figure 12 shows the standard feedback PI controller closed loop connection.

Integral action is incorporated in the system by augmenting the state with the integral of

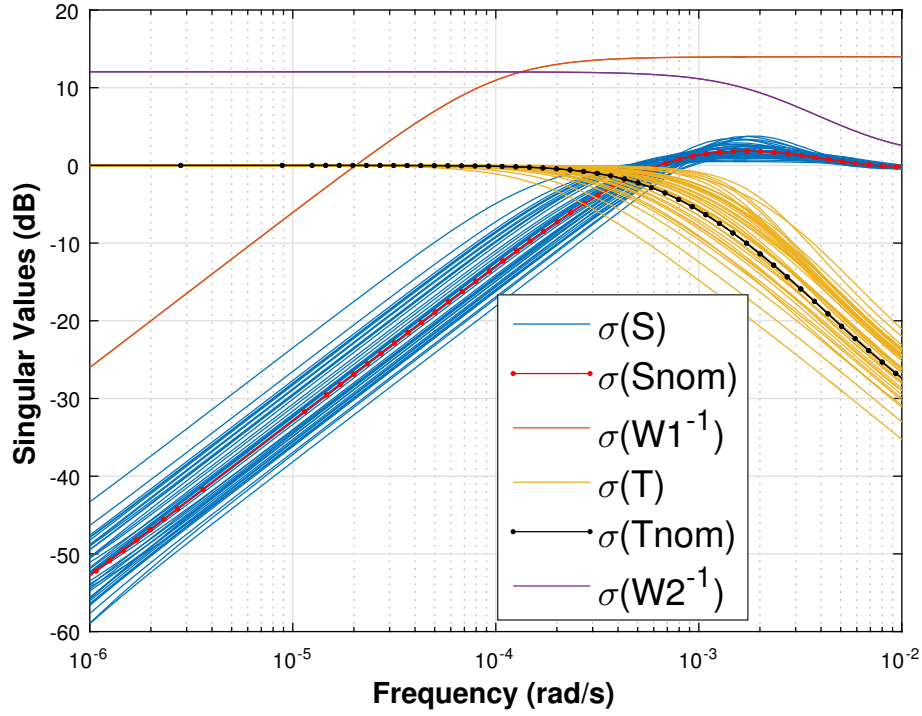


Figure 10: Design 2 : Loop Shape

the error, $x_k = \int edt$, where $e = r - y = r - Cx$. The system hence takes the general form,

$$\begin{bmatrix} \dot{x} \\ \dot{x}_k \end{bmatrix} = \begin{bmatrix} A - BK_p & BK_i \\ -C & 0 \end{bmatrix} \begin{bmatrix} x \\ x_k \end{bmatrix} + \begin{bmatrix} BK_p \\ I \end{bmatrix} \begin{bmatrix} r \end{bmatrix} \quad (4.17)$$

$$y = \begin{bmatrix} C & 0 \end{bmatrix} \begin{bmatrix} x \\ x_k \end{bmatrix} \quad (4.18)$$

with standard feedback,

$$u = \begin{bmatrix} K_i & K_p \end{bmatrix} \begin{bmatrix} x_k \\ e \end{bmatrix} \quad (4.19)$$

The values of the gains K_i and K_p can be chosen using pole placement.

4.2.1 Pole Placement Design

The gains are determined from the nominal plant G_0 , the actuator and measurement dynamics are ignored. The PI control scheme for each channel using state feedback technique is as follows

$$u_{\text{inc}} = -k_{pi}e_{\text{inc}} + k_{ii} \int e_{\text{inc}} dt \quad (4.20)$$

$$u_{\text{azi}} = -k_{pa}e_{\text{azi}} + k_{ia} \int e_{\text{azi}} dt \quad (4.21)$$

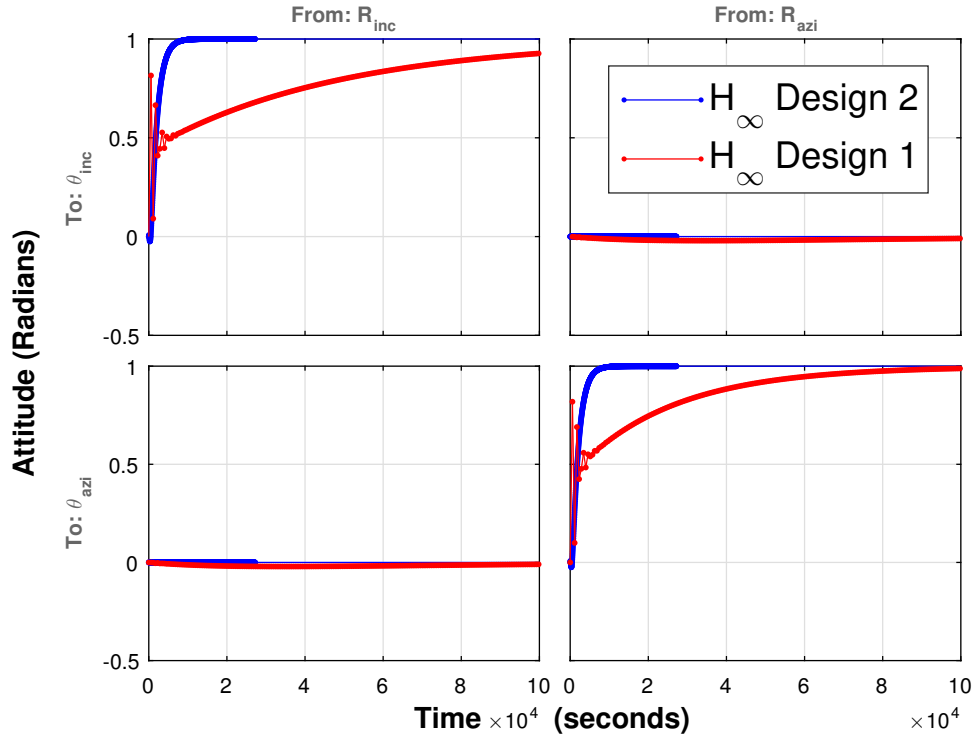


Figure 11: Nominal Closed Loop Response Comparison

where, $e_{inc} = r_{inc} - x_{inc}$ and $e_{azi} = r_{azi} - x_{azi}$.

The controllers for both the channels are appended in diagonal matrix form to give us the following

$$K(s) = 1/s \begin{bmatrix} k_{ii} & 0 \\ 0 & k_{ia} \end{bmatrix} + \begin{bmatrix} k_{pi} & 0 \\ 0 & k_{pa} \end{bmatrix} \quad (4.22)$$

Closing the loop in standard state space form as given by Equations (4.17) and (4.18) with state vector, $x = (x_{inc}, x_{azi}, x_{k1}, x_{k2})$ the closed-loop matrices are calculated as follows,

$$A_{cl} = \begin{bmatrix} -ak_{pi} & 0 & ak_{ii} & 0 \\ -a\alpha_1\alpha_2 & -a\alpha_1k_{pa} & 0 & a\alpha_1k_{ia} \\ -1 & 0 & 0 & 0 \\ 0 & -1 & 0 & 0 \end{bmatrix} \quad (4.23)$$

$$B_{cl} = \begin{bmatrix} ak_{pi} & 0 \\ 0 & a\alpha_1k_{pa} \\ 1 & 0 \\ 0 & 1 \end{bmatrix} \quad (4.24)$$

$$C_{cl} = \begin{bmatrix} 1 & 0 & 0 & 0 \\ 0 & 1 & 0 & 0 \end{bmatrix} \quad (4.25)$$

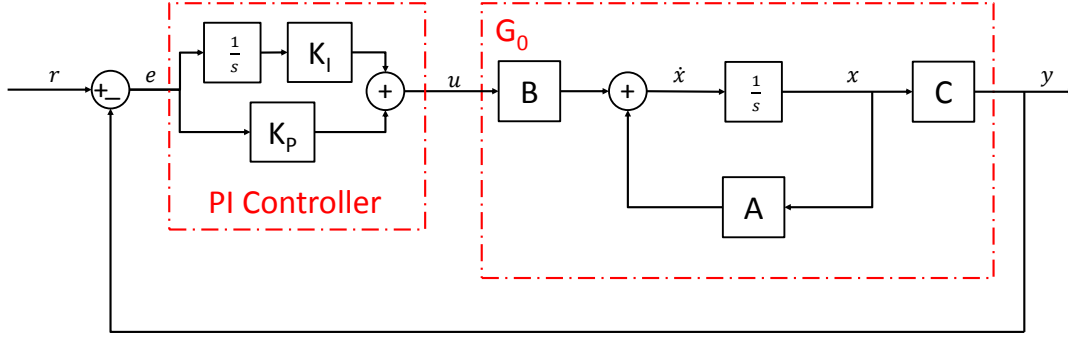


Figure 12: PI Controller Scheme

The characteristic equation for a general state space representation is shown in Section 3.4. Similarly, the determinant of the closed-loop A_{cl} matrix yields the system characteristic equation as follows:

$$q(s) = (s^2 + a\alpha_1 k_{pa}s + a\alpha_1 k_{ia})(s^2 + ak_{pi}s + ak_{ii}) \quad (4.26)$$

It is possible to choose the PI controller gains by pole placement, if it is possible to operate at near constant V_{rop} and θ_{inc} . The closed loop characteristic equation is compared with an ideal fourth order equation of the form,

$$q(s) = (s^2 + 2\tau\omega_a s + \omega_a^2)(s^2 + 2\tau\omega_i s + \omega_i^2) \quad (4.27)$$

where ω_a and ω_i are the closed-loop azimuth and inclination natural frequencies. The damping ratio ζ is set to $1/\sqrt{2}$ to insure maximum rise time and minimal overshoot 5%, then by equating Equations (4.26) and (4.27) the gains for the PI controllers in both the inclination and azimuth loops can be obtained as functions of ω_a and ω_i natural frequencies at near operating point conditions. The gains are hence expressed as follows

$$k_{ii} = \frac{\omega_i^2}{a} \quad (4.28)$$

$$k_{ia} = \frac{\omega_a^2}{a\alpha_1} \quad (4.29)$$

$$k_{pa} = \frac{\sqrt{2}\omega_a}{a\alpha_1} \quad (4.30)$$

$$k_{pi} = \frac{\sqrt{2}\omega_i}{a} \quad (4.31)$$

PI Pole Placement Design: Closed Loop Analysis

The controller is designed for the system parameters as given in Table 1. The designed controller gains are now applied to the plant G_{wd} which includes the lag and delays.

Figure 13 shows the transient response of the nominal plant model and it can be seen that good transient response is achieved for the inclination channel, while the response of the azimuth channel is highly oscillatory, indicating a design that is not ideal for a system with actuator lags and time delays. The controller is tested for the uncertain plant G_{wd} and a worst case is chosen using trial and error similar to H_∞ design 1. The nominal and uncertain closed loop eigenvalue analysis indicates that the design is not robust stable. The eigenvalues for both cases are

$$\begin{aligned} \lambda_{T_{nom}} = \{ & -0.098954; -0.014465; -0.097363; \\ & -0.0022422; -0.00050266 \pm 0.00052482j; \\ & -0.01771; -9.1354 \times 10^{-5} \pm 0.0020684j; -0.0014114 \} \quad (4.32) \end{aligned}$$

$$\begin{aligned} \lambda_{T_{wc}} = \{ & -0.078971; -0.077397; -0.011731; -0.014587; \\ & 0.00030875 \pm 0.0017667j; -0.00047975 \pm 0.00077998j; \\ & -0.00093092; -0.0012257; -1.1963 \times 10^{-11}; 1.1963 \times 10^{-11} \} \quad (4.33) \end{aligned}$$

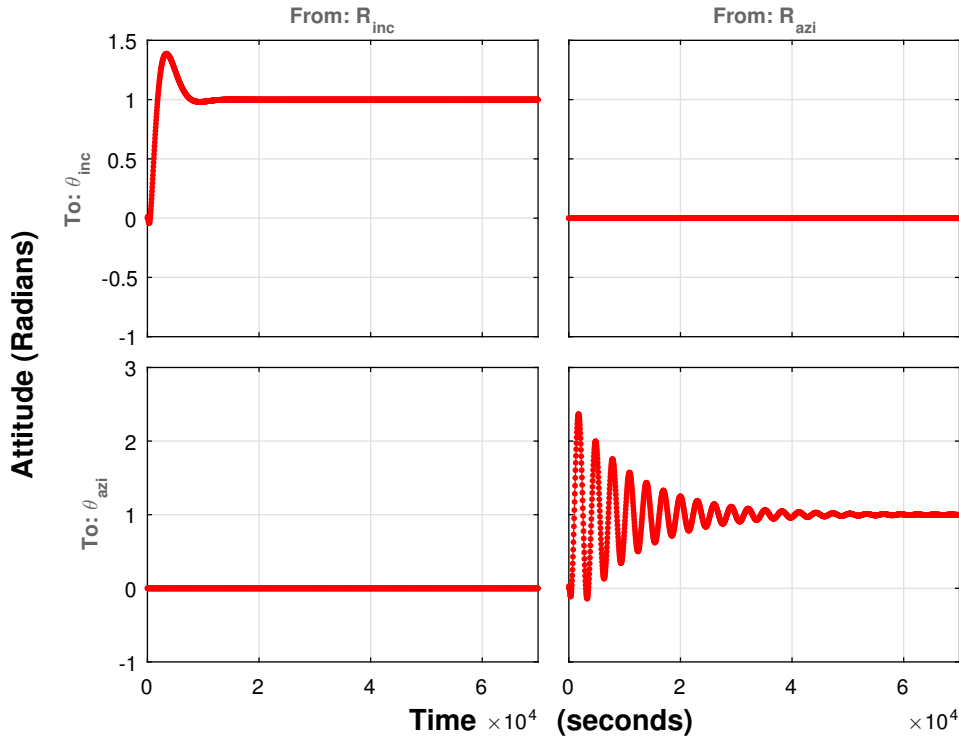


Figure 13: Nominal Closed Loop Step Response PI Pole Placement

4.2.2 Robust PI Controller Design

The robust PI controller is designed in Simulink using the Control System Tuner application. For this design, the plant G_{wd} as given by Equation (3.21) is used. This design includes the input and output delays as well as the lag which are described in Section 3.1.2.

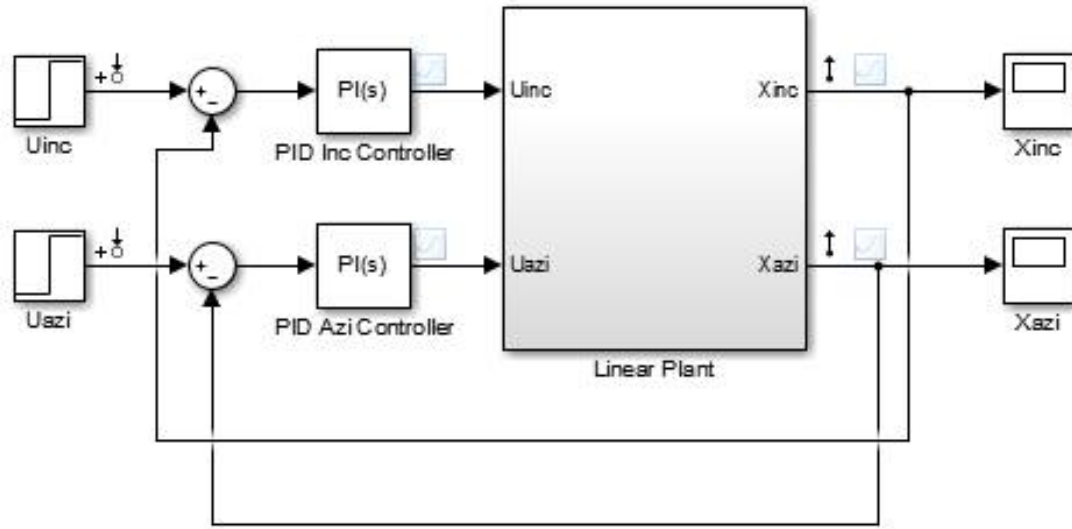


Figure 14: Simulink Closed Loop Interconnection

The following steps are carried out for the successful implementation of the Control System Tuner application. The closed loop interconnection is made in MATLAB Simulink for the nominal plant G_{wd} as shown in the Figure 14. The uncertain real parameters are created using the MATLAB function *ureal* and uncertainty is described for a percentage variation in the parameters. Specific linearization using the Linear Analysis Tool is applied for each uncertain system parameter in Simulink. The uncertain model is now ready to be tuned. The control system tuner application allows the selection of the tunable blocks, the two PID controller blocks. The proportional and integral gain values are initialized at unity. The next step is the selection of the tuning goals. The goals can be set in Simulink as shown in Figure 15. The following tuning goals are to be met

1. *Step Tracking.* The input and output signals are selected to specify the closed loop transfer function to which we need to apply the step tracking goal. A custom reference model which is similar to the nominal closed loop transfer function obtained in the H_∞ Design 2 is used as the tracking goal.
2. *Sensitivity Goal.* The sensitivity goal is the desired performance bound. This is similar to the performance bound used in the H_∞ Design 2. The performance requirement is set by the inverse of the weighting function W_1 . The signals associated with the sensitivity transfer function are selected and the tuning is forced on the desired frequency range of interest which is from 10^{-6} to 10^{-2} rad/s.
3. *Gain Goal.* For this goal the closed loop transfer function is specified by selecting the input and output signals. The gain goal is the desired robustness bound. This is given by the inverse of the weighting function W_2 which is described in the H_∞ controller Design 2. Similarly to the sensitivity goal, its application is limited to the desired frequency range.
4. *Overshoot Goal.* The overshoot goal is set to an overshoot of less than 10%.

When each of the goal is set, a graphical representation of the tuning goal can be obtained.

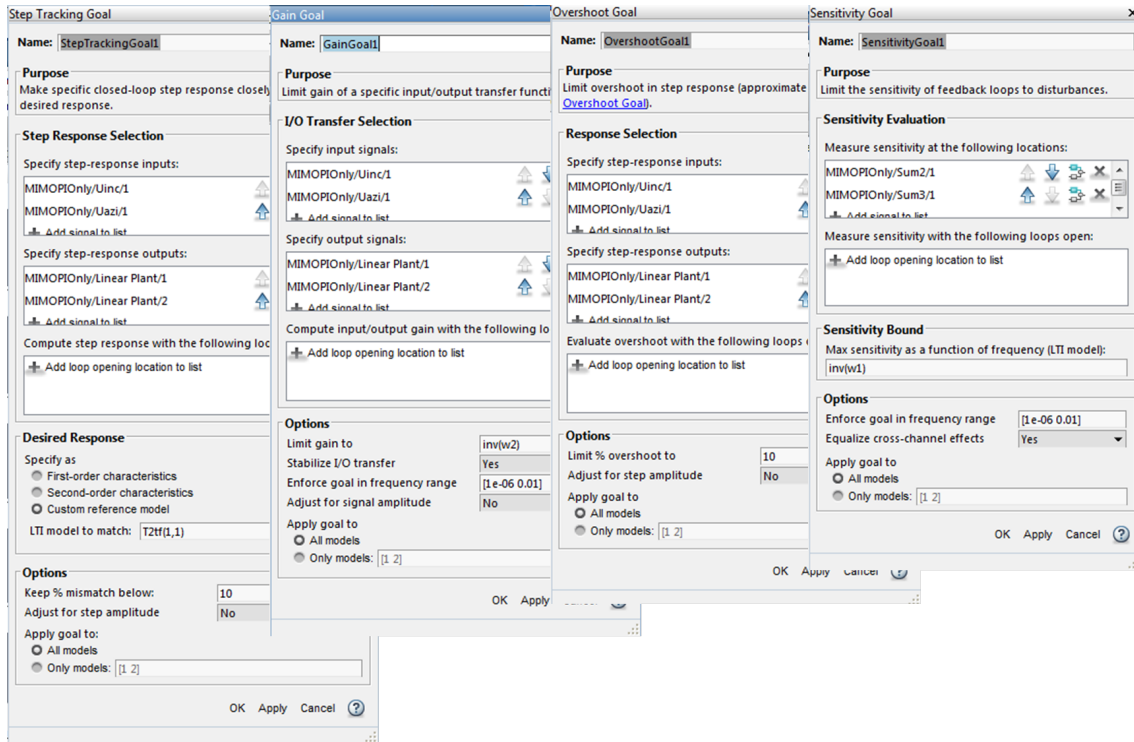


Figure 15: Tuning Goals

The step tracking tuning goal for the un-tuned plant is illustrated in Figure 16 as an example. The other tuning goals can be found in Appendix B. After tuning the control this can be used as a graphical representation of how well the controller has been tuned.

The control system is now tuned for the prescribed goals. On tuning the model, Control System Tuner converts each tuning goal to a function of the tuneable parameters of the system. It adjusts the parameters to minimize the value of those functions and generates a tuning report as given in Figure 17. The tuning report shows that the final values for the second and third goals are close to 1, which indicates that the requirements are nearly met. A value closer to 1 indicates successful tuning. The step tracking goal is nearly impossible to meet due to the presence of large parametric uncertainty which makes it difficult to track every perturbed case. The Appendix B is a graphical illustration of the tuning procedure in the control system tuner application.

Robust PI Closed Loop Analysis

The controller design can be validated by updating the two PI controller blocks in Simulink or by using the devised control gains for the plant model imported in MATLAB. Figure 18 shows the transient response of the nominal and uncertain plant which includes lag and delays. It can be seen that the system response for both the channels is stable, with minimum overshoot for the set of perturbed plants. Further, in Figure 19 it can be seen that performance and robustness criteria established while tuning is met for both the nominal and uncertain plants. The eigenvalues of the nominal plant and selected worst

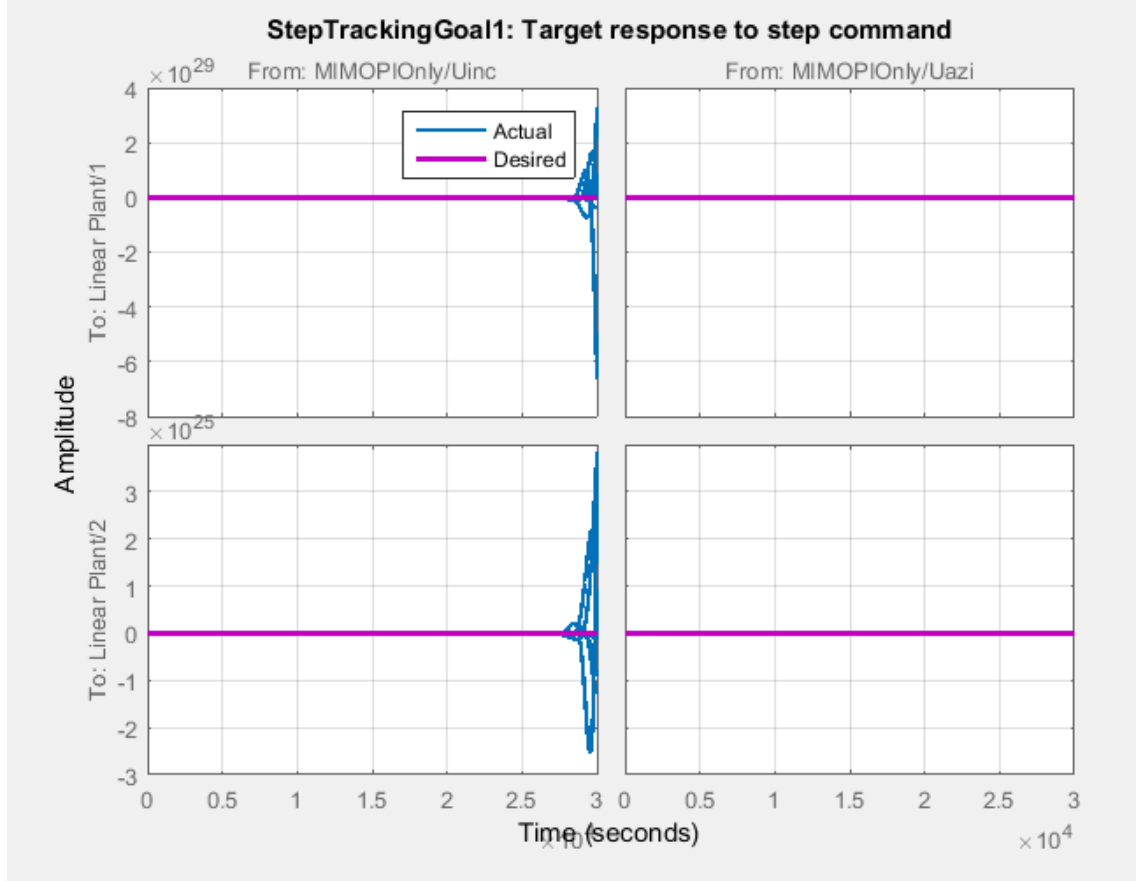


Figure 16: Unstable Plant: Step Tracking Response

case combination are

$$\begin{aligned} \lambda_{T_{nom}} = \{ & -0.099161; -0.013984; -0.099144; -0.0024369; \\ & -0.014029; -0.0010849; -0.0023495; -0.0011439; \\ & -1. \times 10^{-7}; -1.1272 \times 10^{-7} \} \quad (4.34) \end{aligned}$$

$$\begin{aligned} \lambda_{T_{wc}} = \{ & -0.078625; -0.07787; -0.01254; -0.013998; \\ & -0.00071384 \pm 0.001452j; -0.0003627 \pm 0.0018683j; \\ & -1.127 \times 10^{-7}; -1.0 \times 10^{-7} \} \quad (4.35) \end{aligned}$$

The eigenvalues for this closed-loop system for both it's nominal and selected worst case indicate robust stability. The PI controllers designed in this section will be subjected to a robustness analysis test for a frequency range of interest to confirm their robustness in Section 6.1.3.

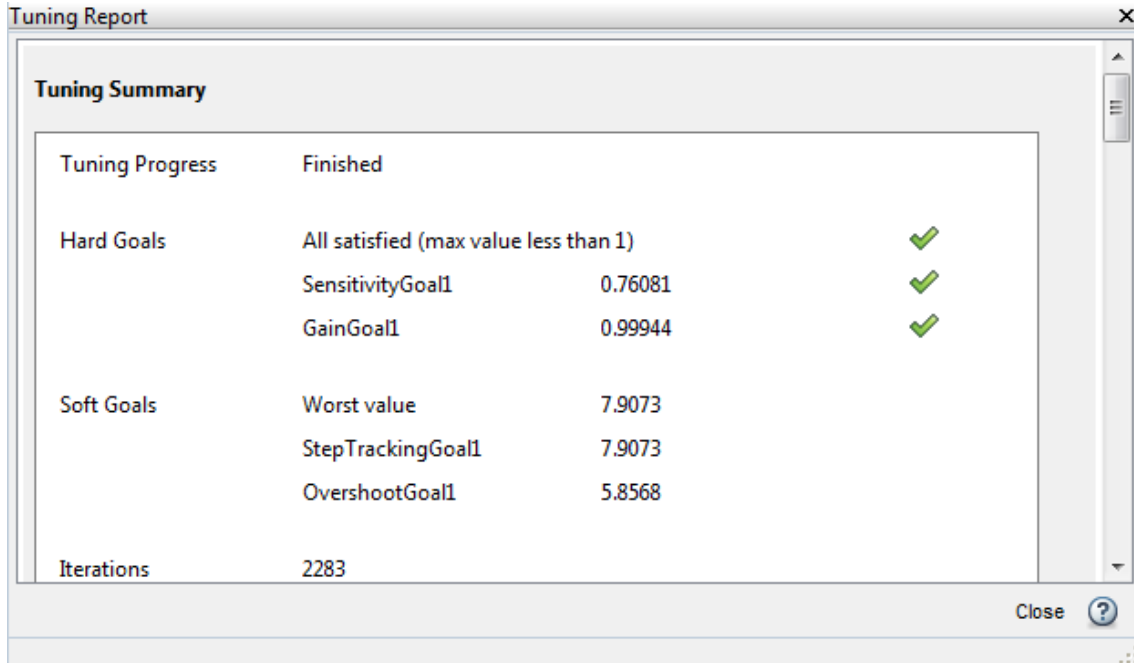


Figure 17: Tuning Report

4.3 Conclusion

In this chapter two controllers, namely PI and H_∞ were designed for two separate cases. The first case ignored the effect of the unmodelled dynamics in the controller design while the second case included these effects. The closed loop analysis was conducted on the plant model which includes the lag and delays and the parametric uncertainties for both the cases. Eigenvalue analysis for nominal and worst case for the first case designs confirmed that both the designed controllers are not robust. To achieve better control over the plant model the second controller design includes the effects of the lag and delays. The uncertain closed loop analysis for both the robust PI controller and the H_∞ controller suggest both robust stability and robust performance considering the restrictions imposed by system weighting functions. The controller designs are confirmed to be robust subject to their closed loop analysis. The designed controllers successfully stabilize the dynamics however the presence of delay is found to be significant which is dealt with it the next section.

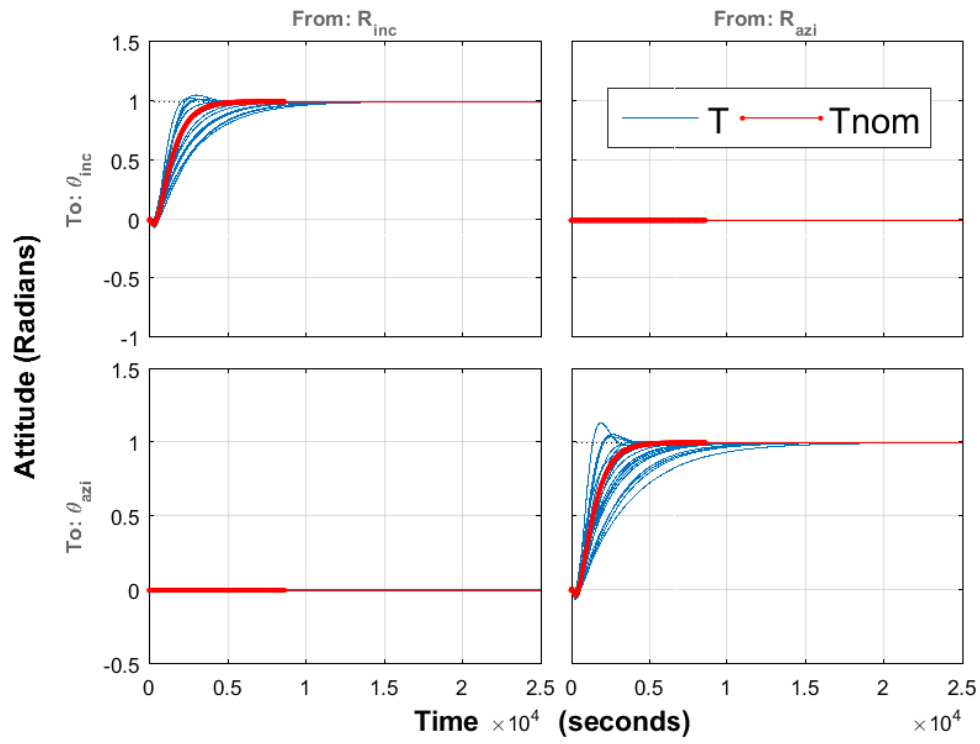


Figure 18: Robust PI Controller Transient Response

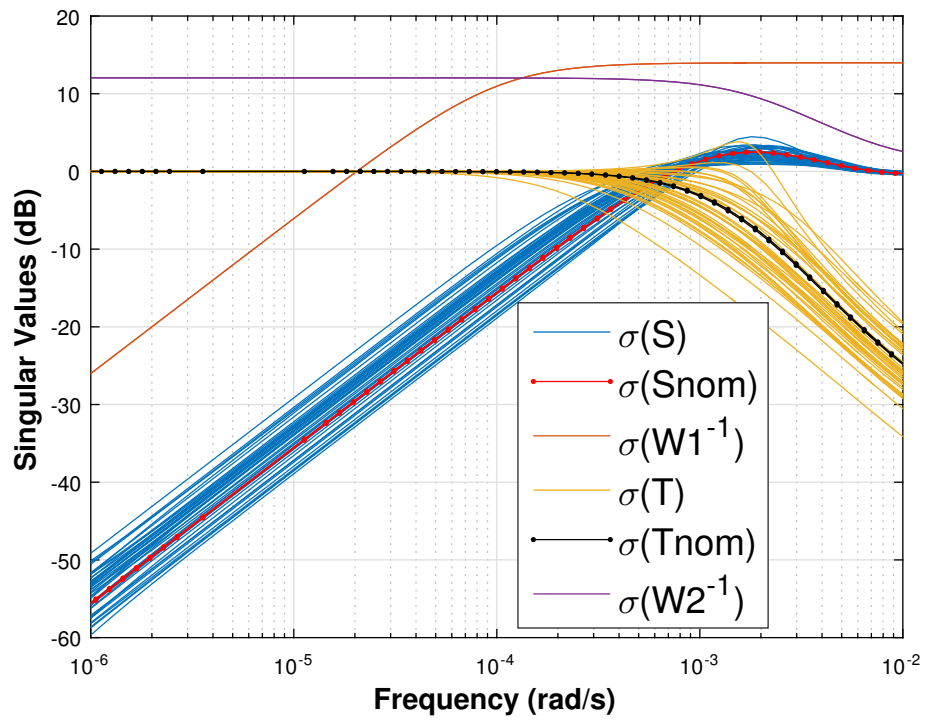


Figure 19: Robust PI Controller Loop Shapes

Chapter 5

Smith Predictor Controller

5.1 Generalized Smith Predictor

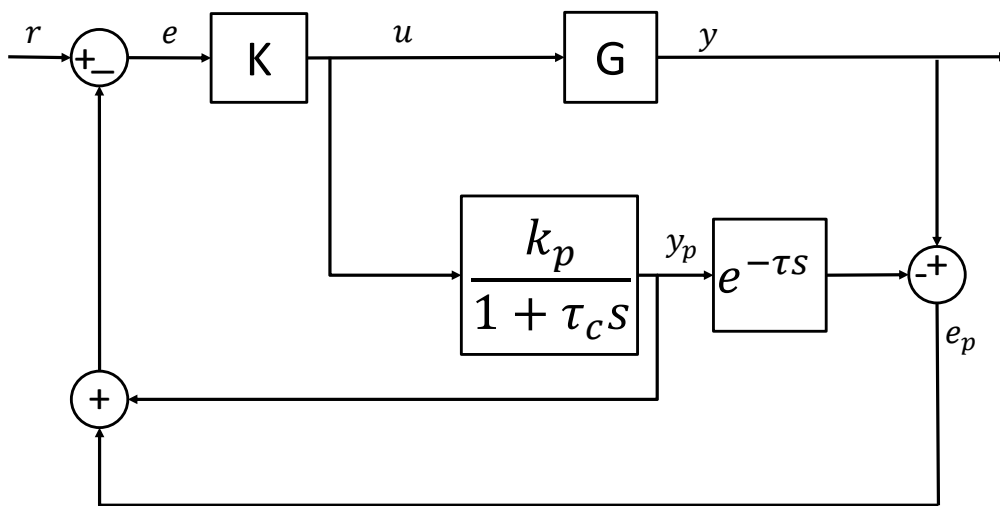


Figure 20: Structure of the Smith Predictor

In the industry, there are various types of processes such as stable process, unstable and integrating process. Apart from these processes, there is also lag dominated and delay dominated. The Smith predictor controller is generally used for delay dominated processes. For the majority of simple control loops, the amount of dead time is usually not significant when compared to the time constant. For more complicated control loops like those used for quality control, dead time can be very significant and may even be longer than the system time constant (Albertos et al.; 2015). The reasons for this may be due to analysis delay and the down stream location of sampling point for quality analyzer. It is well known that good control of processes with long time delays is difficult using PID control. The consequence is that many important control loops such as those for quality control are either poorly regulated or left on manual status, which then necessitates the frequent and close attention of the plant operators. In 1957, Smith (1957; 1959) developed the Smith predictor structure to compensate systems with time delay. This structure is a

model-based controller shown in Figure 20, which has an inner loop with a main controller that can be simply designed without the dead time. The outer loop helps in correcting the effects of load disturbances and modeling error. The principle of the Smith predictor can easily be illustrated through the control of a process with the following transfer function

$$G(s) = \frac{k_p e^{-s\tau}}{1 + s\tau_c} \quad (5.1)$$

where, k_p , τ and τ_c are the process' static gain, dead time, and time constant respectively. As seen in Figure 20, the Smith predictor is a model based controller that has two loops. The inner loop uses the process model without the dead time to predict the output y_a which is fed back to the main controller $K(s)$ to generate the appropriate control signal, u , so that the process output will track the setpoint or reference signal, r . As this loop does not contain the dead time, the controller gain can be selected to be high, in order to achieve fast and well damped setpoint responses. One of the advantages of the Smith predictor structure is that it can be easily extended from a single input-single output (SISO) system to a multiple-input multiple-output (MIMO) system (Sourdille, P. and Dwyer; 2003).

5.2 Modifications and extensions

Over the years, many modifications to the Smith predictor structure have been proposed to improve the servo response, the regulator response, or both. These modifications were accomplished to adapt the structure to stable, integrative or unstable systems. However, most of the research is about SISO systems. Only a few works, in the past several decades, are about the Multi-Input/Multi-Output (MIMO) Smith predictor (Maciejowski; 1994; Niculescu and Gu; 2004). B. Ogunnaike and W. Ray (1979), pioneers in the design problem of the multivariable Smith predictor, extended the Smith predictor to MIMO systems. In their method, the delay free part is taken to be the same as the plant with no delays. If the model is exact, the Smith predictor can remove the time delays from the closed-loop characteristic equation. In the MIMO Smith predictor of Jerome and Ray. (1986), a diagonal matrix with time delays is first determined and then a quasi delay free part is derived. The model is split into two parts, the non-delayed and delayed part.

The design is difficult to carry out because no effective rules are given for the choice of the diagonal matrix with pure time delays. To overcome these disadvantages and improve the performance of the Multivariable Smith predictor, Wang et al. (2000) proposed a new scheme. A decoupler is first introduced in this scheme. With this decoupler the multivariable Smith predictor design is simplified to multiple single loop Smith predictor designs.

5.3 MIMO Smith Predictor(Albertos et al.; 2015)

Let us consider a MIMO system with m -inputs and p -outputs represented by the transfer matrix:

$$P(s) = \begin{bmatrix} p_{11}(s) & \dots & \dots & p_{1m}(s) \\ p_{21}(s) & \dots & \dots & p_{2m}(s) \\ \dots & \dots & \dots & \dots \\ p_{p1}(s) & \dots & \dots & p_{pm}(s) \end{bmatrix} \quad (5.2)$$

This approach is partially formulated in discrete time for its convenient implementation to just the pre-filter construction shortly. This is different from the approach in Albertos et al. (2015) where the entire problem is constructed in discrete time. Converting $P(s)$ to discrete time using the Zero Order Hold (ZOH) method,

$$P(z) = \begin{bmatrix} p_{11}(z) & \dots & \dots & p_{1m}(z) \\ p_{21}(z) & \dots & \dots & p_{2m}(z) \\ \dots & \dots & \dots & \dots \\ p_{p1}(z) & \dots & \dots & p_{pm}(z) \end{bmatrix} \quad (5.3)$$

whose elements are $p_{ij}(z) = g_{ij}(z)z^{d_{ij}}$, where $g_{ij}(z)$ is the undelayed transfer function corresponding to the output-input pair ij , that is $y_i(z) = \sum_{j=1}^m g_{ij}(z)z^{d_{ij}}u_j(z)$. Some of these elements are assumed to be unstable. Thus, any estimation based on the model plant will be unstable and the SP cannot be implemented. Let us denote by $G(z)$ the rational model of the plant, with internal representation (A,B,C), that is:

$$\begin{aligned} G(z) &= C(zI - A)^{-1}B \\ &= \begin{bmatrix} c_1 \\ \vdots \\ c_m \end{bmatrix} (zI - A)^{-1} [b_1 \dots b_m] \end{aligned} \quad (5.4)$$

Defining $\Phi(z)$ as:

$$\Phi(z) = \begin{bmatrix} \phi_{11}(z) & \dots & \dots & \phi_{1m}(z) \\ \phi_{21}(z) & \dots & \dots & \phi_{2m}(z) \\ \dots & \dots & \dots & \dots \\ \phi_{p1}(z) & \dots & \dots & \phi_{pm}(z) \end{bmatrix} \quad (5.5)$$

where each element, as defined in (Albertos et al.; 2015) for the SISO case, being

$$\phi_{ij}(z) = c_i A^{-d_{ij}} \sum_{k=1}^{d_{ij}} A^{k-1} b_j z^{-k} \quad (5.6)$$

Denoting $gt_{ij}(z) = \phi_{ij}(z) + p_{ij}(z)$, thus

$$G_T(z) = \begin{bmatrix} gt_{11}(z) & \dots & \dots & gt_{1m}(z) \\ gt_{21}(z) & \dots & \dots & gt_{2m}(z) \\ \dots & \dots & \dots & \dots \\ gt_{p1}(z) & \dots & \dots & gt_{pm}(z) \end{bmatrix} \quad (5.7)$$

Now, the prefilter Φ and undelayed plant G_T are converted back to continuous time for designing continuous time stabilizing controllers. Figure 21 shows the undelayed computed plant output as $y(s) = G(s)u(s)$. The control can be designed based on this output without considering the multiple and different delays.

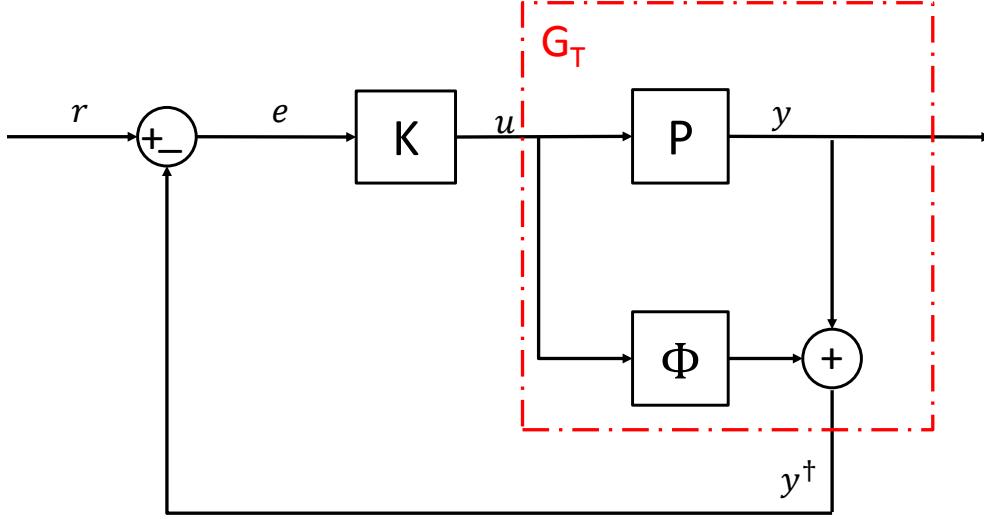


Figure 21: Unstable MIMO Stabilization

Based on the delay-free computed output $y(s)$, any classical control design technique can be used to stabilize the plant.

1. *Stabilization of delayed unstable MIMO systems:* A controller $K(s)$ can be designed to stabilize the plant, for the delay-free model $G_T(s)$ shown in Figure 21, leading to

$$y(s) = G_T K(s) [I + G_T K(s)]^{-1} r(s) \quad (5.8)$$

The output/reference response is obtained as:

$$y(s) = P(s) K(s) [I + (\Phi(s) + P(z)) K(s)]^{-1} r(s) \quad (5.9)$$

Using Equation 5.7, we get,

$$y(s) = P(s) K(s) [I + G_T(s) K(s)]^{-1} r(s) \quad (5.10)$$

Denoting the sensitivity function as

$$S_m(s) = [I + G_T(s) K(s)]^{-1} \quad (5.11)$$

we get

$$y(s) = P(s) K(s) S_m(s) r(s) = H(s) r(s) \quad (5.12)$$

For stabilization of the plant $P(s)$, the controller $K(s)$ in Figure 21 is designed such that the matrix $[I + G(z)K(s)]$ is Hurwitz. Until now, steady state behaviour has not been considered.

5.3.1 Application to Drilling Plant

The Smith predictor scheme/DTC to remove the delay associated with the input and output channels of the plant is applied to the drilling plant. The input and output delays are different for this unstable and integrating plant and hence the method detailed above and described in [Albertos et al. \(2015\)](#) can be used. However, we must also consider the dynamics associated with actuation lag which is described in Section 3.1.2. However, the lag is stable and hence, the lag can be removed out of the construction of the nominal pre-filter and is added before the dead time compensated construction. Real delays given by the Laplace transform, $e^{-s\tau}$ are used for the problem formulation instead of their Pade approximations used in previous controller designs.

Now we can describe the drilling plant as,

$$G_{wd}(s) = H_2(s)G_0(s)H_1(s)H_{lag}(s) \quad (5.13)$$

where G_0 is given by Equation (3.19) and

$$H_1(s) = e^{-\tau_1 s} \begin{bmatrix} 1 & 0 \\ 0 & 1 \end{bmatrix} \quad (5.14)$$

and

$$H_2(s) = e^{-\tau_2 s} \begin{bmatrix} 1 & 0 \\ 0 & 1 \end{bmatrix} \quad (5.15)$$

Now, the required nominal plant after the lag is given is

$$P(s) = H_2(s)G_0(s)H_1(s) \quad (5.16)$$

$$P(s) = \begin{bmatrix} \frac{ae^{-(\tau_1+\tau_2)s}}{s} & 0 \\ \frac{a\alpha_1\alpha_2e^{-(\tau_1+\tau_2)s}}{s^2} & \frac{\alpha_1e^{-(\tau_1+\tau_2)s}}{s} \end{bmatrix} \quad (5.17)$$

Now, for the application of the DTC method as described in Section 5.3, the plant in Equation (5.17) is converted to discrete time by using the *ZOH* method using the nominal parameters as described in Table 1 ([Perdikaris; 1991](#)). The sample time T_s is chosen to be 3 seconds. More about the selection of sampling time at the end of this section. The continuous domain nominal plant $P(s)$ as obtained in MATLAB is

$$P(s) = \begin{bmatrix} \frac{2.424 \times 10^{-5}e^{-540s}}{s} & 0 \\ 0 & \frac{2.424 \times 10^{-5}e^{-540s}}{s} \end{bmatrix} \quad (5.18)$$

Discrete time domain of the delay is

$$e^{-(\tau)s} \Rightarrow z^{-\tau/T_s} \quad (5.19)$$

For the different input and output delays this can be written as

$$\frac{\tau_1 + \tau_2}{T_s} = \frac{540}{3} = 180 \quad (5.20)$$

So,

$$e^{-(540)s} \Rightarrow z^{-180} \quad (5.21)$$

The rest of the function can now be transformed. Multiplying the function by an integrator,

$$\frac{2.42 \times 10^{-5}}{s} \times \frac{1}{s} = \frac{2.42 \times 10^{-5}}{s^2} \quad (5.22)$$

Applying the \mathcal{Z} transform,

$$\mathcal{Z} \left[\frac{2.42 \times 10^{-5}}{s} \right] = 2.42 \times 10^{-5} \mathcal{Z} \left[\frac{1}{s^2} \right] \quad (5.23)$$

Now,

$$\mathcal{Z} \left[\frac{1}{s^2} \right] = \frac{T_s z}{(z-1)^2} \quad (5.24)$$

The *ZOH* method equation is

$$ZOH(f(s)) = (1 - z^{-1}) \mathcal{Z} \left(\frac{1}{s} f(s) \right) \quad (5.25)$$

Multiplying Equation (5.23) by $1 - z^{-1} = \frac{z-1}{z}$ we get,

$$ZOH(f(s)) = \frac{z-1}{z} \left(\frac{T_s z}{(z-1)^2} \right) 2.42 \times 10^{-5} \quad (5.26)$$

$$ZOH(f(s)) = \frac{3.424 \times 10^{-5} \times T_s}{z-1} = \frac{7.272 \times 10^{-5}}{z-1} \quad (5.27)$$

This discretization is made possible in MATLAB using the *c2d* command and further information about the code is available in the Appendix A. Hence we get the plants $P(z)$ and $G(z)$ as follows

$$P(z) = \begin{bmatrix} \frac{7.272 \times 10^{-5}}{z-1} z^{-180} & 0 \\ 0 & \frac{7.272 \times 10^{-5}}{z-1} z^{-180} \end{bmatrix} \quad (5.28)$$

$$G(z) = \begin{bmatrix} \frac{7.272 \times 10^{-5}}{z-1} & 0 \\ 0 & \frac{7.272 \times 10^{-5}}{z-1} \end{bmatrix} \quad (5.29)$$

The plant $G(z)$ is used to compute the $G_T(z)$ and $\Phi(z)$. The state space representation of the plant $G(z)$ is computed in MATLAB and we get the following state-space matrices

$$A = \begin{bmatrix} 1 & 0 \\ 0 & 1 \end{bmatrix} \quad (5.30)$$

$$B = \begin{bmatrix} 0.0078 & 0 \\ 0 & 0.0078 \end{bmatrix} \quad (5.31)$$

$$C = \begin{bmatrix} 0.0093 & 0 \\ 0 & 0.0093 \end{bmatrix} \quad (5.32)$$

With this state-space representation we can compute the pre-filter predictor $\Phi(z)$ using the Equation (5.6), where, c_i = row vector with elements in C, b_j = column vector with elements in B, A = state space matrix, see Equation (5.30), and d_{ij} = delay in discrete time in the positions i, j .

We obtain the pre-filter matrix $\Phi(z)$ and the undelayed plant $G_T(z)$ using a MATLAB program. The pre-filter matrix is of very high order and Hankel order reduction is made to reduce the order from 180 to 32 to simplify the tuning. This is the least possible reduction which needs to be applied for the successful implementation of the MIMO Smith predictor. The pre-filter and the undelayed matrix are converted to continuous time for the design of the stabilizing controllers.

Two stabilizing controllers K are formulated for the Smith predictor configuration detailed above. The first controller which is used is a PI controller and tuned for the uncertain linear SP plant using the control system tuner application. The system connection made in Simulink is shown in Figure 22. The control tuning goals for the SP are the same as the ones used in the tuning of the robust PI controller. The controller is seen to achieve good transient response for all uncertain perturbations as seen in Figure 23 and the tuning goals are met. The eigenvalues of the nominal and selected worse case are seen in the pole-zero map in Figure 24. Both the cases are found to be stable indicating robust stability.

The second stabilizer developed for the SP is a H_∞ controller with the same weighting functions as used in H_∞ Design 2. The controller is designed for the undelayed plant G_T . The controller again obtains good step tracking in the presence of uncertain perturbations and is stable as can be seen from Figure 25. These developed control schemes will further be subjected to a structured singular value analysis for confirming robustness. The eigen values of the nominal and selected worse case are seen in the pole-zero plot in Figure 26. There is a pair of poles and zeros at the origin. Pole-zero cancellation occurs and this does not cause instability. The indicated robust stability is confirmed in Section 6.4. These developed Smith predictor control schemes are also assessed for their time response in comparison with the previously developed controllers in Section 7.

Sampling Time

A general guideline for the selection of sampling time is the Nyquist criterion. It suggests that a sufficient sample rate is $2B$ samples/second, or anything large, where B is the bandwidth of the system in Hertz. For a given sample rate f_s , perfect reconstruction is guaranteed possible for a band limit $B < f_s/2$ (Perdikaris; 1991). The sample time, T_s is given by $1/f_s$. The bandwidth of the system for the smith predictor is $3.46e - 5/(2\pi i)$ hence from the Nyquist criteria the maximum sampling time is 90797 seconds for the Smith predictor. The first thing to be taken in consideration to choose the sample time is the effort of the software in computing the discrete systems and variables, in this sense

it is better to choose a greater value of sample time, for this implies working with a less degree polynomial. If the sample time is chosen to be very big then the discrete system is not able to represent the continuous time system due to a large sampling signal. This means that the maximum sample time that represent a good resolution of the continuous system should be selected. By running the ZOH transformation of the system with some sample times, using trial and error the sampling time T_s for this system is chosen as 3 seconds. This allows faster simulation time and with a good quality signal.

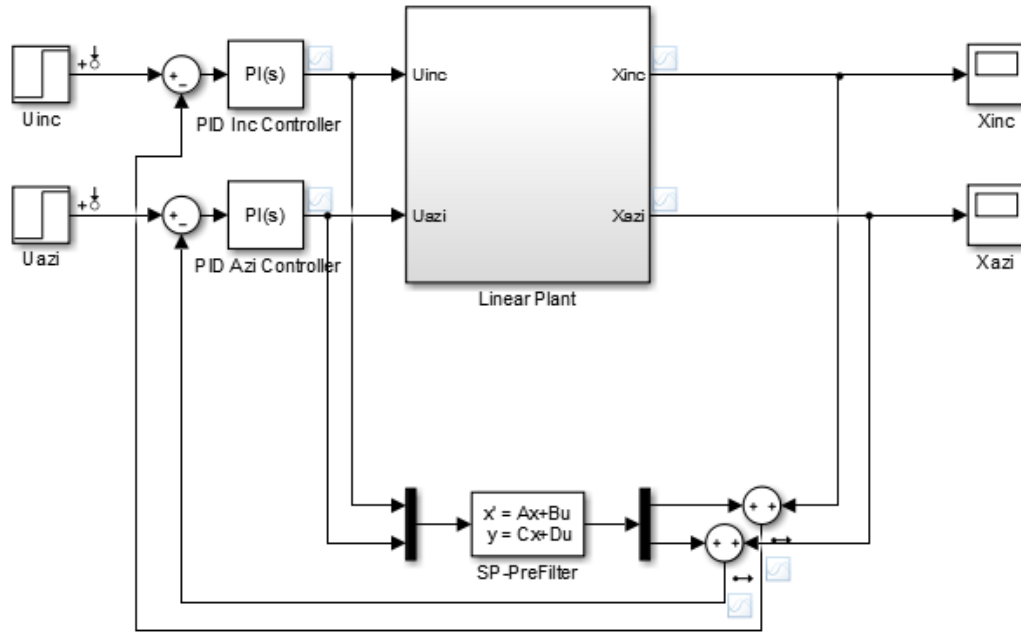


Figure 22: PI-SP Closed Loop Simulink Interconnection

5.4 Conclusion

In this chapter to accommodate the effect of delay in the drilling plant a Smith predictor inspired MIMO dead time compensator has been designed. Two stabilizing controllers, PI and H have been designed for the DTC predictor scheme and successfully ameliorate the effect of the delay associated with the plant. The PI-SP design is the best design as it achieves the best combination between robustness and time response of closed loop. Both the SP designs are better than the previously designed controllers.

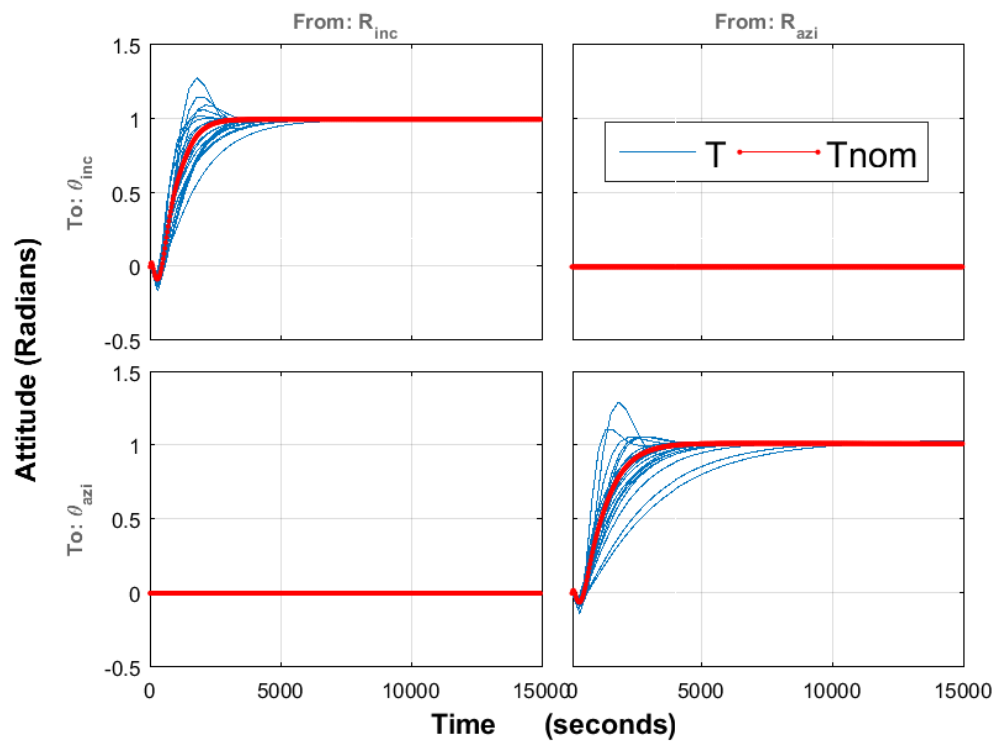


Figure 23: PI-SP Closed Loop Transient Responses

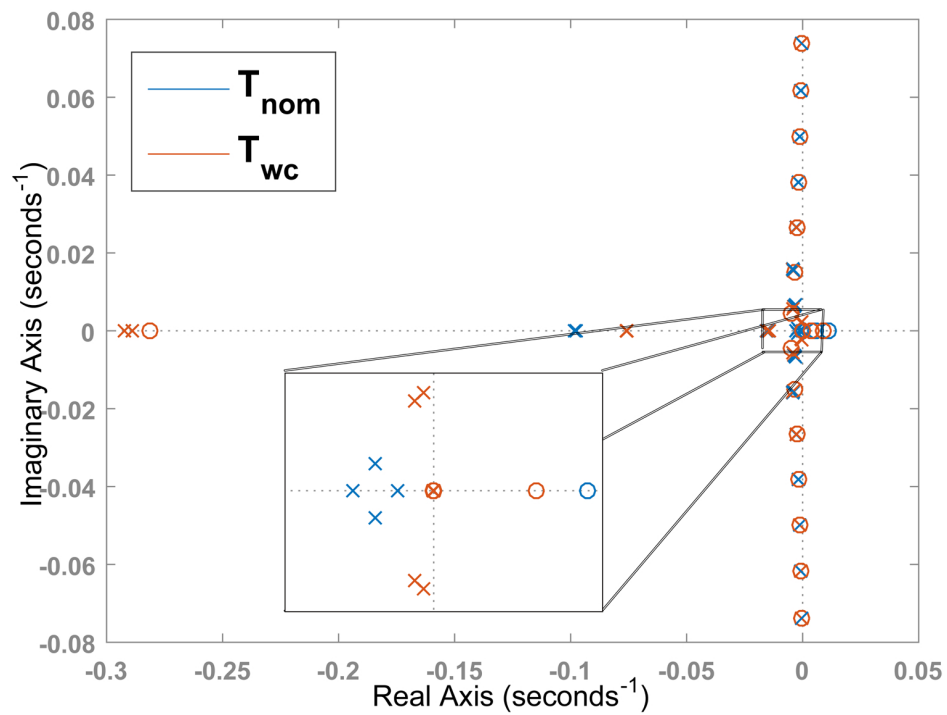
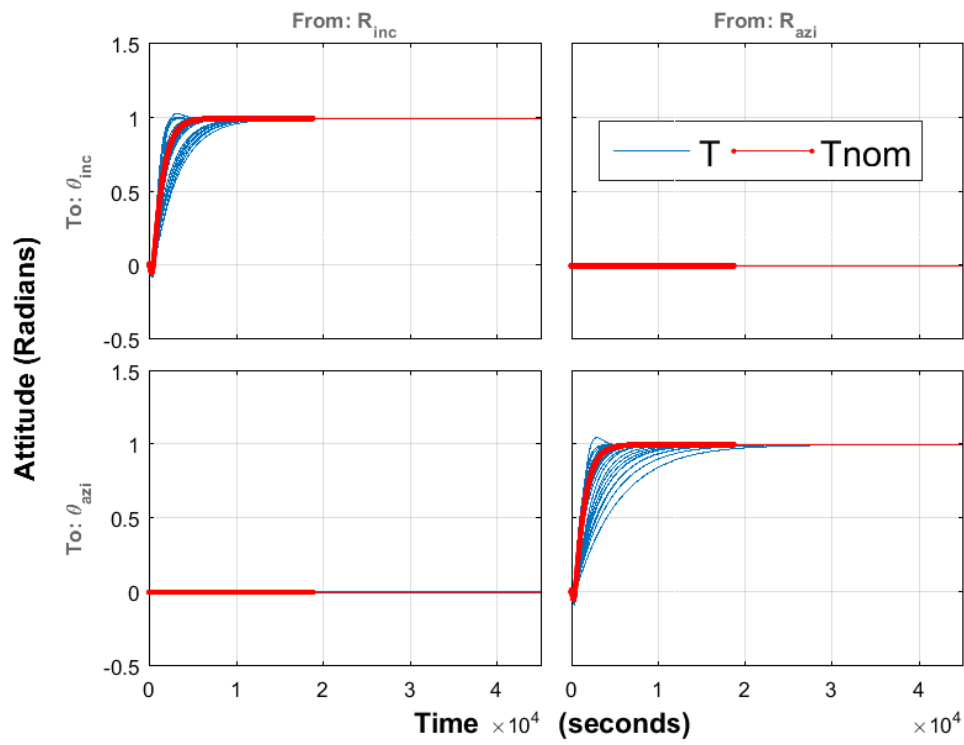
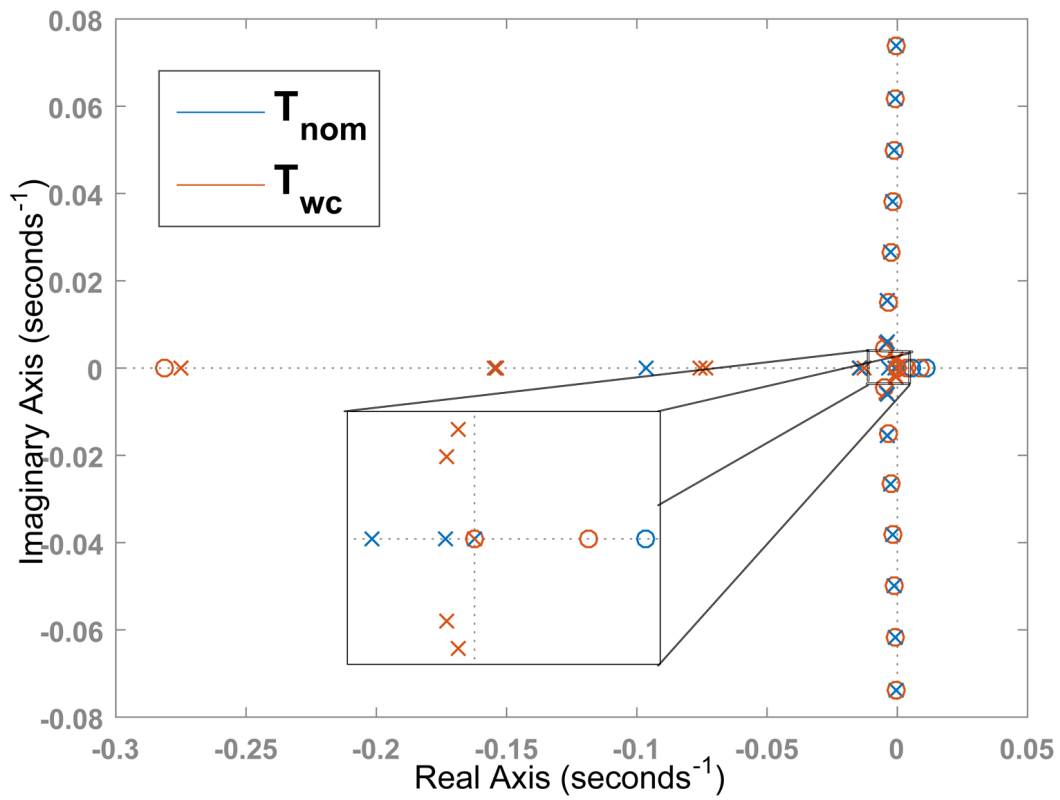


Figure 24: PI-SP Pole Zero Plot

Figure 25: H_∞ -SP Closed Loop Transient ResponsesFigure 26: H_∞ -SP Pole Zero Plot

Chapter 6

Controller Robustness Analysis

6.1 Theoretical Background: Measures of Robustness

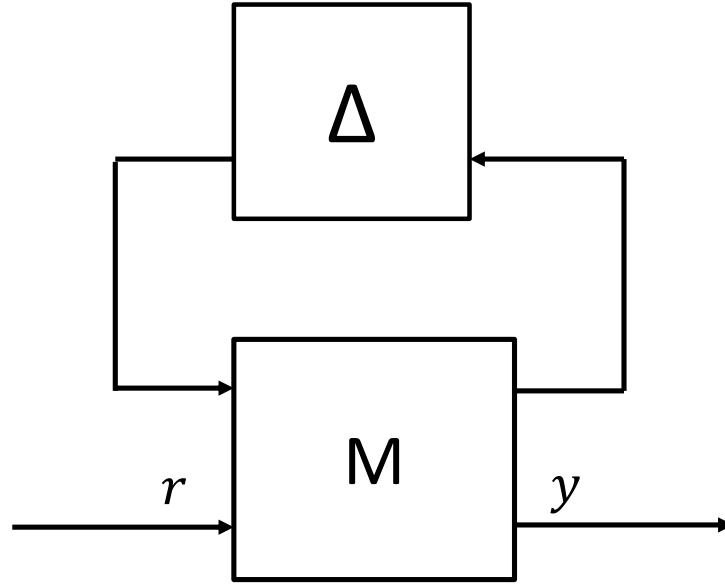
Feedback gains have been designed using the three types of controllers previously discussed to ensure nominal stability and performance at a certain operating point condition. It is also essential to assess the formulated gains, at each operating point to confirm robust stability and performance. The corresponding theoretical background for this frequency domain analysis is presented and applied.

6.1.1 Uncertainty

Uncertainties can be described as unstructured and structured. Unstructured uncertainty usually represents the unmodelled dynamics of the systems ([Gu et al.; 2005](#)) and usually represent high-frequency range dynamics that unmodelled delays and/or other nonlinearities introduce. *Parametric uncertainty* arises from the inaccurately known parameters of an accurately modeled plant. Variations in the gain or time-constant of the plant are also considered as parametric uncertainty. Parametric uncertainties are usually avoided for it takes huge effort to model them. It is an over accurate and detailed description of a possibly lesser known physical system. Real perturbations which tend to be more difficult mathematically are required for controller synthesis ([Skogestad and Postlethwaite; 2001](#)). These affect low-frequency range dynamics. Parametric uncertainties are sometimes known as structured uncertainties, since all the perturbations can be lumped into a single-block diagonal matrix. Parametric uncertainties can further be assumed to be additive or multiplicative. However, both these formulations can be accommodated into a structured set. For further information refer to [Skogestad and Postlethwaite \(2001\)](#).

6.1.2 Linear Fractional Transformation

Linear fractional transformations (LFT) can be accurately used to represent uncertainty in matrices and systems ([Balas et al.; 1991](#)). LFT's dictate how the uncertainty affects the input/output relationship of a certain control system.

Figure 27: Standard $M - \Delta$ configuration

The partitioned interconnection transfer function matrix M in Figure 27 is

$$M = \begin{bmatrix} M_{11} & M_{12} \\ M_{21} & M_{22} \end{bmatrix} \quad (6.1)$$

Here, only M_{11} corresponds to the dimensions of Δ . It can be easily derived that

$$z = [M_{22} + M_{21}\Delta(I - M_{11}\Delta)^{-1}M_{12}]w \quad (6.2)$$

Now if $(I - M_{11}\Delta)$ is invertible, we can define

$$F(M, \Delta) = M_{22} + M_{21}\Delta(I - M_{11}\Delta)^{-1}M_{12} \quad (6.3)$$

$F_U(M, \Delta)$ is known as an upper linear fractional transformation of M and Δ as the upper loop of M is closed by the block Δ . Similarly, there are lower LFT's which are usually used to represent the incorporation of a controller K into the system.

6.1.3 Structured Singular Value

The structured singular value, which is usually denoted by μ is a function which provides a generalization of the singular value, $\bar{\sigma}$, and the spectral radius, ρ . μ is used to get necessary and sufficient conditions for robust stability and robust performance. The structured singular value defined in Skogestad and Postlethwaite (2001) is the following.

1. *Definition: Structured Singular Value.*

Let M be a given complex matrix and let $\Delta = \text{diag}(\Delta_i)$ denote the set of complex

matrices with $\bar{\sigma}(\Delta) \leq 1$ and with a given block-diagonal structure (in which some of the blocks may be repeated and may be real or complex). The real non-negative function $\mu(M)$, called structure singular value, is defined by,

$$\mu(M) \triangleq \frac{1}{\min k_m \mid \det(I - k_m M \Delta) = 0 \forall \Delta, \bar{\sigma}(\Delta) \leq 1} \quad (6.4)$$

If no such structure Δ exists then $\mu(M) = 0$. A value of $\mu = 1$ means that there exists a perturbation with $\bar{\sigma}(\Delta) = 1$ which is just large enough to make $I - M\Delta$ singular. A large value of μ is bad as it means that small perturbations make $I - M\Delta$ singular, whereas a smaller value of μ is good.

6.1.4 Nominal Performance

H_∞ norm of the system transfer function is a well known measure for indicating system performance. The H_∞ norm of the nominal closed loop system, N , as shown in Figure 28 is the supremum of the maximum singular value of the frequency response of the system (Scherer and Weiland; 2005). Hence, the nominal performance criteria is given as

$$\|N\|_\infty = \sup_{\omega \in R} \sigma_{max}(T(j\omega)) \quad (6.5)$$

6.1.5 Robust Stability

For the $M\Delta$ structure described in Section (6.1.2), the robust stability condition is described as in Skogestad and Postlethwaite (2001) where the loop transfer function comprises of two parts. M is the nominal part which is separated from Δ , the block diagonal perturbations. In the general case of structured uncertainty we can use the structured singular value for studying robust stability. In the computation of the structured singular value, the uncertainty Δ is scaled by a k_m , the factor by which the system is robustly stable. We seek the smallest k_m which yields borderline instability and is given by,

$$\det(I - k_m M \Delta) = 0 \quad (6.6)$$

The definition of μ given in Equation (6.4), we get $k_m = \frac{1}{\mu(M)}$ gives the following condition for robust stability

Theorem: RS for block-diagonal perturbations (real or complex).

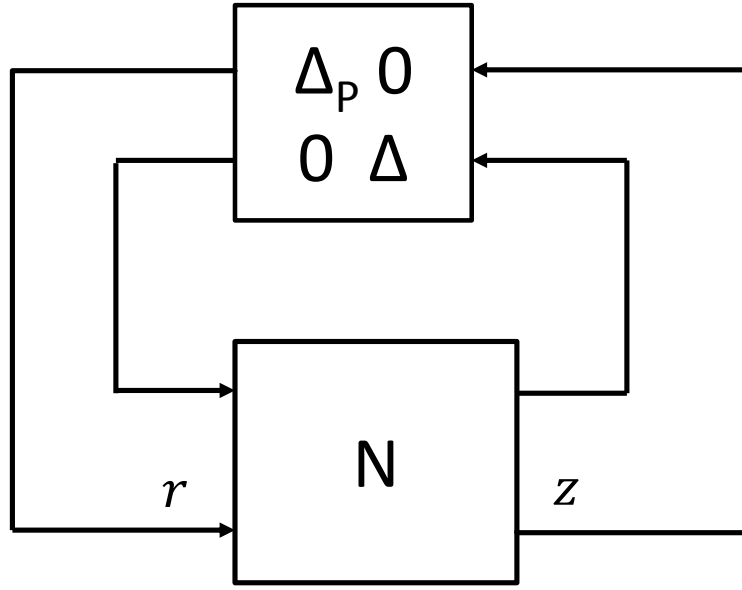
Assume that the nominal system M and the perturbations Δ are stable. The $M\Delta$ system in figure xx is stable for all perturbations with $\bar{\sigma}(\Delta) \leq 1, \forall \omega$, if and only if

$$\mu(M(j\omega)) < 1, \forall \omega \quad (6.7)$$

Equation (6.7) can be re written as

$$RS \Leftrightarrow \mu(M(j\omega))\bar{\sigma}(\Delta(j\omega)) < 1, \forall \omega \quad (6.8)$$

This can be interpreted as a generalized small gain theorem, which takes into account the structure of Δ .

Figure 28: Robust Stability $N\Delta$ structure

6.1.6 Robust Performance

Robust performance (RP) implies that the performance objective is satisfied for all possible plants in the uncertainty set, inclusive of the worst-case plant. The RP - condition is identical to a RS condition with an additional perturbation block, Δ_P . The block Δ_P is a full matrix and is a fictitious uncertainty block representing the H_∞ performance specification.

The uncertain perturbations are pulled out similar to the RS condition into the $N\Delta$ form of figure. The RP requirement in term of μ can be exactly computed as in the following theorem of *Robust Performance*.

Rearrange the uncertain system into the $N\Delta$ structure of Figure 28. Assume nominal stability such that N is internally stable. Then

$$RP \Leftrightarrow \|F\| = \|F_u(N, \Delta)\|_\infty < 1, \forall \|\Delta\|_\infty \leq 1 \quad (6.9)$$

The condition in Equation (6.9) can now be generalized as

$$RP \Leftrightarrow \mu_{\hat{\Delta}}(N(j\omega)) < 1, \forall \omega \quad (6.10)$$

where μ is computed with respect to the structure

$$\hat{\Delta} = \begin{bmatrix} \Delta & 0 \\ 0 & \Delta_P \end{bmatrix} \quad (6.11)$$

and Δ_P is the full complex perturbation matrix with the same dimensions as F^T . The definition of robust performance is as obtained in Skogestad and Postlethwaite (2001).

6.2 Plant Specific Uncertainty

Now the uncertainties are defined for the plant model, G_0 , given by Equation (3.19). The parameter V_{rop} is directly related to the weight on bit applied by the driller in the loop and it is also affected by the geological aspects of the reservoir being drilled. Similarly, the parameter K_{dls} is subject to variation as it can only be estimated offline and requires previous experience related to the drill bit and the location where drilling is being carried out (Panchal et al.; 2010). The same assumption as in Panchal et al. (2010) is used where the parametric uncertainty on V_{rop} is 50% and K_{dls} is 10%.

The $\csc(\alpha_1)$ and $\cot(\alpha_2)$ parameters are evaluated at a nominal inclination angle of $\pi/2$ radians with a ± 0.0175 perturbation on α_2 and ± 1 perturbation on α_1 , which allows to calculate the nominal values for the \csc and \cot parameters.

The uncertainties associated with input delay τ_1 are assumed to be 25% for a nominal value equal to half of the drilling cycle time. More about the drilling cycle is explained in Section 8.1. The measurement delay τ_2 for a nominal value of 360 seconds as described in section is assumed to have a delay of 50%. The uncertainty on the nominal actuation lag, τ_D is assumed to be 10%.

6.2.1 Uncertainty Modelling

The actual plant is modeled taking into account the parametric uncertainties and the unmodeled dynamics of the lags and delays. This is a requirement for structured singular value analysis. The MATLAB function *ureal* facilitates the creation of real uncertain system parameters. The uncertainty can be expressed as a percentage variation or as a range. No matter how the uncertainty is specified it can be pulled out of the uncertain plant, G_{unc} to get the form

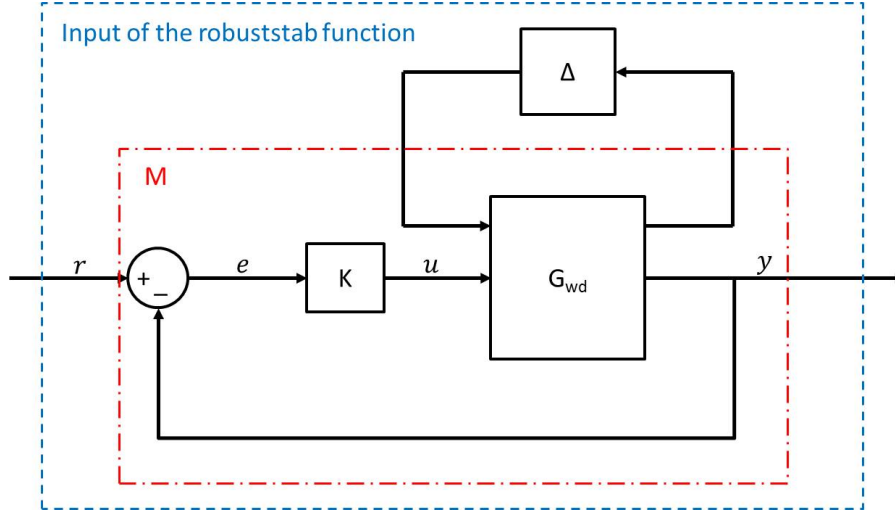
$$G_{unc}(s) = G_{wd}(s) + \Delta(s) \quad (6.12)$$

where, $G_{wd}(s)$ is the nominal plant model and $\Delta(s)$ is the structured combined uncertainty. This is facilitated within the *robustperf* command. The uncertain system parameters are as described in Table 3. The closed loop is constructed using the MATLAB function *sysic* which facilitates uncertain closed loop construction. There are 7 uncertain parameters in total, V_{rop} , K_{dls} , τ_1 , τ_2 , τ_d , α_1 and α_2 .

6.3 Robustness Analysis Plant interconnection

6.3.1 Robust Stability

The closed-loop system achieves robust stability if the closed loop system is internally stable for each of the perturbed plant dynamics given by G_{unc} . The structured singular value is computed using the MATLAB command *robuststab*. The command gives a detailed report about the robust stability margins, destabilizing frequencies and also makes the structured singular value analysis. The uncertainty block pulled out has dimension 19×19 as the uncertainties in the parameters V_{rop} , K_{dls} , τ_1 and τ_2 are repeated four times each. The closed loop $M\Delta$ structure for robust stability is made as in Figure 29. The

Figure 29: Robust Stability $M\Delta$ Structure

desired frequency range of interest for the analysis is given by $[\omega_l \omega_u]$. These frequencies are defined as $\omega_l = 1.0 \times 10^{-6}$ rad/s and $\omega_u = 1.0 \times 10^{-2}$. The $M\Delta$ structure for the SP is shown in Figure 30.

6.3.2 Robust Performance

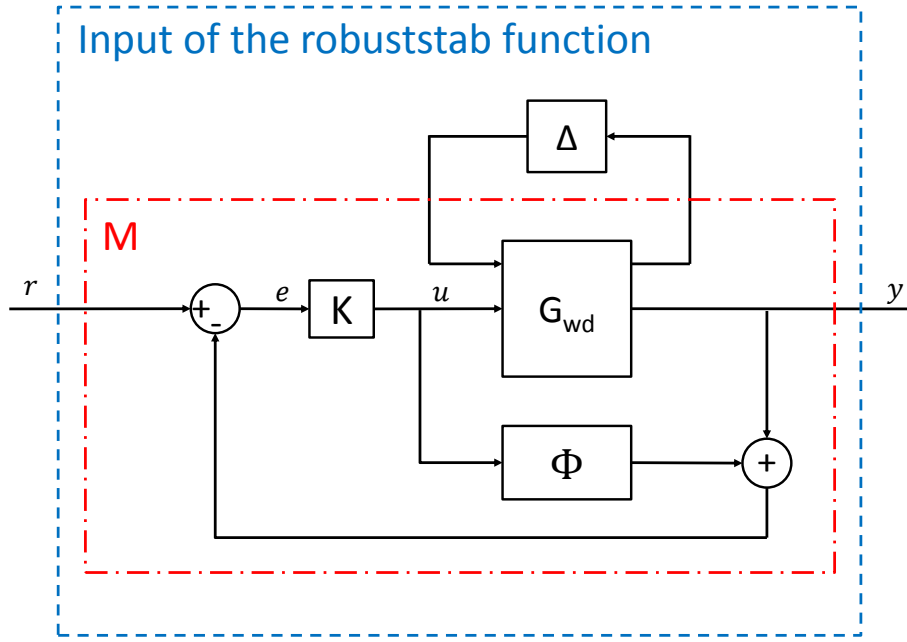
If robust stability is achieved, a robust performance assessment can be made as detailed in Section 6.1.6. The closed loop interconnection for robust stability is shown in Figure 31 for the PI and H_∞ controllers and in Figure 32. The sensitivity weight is augmented in the plant to get the required $N\Delta$ structure. The fictitious uncertainty is a 2×2 complex uncertainty matrix. Robust performance analysis is also subject to the same frequency range of interest. The entire mathematical formulation is facilitated within the *robustperf* command in MATLAB.

6.4 μ -analysis Results

6.4.1 PI Controllers

The PI controller design using the pole placement technique is found to be nominally stable subject to its eigenvalue analysis and hence can be analyzed using μ as detailed in Sections 6.1.3, 6.1.5 and 6.1.6. MATLAB generates a report which indicates the robust stability and performance characteristics of the closed loop system for this design, shown in Appendix B.

The results of the frequency domain robustness analysis are shown in Figure 33, which shows the nominal stability, $\mu(M(j\omega))$ and $\mu(N(j\omega))$. It can be seen that the controller does not meet the RS and RP requirements defined by Equations (6.9) and (6.9) over the frequency range of interest $\omega \in [\omega_n, \omega_l]$. The nominal performance requirement is met. The controller has high peaks closed to the the frequency 10^{-3} for both RS and RP.

Figure 30: Robust Stability $M\Delta$ Structure-SP

The robust PI controller designed for an uncertain plant in Section (4.2.2) is analysed using μ . The following report indicating the RS, NP, RP as generated in MATLAB is shown as an example. Similar reports are obtained for robust stability and performance for all the controllers and are shown in the Appendix (C). The results of the μ analysis are shown in Figure 35. The RS, NP and RP criteria are seen to be met comfortably for the robust PI controller.

6.4.2 H_∞ Controllers

The H_∞ design 1 as formulated in Section 4.1.2 is passed through a SSV analysis which allows to discuss the designed controllers nominal performance, robust stability and robust performance specifications as addressed in Section 6.3. The frequency plots of the SSV are shown in Figure 36.

The closed loop system with the H_∞ Design 1 does not achieve robust stability or robust performance, the maximum value of μ exceeds 1 at frequency close to 10^{-3} radians/second indicating instability closer to the upper frequency limit. It follows from the report that all the uncertain parameters practically do not affect the robust stability margins.

The Design formulated in Section 4.1.3 is analyzed here for robustness. Figure 37 indicates that the designed H_∞ controller meets the NP, RS, RP criteria.

The closed loop system with the H_∞ Design 2 is a better design since it accommodates the presence of the inherent lag and delays associated with the drill's dynamics. As indicated above, the closed loop system for the proposed controller meets all the requirements and is robustly stable and achieves robust performance for the frequency range of interest.

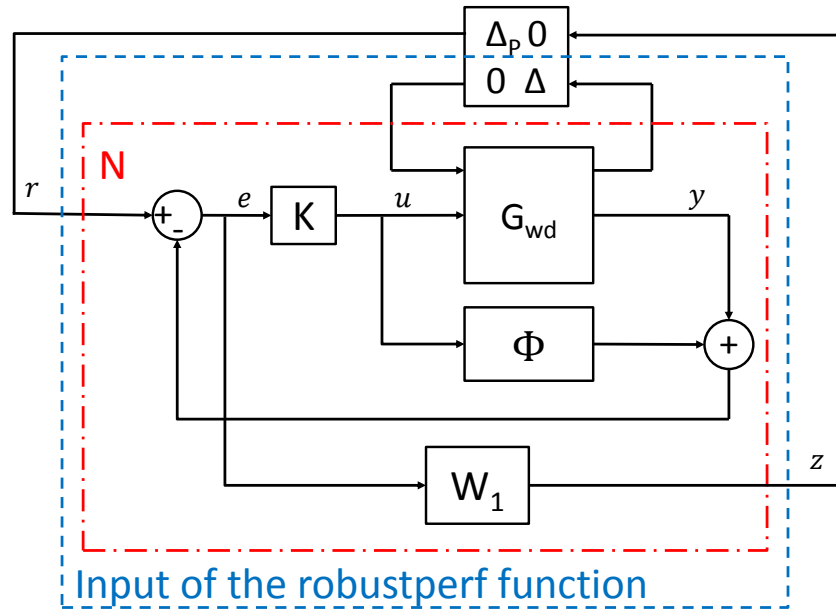
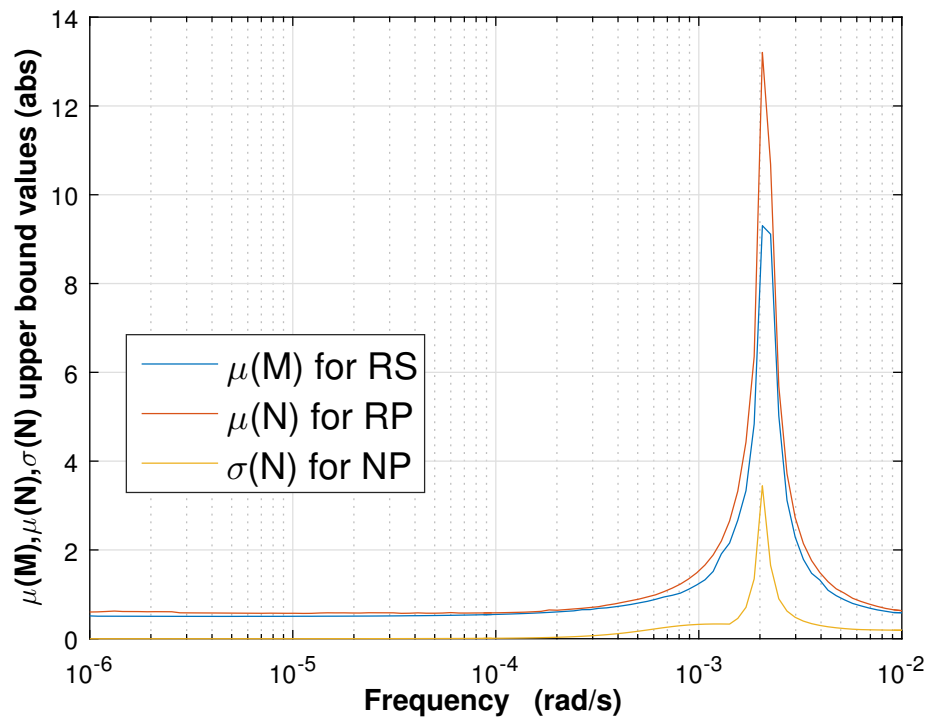
Figure 32: Robust Performance $N\Delta$ Structure-SP

Figure 33: NP,RS,RP for Pole Placement Design

```

stabReportD2 =
Assuming nominal UFRD system is stable...
Uncertain system is robustly stable to modeled uncertainty.
-- It can tolerate up to 167% of the modeled uncertainty.
-- A destabilizing combination of 180% of the modeled uncertainty was found.
-- This combination causes an instability at 0.00187 rad/seconds.
-- Sensitivity with respect to the uncertain elements are:
  'Kdls_un' is 16%. Increasing 'Kdls_un' by 25% leads to a 4% decrease in the margin.
  'Vrop_un' is 92%. Increasing 'Vrop_un' by 25% leads to a 23% decrease in the margin.
  'alpha1_un' is 18%. Increasing 'alpha1_un' by 25% leads to a 5% decrease in the margin.
  'alpha2_un' is 16%. Increasing 'alpha2_un' by 25% leads to a 4% decrease in the margin.
  't1_un' is 18%. Increasing 't1_un' by 25% leads to a 5% decrease in the margin.
  't2_un' is 15%. Increasing 't2_un' by 25% leads to a 4% decrease in the margin.
  'td_un' is 13%. Increasing 'td_un' by 25% leads to a 3% decrease in the margin.

```

Figure 34: Robust Performance Report

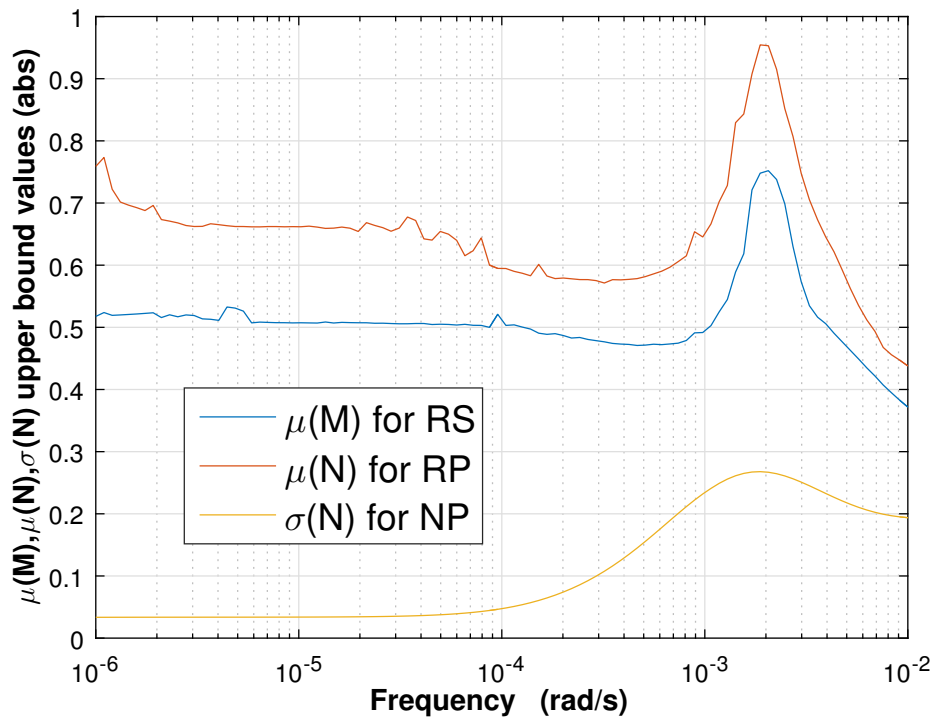
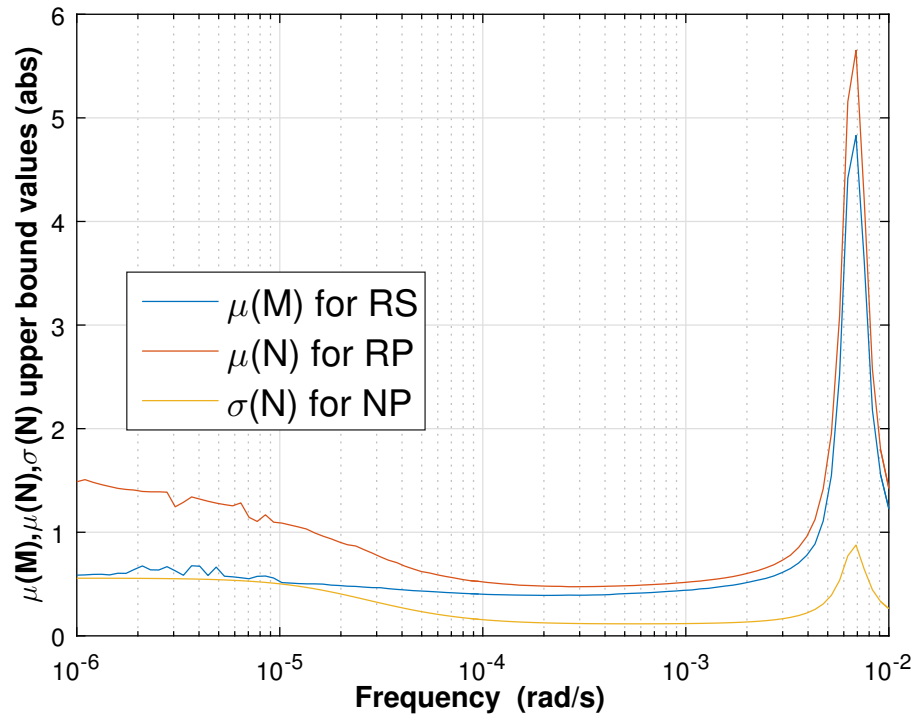
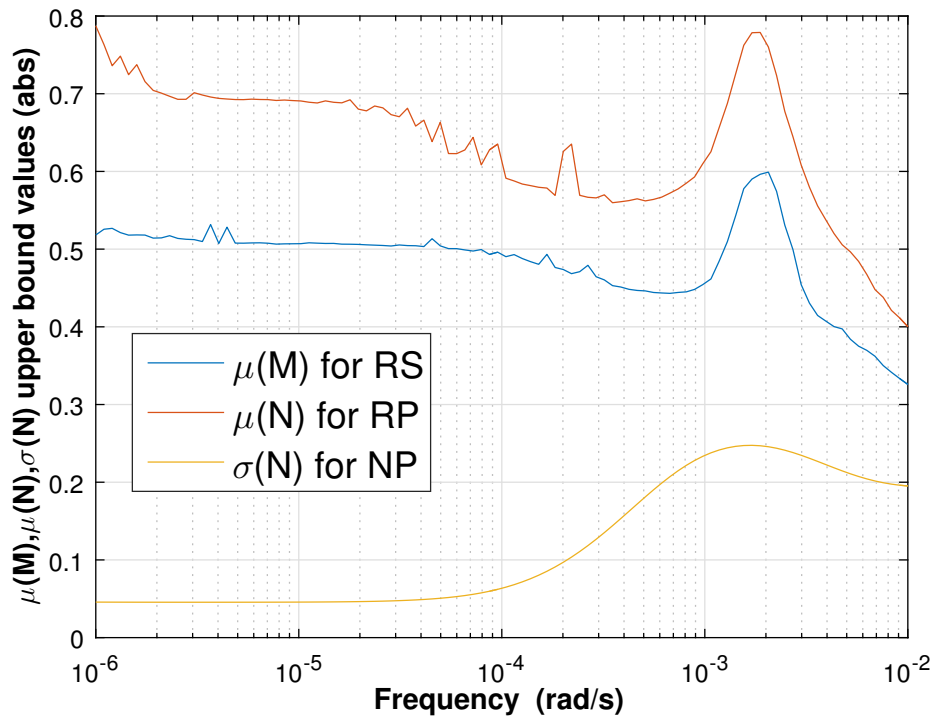
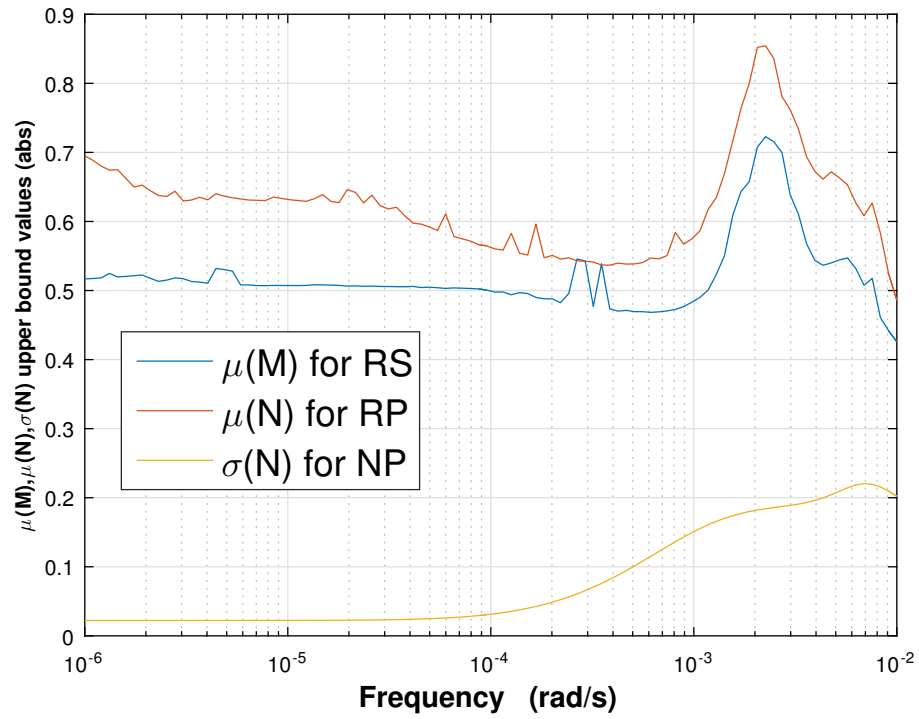
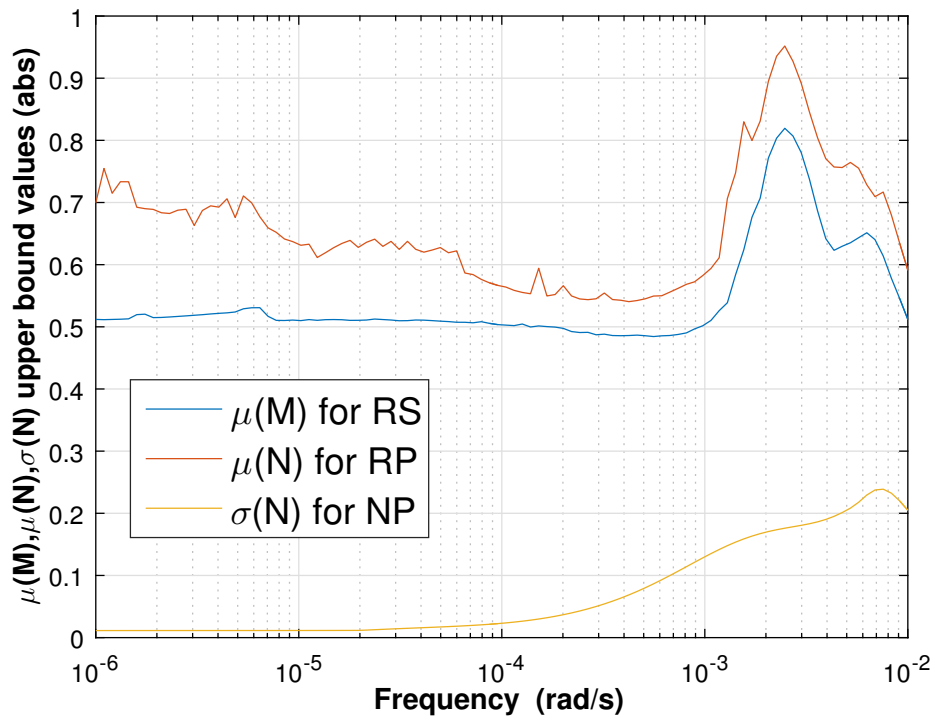


Figure 35: NP,RS,RP for Robust PI Controller Design

Figure 36: NP,RS,RP for H_∞ Design 1Figure 37: NP,RS,RP for H_∞ Design 2

Figure 38: NP,RS,RP for $H_\infty - SP$ DesignFigure 39: NP,RS,RP for $PI - SP$ Design

Chapter 7

Comparison of Designed Controllers

7.1 Transient Response Comparison

In this section the transient response of the designed controllers in terms of the nominal and worst case performance is considered. The worst case is obtained from the [MATLAB \(2015\)](#) function *wcgain* which yields the frequency dependent curve of the maximum gain across the frequency range. From this, the upper bound gain value for the specific uncertainty combination beyond which the system is unstable is obtained. Instead of comparing for each perturbed plant, we consider the worst case for which the system achieves the fastest transient response. Figure 40 illustrates the transient responses of the H_∞ design 2 and the robust PI transient response. It can be seen that the Robust PI controller is the quickest for the worst case. Both controllers achieve good nominal response, however, despite being quicker, the worst case response is seen to be oscillatory and the settling time is larger than that of the nominal case as indicated in the azimuth channel. The delay is made with a first order Pade approximant which also explains the oscillatory nature of the transient response and explains the presence of the undershoot.

Figure 41 compares the closed loop transient response of the two formulated Smith predictor controllers. Similar characteristics are applicable to the explanation of the oscillatory system dynamics and slow settling time of the worst case transient response. The robust PI-SP controller has a faster response than the H_∞ -SP controller for both the nominal and the worst case.

Similarly, the transient response comparison of the robust PI design and the PI-SP is made and showcases the better design of the SP scheme. The SP configuration is known to ameliorate the effect of the delay and this is noticed from this comparison. Similar characteristics pertaining to the oscillatory response and slow settling time of the perturbed worst case are observed in all the designs. Figure 42 illustrates this example.

Lastly, the transient response of the H_∞ design 2 and H_∞ -SP is compared. Figure 43 indicates the effectiveness of the smith predictor controller scheme. The transient response of both the nominal and the worst case is quicker for the H_∞ -SP. The SP is known to be able to remove the effect of the delay and this is confirmed by this comparison.

Table (5) compares the maximum rise time for the different controllers for the nominal and worst case closed loop systems. The two SP control configurations achieve a quicker rise time for the indicated channel as can be seen in the figures and respond faster than the other controller designs.

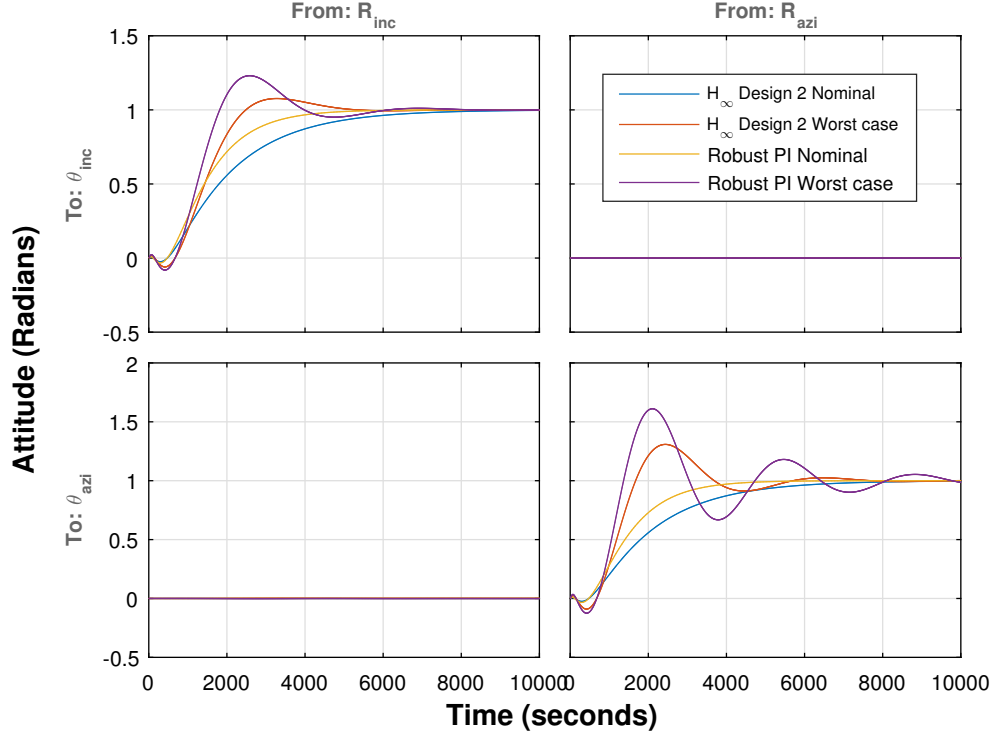


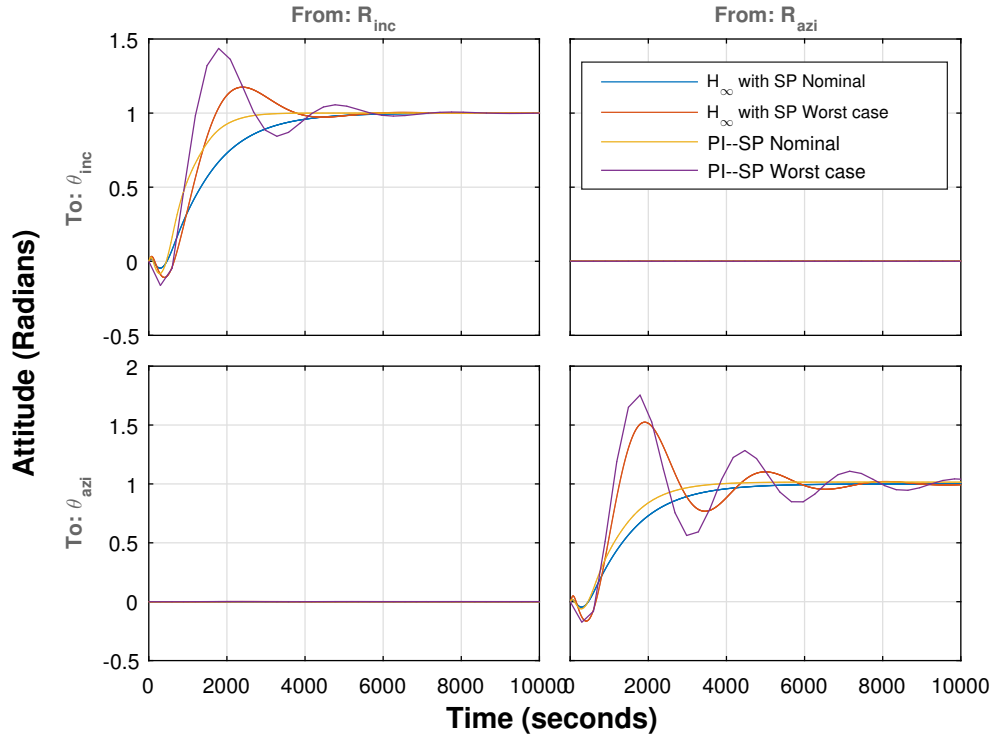
Figure 40: H_∞ Design 2 vs Robust PI Transient Response

Design	Max. Nominal Rise Time(s)		Max. Worst Case Rise Time(s)	
	θ_{inc}	θ_{azi}	θ_{inc}	θ_{azi}
H_∞ Design 1	8.38×10^4	4.39×10^4	-	-
H_∞ Design 2	4.41×10^3	4.41×10^3	2.15×10^3	1.57×10^3
PI Pole Placement	1.68×10^3	945	-	-
Robust PI	2.99×10^3	2.91×10^3	1.68×10^3	1.3×10^3
H_∞ -SP	3.06×10^3	3.06×10^3	1.57×10^3	1.2×10^3
PI-SP	1.86×10^3	2.33×10^3	1.15×10^3	1.07×10^3

Table 5: Rise Time Comparison

7.2 Nominal and Robustness Comparison

All the designed controllers are seen to be nominally stable as previously indicated by their step response and eigenvalue assessment. However, the PI pole placement controller is almost nominally unstable. It is found that the main reason for this is the presence of the large output delay and also the fact that the controller design excludes the presence of the dynamics associated with the lag and delay.

Figure 41: PI-SP vs H_∞ -SP Transient Response

A comparison of the results of nominal performance, robust stability and robust performance analysis obtained in Section 6.4 is made. The result of the nominal performance analysis is given in Figure 44, which shows $\mu(N(j\omega))$ for the 6 formulated control schemes for the nominal plants. All the controllers achieve nominal performance except for the PI Pole placement design which is seen to have bad performance margins at frequencies close to 10^{-3} radians/second for the frequency range of interest $\omega \in [\omega_l, \omega_u]$ as previously described. The Robust PI with SP design is seen to have the best nominal performance margins.

Similarly, a comparative result of the robust stability analysis obtained in Section 6.4 is presented. The robust stability results for all the controllers is given in Figure 45, which shows $\mu(M(j\omega))$ for all the controllers. It can be seen that the PI Pole Placement design and H_∞ design 1 do not achieve robust stability for the given frequency range. All the other controllers easily meet the robust stability criteria. The robust stability margins of these controllers are nearly similar.

Lastly, the results of robust performance analysis are given in Figure 46, which shows $\mu(N(j\omega))$ for all the designed controllers. The H_∞ Design 2, robust PI, PI-SP and H_∞ -SP controllers all satisfy the robust performance criteria. All these designs are seen to have similar performance margins. However, the two designs formulated for the nominal plants do not meet this requirement.

It can be seen for the plant of interest that it is essential to include the presence of the various parametric uncertainties in the design of the controllers. Large parametric variations associated with the system parameters leads to a bad design when the un-

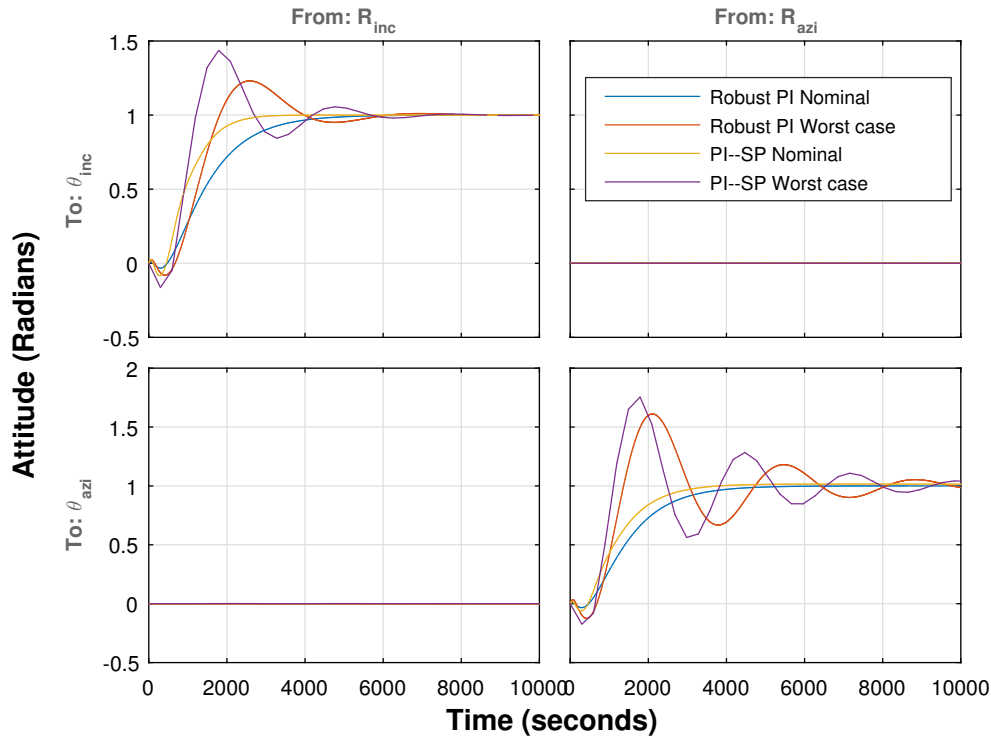


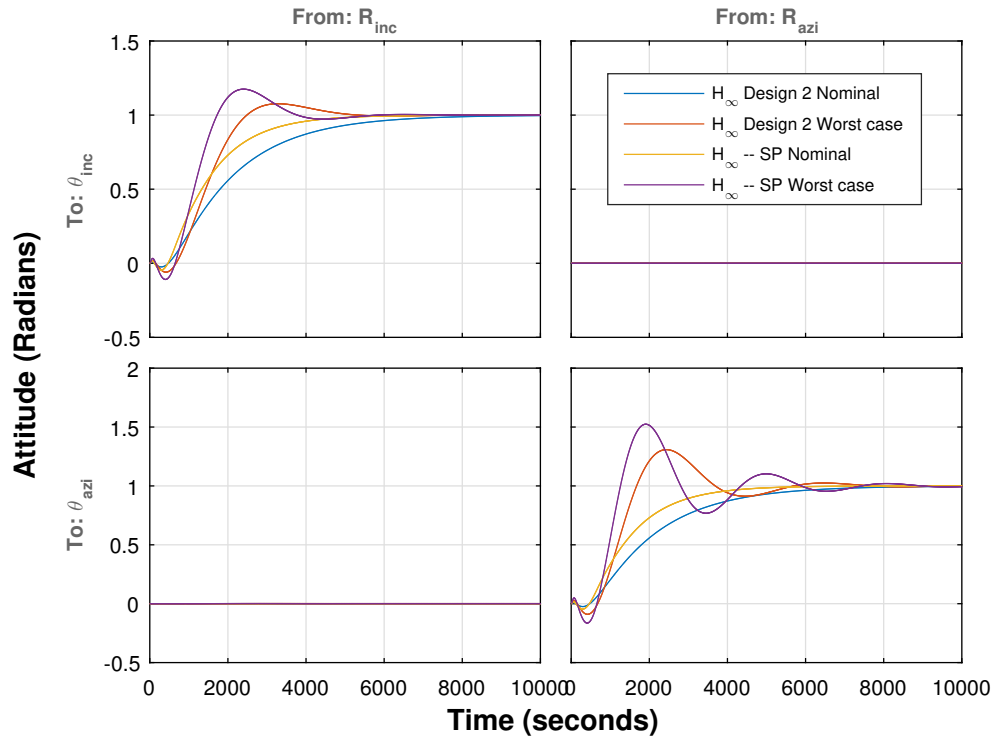
Figure 42: PI vs PI-SP Transient Response

modelled dynamics and perturbations are included. It is also seen that the controllers, when designed for the plant model augmented with the lags and delays, allow better control of the drilling dynamics.

Table 7.2 shows the trade-off in performance and stability of the designed controller in terms of performance margins and uncertainty tolerance for stability in terms of percentage. It can be seen that the H_∞ Design 2 is the best in terms of stability and performance margins. However, both the SP controllers are also seen to have good robustness margins and also have better transient responses as seen earlier. The H_∞ design 1 and PI pole placement controllers are seen to have degraded performance and stability margins which is indicated by their μ analysis. More information about the stability and performance trade offs of the designed controllers can be seen in Appendix B.

Design	Performance Trade off (%)	Stability Tolerance (%)
H_∞ Design 1	17.7	20.7
H_∞ Design 2	127	167
PI Pole Placement	7.57	10.7
Robust PI	105	133
H_∞ -SP	117	151
PI-SP	105	122

Table 6: Robust Performance and Robust Stability Trade-off

Figure 43: H_∞ vs H_∞ -SP Transient Response

7.3 Conclusion

In this chapter a comparative analysis of the system response and robustness criteria helped indicate the better controller designs when the lag and delays are included. The transient response analysis confirms the application of the SP to reduce the effect of the time delay. The robustness comparison indicates that the PI-SP controllers achieves the best robust stability and robust performance margins.

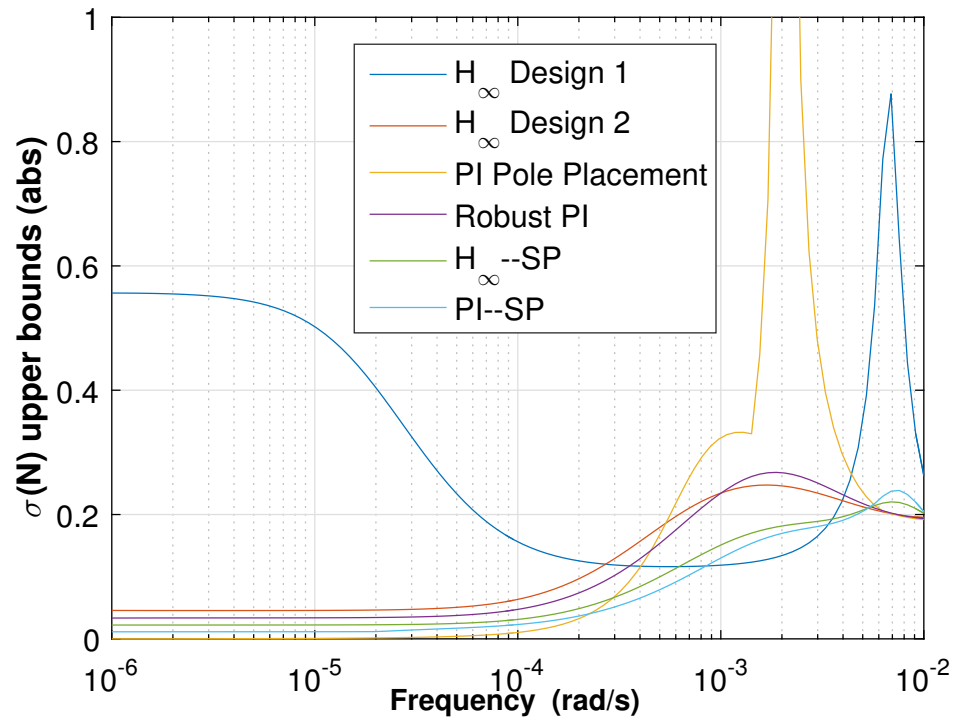
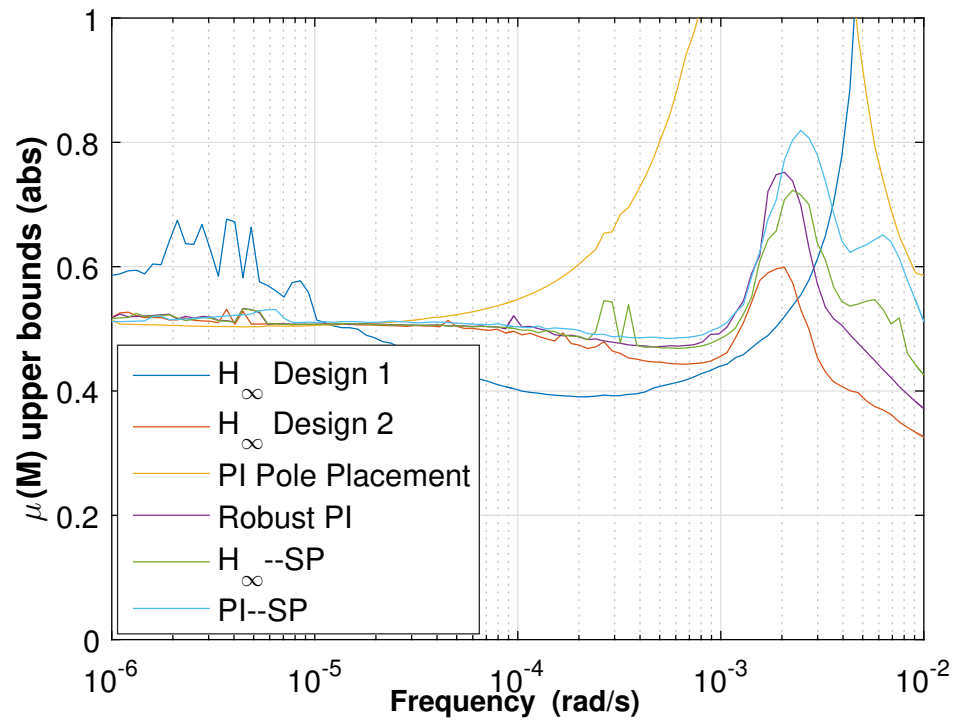
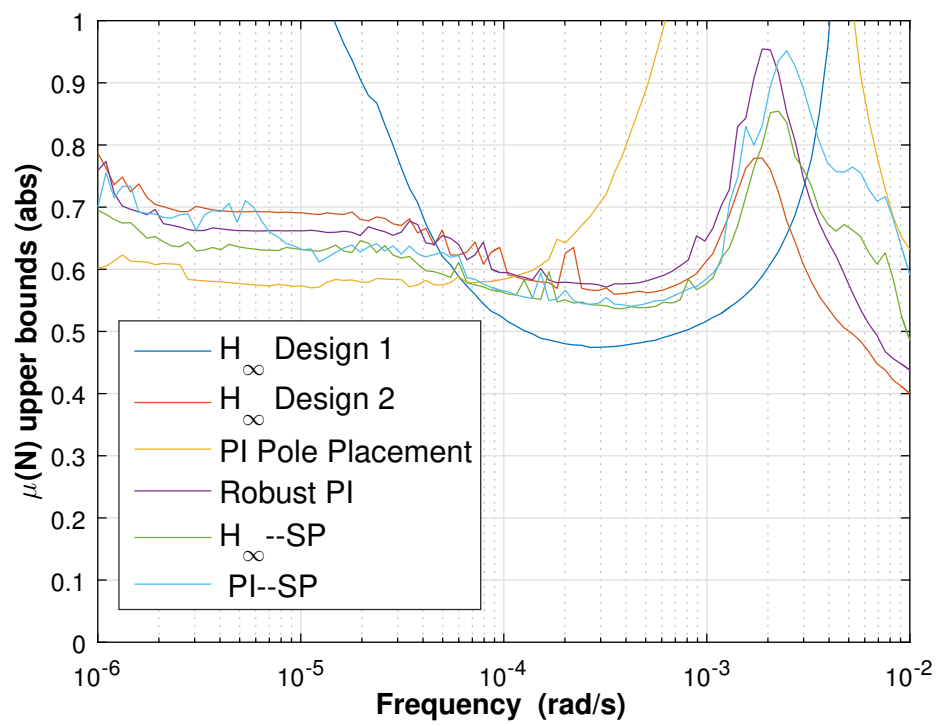


Figure 44: Nominal Performance Analysis

Figure 45: Robust Stability μ_M Comparison

Figure 46: Robust Performance μ_N Analysis

Chapter 8

High Fidelity Simulations

8.1 Drill Cycle

Drilling tools are made to drill in drilling cycles to generate curvatures less than their maximum curvature response. The drilling cycle is divided quantitatively into regular spaced intervals across the drilling cycle, which are the neutral and bias periods. In the neutral phase the input tool face U_{tf} is cycled at a constant rate. In the bias period the input tool face is held constant and the tool responds with maximum curvature. The average curvature over a drilling cycle is varied anywhere between 0 and maximum curvature response.

The drilling cycle has been designed in MATLAB and Simulink taking into account these factors. The drilling cycle depends upon the two inputs U_{tf} and U_{dls} , namely the tool face input and the the dog leg severity or curvature. The two designed modes are the bias (constant) and the neutral, also known as nutate in the industry. In the bias mode, the tool face is held constant to give a curvature equal to the specified maximum, while in the nutate period the tool face is circulated at a constant rate which physically explains rotational motion of the drill string, such that the tool face response is zero. The nutate mode is typically drilling vertically without any curvature definition to eventually stop at our desired curvature response in the bias mode. These two modes make up our drilling cycle which is assumed to be 360 seconds in the simulations undertaken. The drilling cycle block constructed in Simulink can be seen in Appendix E.

$$BR = \frac{U_{dls}}{K_{dls}} = \frac{T_{bias}}{T_{dc}} \quad (8.1)$$

This gives us the bias ratio (BR) which governs the logic behind the drill cycle. The bias ratio takes into consideration the entire drilling cycle. The bias ratio along with the drilling cycle makes our tool respond with maximum curvature response, K_{dls} . The drill cycle definition is illustrated in Figure 47. Now, this effectively helps us to model the dynamics of the input lag and input delay. In Panchal et al. (2012) this delay is modelled as a second order Pade approximant and the concept of the drilling cycle is introduced in Bayliss et al. (2014). By designing the drilling cycle physically and introducing it into the model, we remove the need to model this delay with the help of Pade approximants.

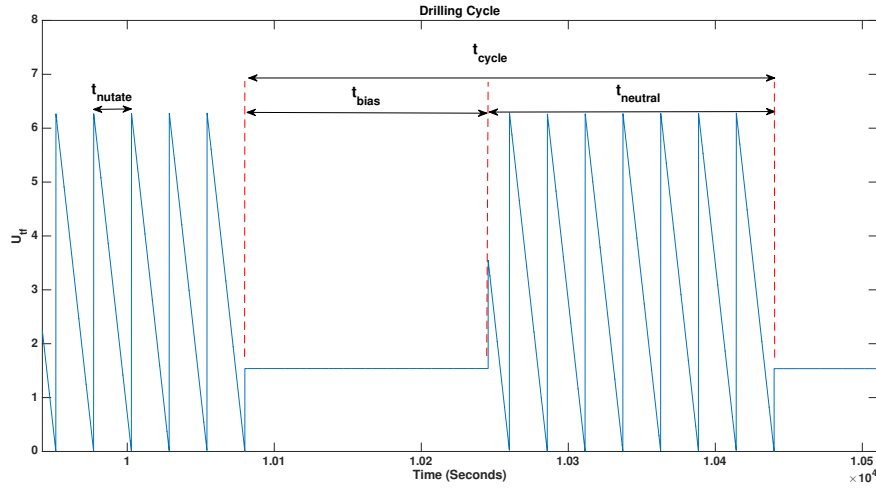


Figure 47: Drill Cycle Definition

8.2 Transient Simulation Description

The non-linear equations governing attitude control as given by Equation (3.1) and (3.2), are used as the controlled plant in Simulink for the transient simulations. The constant disturbances V_{dr} and V_{tr} are included in these equations. The solver settings used for the simulation are ode24 (Bogacki-Shampine) fixed step solver with a time step of 1s, similar to Bayliss et al. (2014). This solver is known to be fast enough and captures well the dynamics of the closed loop bandwidth of interest, which is similar to the one used in the robustness analysis. The simulation includes the engineering constraints of first-order lag applied to the U_{tf} control input and the delay associated with it as described in Section 8.1. Another significant engineering constraint as discussed in Section 3.1.2 included in the simulation is a feedback delay on the measurement of inclination and azimuth. The transient simulation parameters used are only for the nominal plant model and are given in Table 8.2. The Simulink block diagrams for the robust PI and the H_∞ -SP are shown in Figure 48 and 49.

Parameter	Value
Nominal $\theta_{inc}, \theta_{azi}$	$\pi/2$ rad and 2π rad
Nominal K_{dls}	5 deg /100ft
Disturbance drop rate V_{dr}	1 deg /100 ft
Disturbance turn rate V_{tr}	250 ft/hr
Disturbance turn rate V_{rop}	250 ft/hr
Drilling Cycle	360 s

Table 7: Transient Simulation Parameters

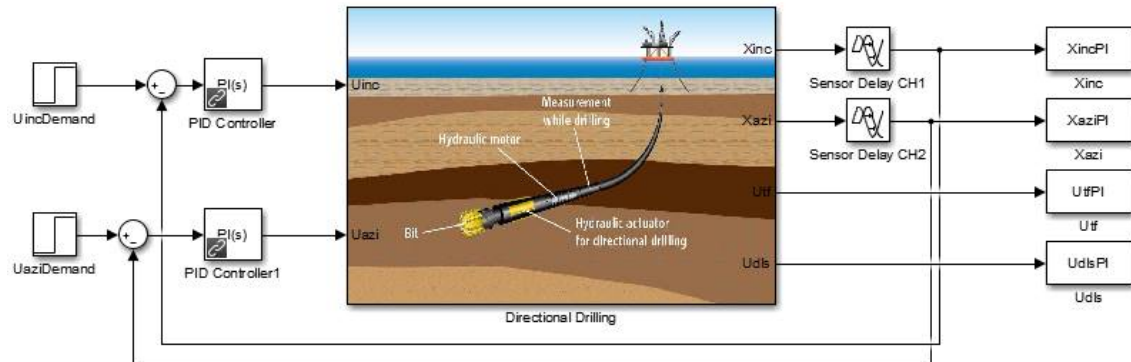
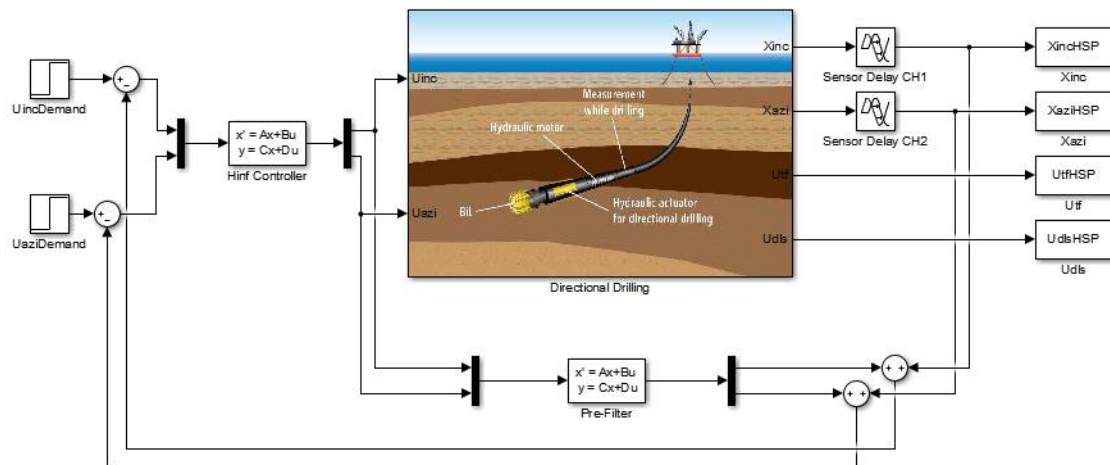


Figure 48: Simulink Block Diagram PI controller

Figure 49: Simulink Block Diagram H_{∞} -SP controller

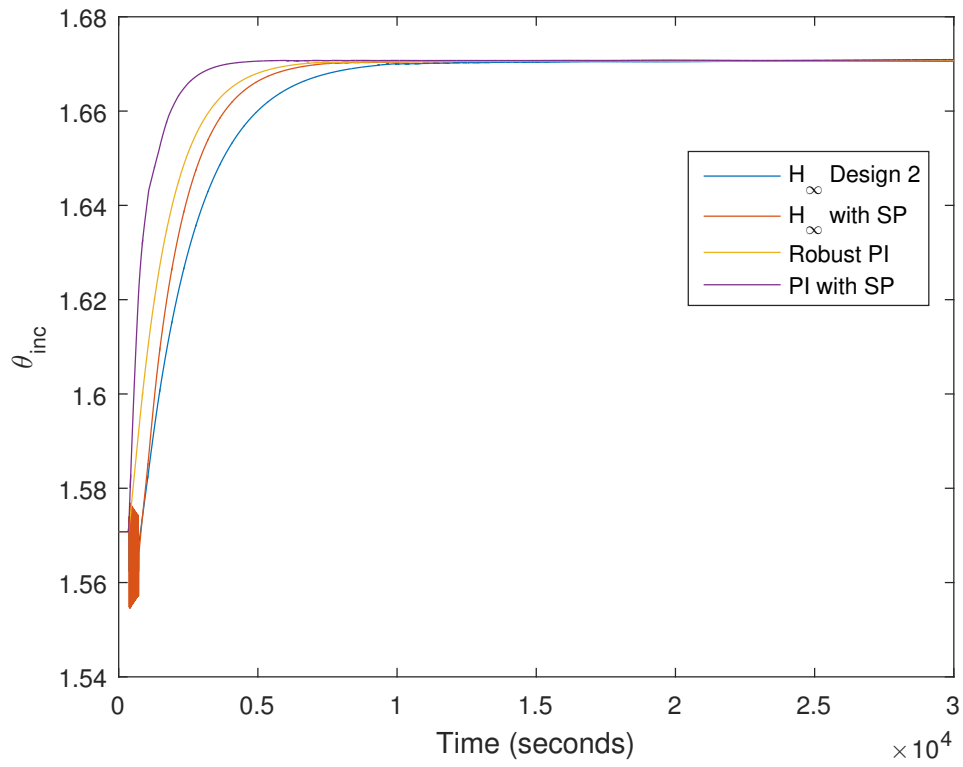
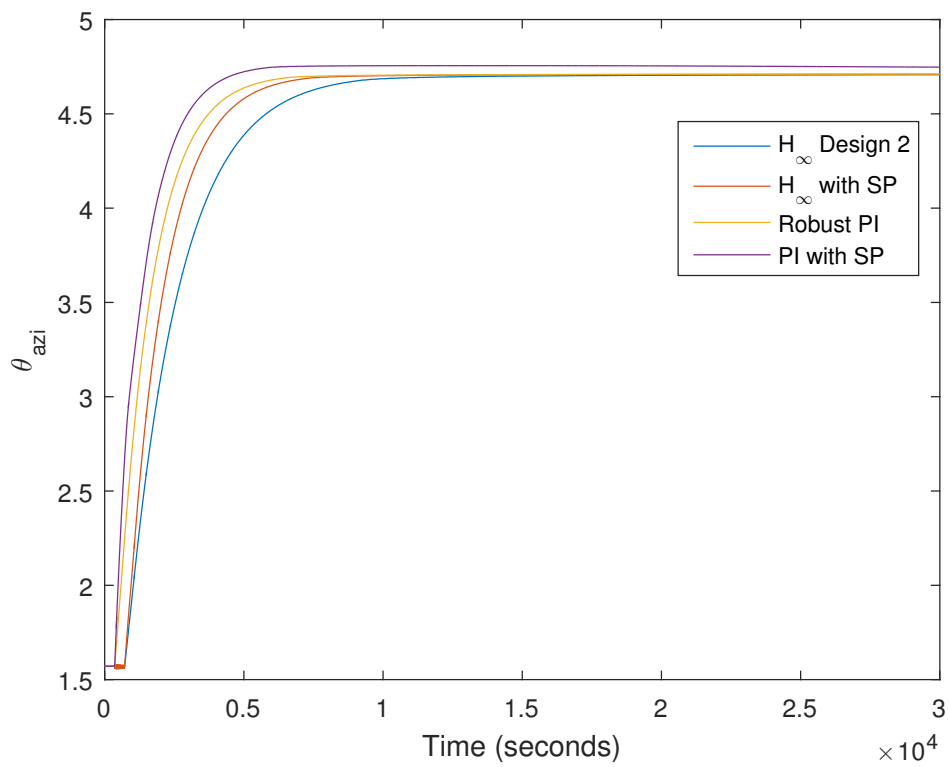
8.3 Transient simulation results

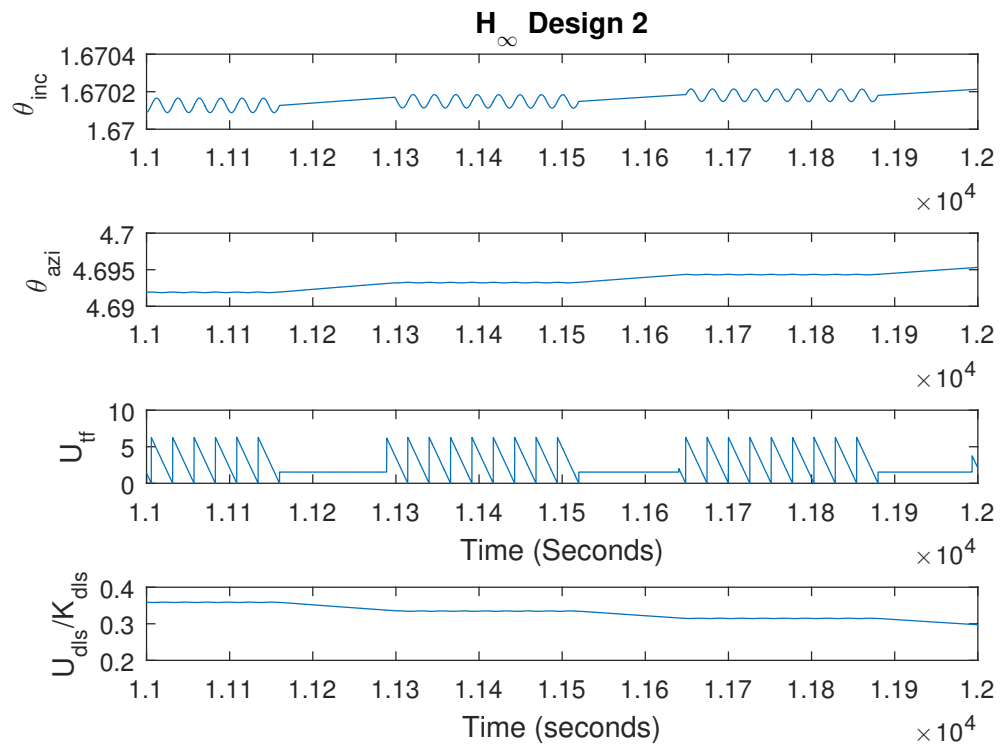
Figures 50 and 51 show the tracking response of the 4 robust controllers. It can be clearly seen that the Smith predictor controllers track the nominal reference inclination of $\pi/2$ and azimuth of 2π radians faster than the PI and H_∞ controllers. The effect of the lags and delays is reduced. Thus the results obtained from the linear analysis of the controllers are validated for the successful implementation of the SP. The units used are all *SI* units. However the Table 8.2 shows them in industry standard for simplicity.

The zoomed view of the attitude response for the H_∞ design 2 is shown in Figure 52 shows a direct correlation between the θ_{inc} and θ_{azi} responses. The non-linear input variable is shown for a detailed drill cycle. It can be seen that when the U_{tf} is held constant in the bias part of the drilling cycle for the entire time span, θ_{inc} and θ_{azi} ramp up/down at the tool's max curvature capacity, while in the neutral phase of the drilling cycle where the input U_{tf} is cycled at a constant rate. Therefore, it is seen as in Bayliss and Whidborne (2015) that in the neutral phase of the drilling cycle, the tool is open-loop while in the bias phase the closed-loop correction is applied and similar results are obtained. This is an interesting phenomena which makes the control system problem complex. To stabilize the plant you need a good controller which would have good response when the controller receives the input signal U_{tf} . The zoomed view of attitude response for the three other robust controllers are shown in Figures 83, 84 and 85 in Appendix D. The bias ratio keeps decreasing as the tool always tends to respond with its maximum radius of curvature which is acceptable while directional drilling. All the controllers behave in a similar manner for this inclination and azimuth hold formulation.

8.4 Conclusion

In this chapter a high fidelity non linear simulation was made for each of the designed controllers and it was seen that the controllers exhibit similar control over the plant. The controllers were found to successfully track the attitude command for all the designs. In the following chapter, the same models will be used with saturation to investigate a link between control action and its effect on system performance.

Figure 50: θ_{inc} Reference TrackingFigure 51: θ_{azi} Reference Tracking

Figure 52: Attitude-Tracking Transient Attitude Response, H_∞ Design, Zoomed View

Chapter 9

Controller Action

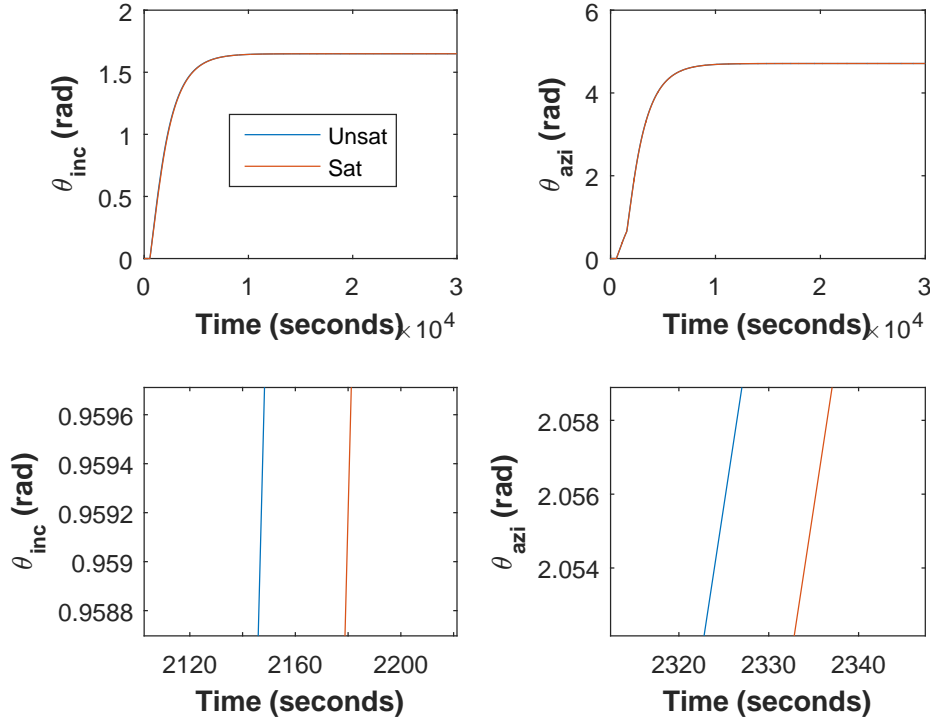
9.1 Effect of Saturation

The controller action and its link to the overall performance of the system is investigated in this section. Saturation of the control signal may affect the performance of the system as a certain system may not perform to its full potential however it is essential to limit the control signal as a real system could be damaged and can be dangerous for some input values. The reason saturation is important is for the security and safe functioning of the system. In the following sections the effect of a saturated and unsaturated signal on the output of the plant is compared to see the effect of the saturation in the controller action and effort; and in the system.

The effect of saturation on the system is initially checked on the linear system and then on the non-linear system. Due to the uncertainty in the system it can be assumed that the saturation on the virtual control signals U_{inc} and U_{azi} is 5% of the maximum value of the unsaturated system. This change is seen to be sufficient to see the effect of saturation in the linear system. The control action of the designed controllers is saturated in the linear simulation in Simulink within the PID controller block for the PI controller and with a saturation block for the H_∞ controller.

The Figures 53 and 54 shows the output performance of the system for a saturated and unsaturated control signal of the H_∞ controller on the linear plant and the PI controller on the non-linear plant. The plots indicate that both the control signals are successful in achieving the desired output. However, it can also be seen in the zoomed plot that the unsaturated control signal has the system performing a bit faster. This implies that on saturating the control signal the controller will have a longer actuation time. This characteristic is not essentially good for the system but implies its secure and safe functioning. Also taking into account the settling time of the system this difference can be neglected. The other 3 controllers namely PI, PI-SP and H_∞ -SP controllers also exhibit the exact same behavior which can be seen from Figures 86, 88 and 87, 89, 91 and 90 for both linear and non-linear systems and can be found in the Appendix D.

From Figure 55 it can be seen that the saturated signal is below the unsaturated system output and the steady state is different for both the attitude channels. It is more visible from the azimuth channel response that there is a delay between the two signals. Satura-

Figure 53: Effect of saturation on Controller Output- H_∞

tion has no effect on U_{tf} however it can be seen from the plots of the control output signals U_{inc} and U_{azi} that saturation delays the control action and hence delays U_{dls} too. This indicates that the saturated signal delays the system output and hence increases actuator effort.

9.2 Conclusion

It is interesting to see how much the saturation affects the control action and to determine the effort the controller needs to control the signal. As it is previously seen that all the designed controllers respond in a similar way, the PI controller is simulated for 9 values of saturation. It can be seen from Figure 56 that the greater the saturation on the control signal the more is the delay in the system output signals. This confirms the results from the previous sections, that more effort will be required by the controller to control the system and it can be seen that for greater values of saturation set point is not reached. For smaller values of saturation it can be assumed that there is no effect on the overall performance of the system since there is a very small difference in the saturated and unsaturated signals. Therefore, it is concluded that saturation has an important effect in the applicability of the controller and on the overall performance of the system and hence could be taken into account in the control system design.

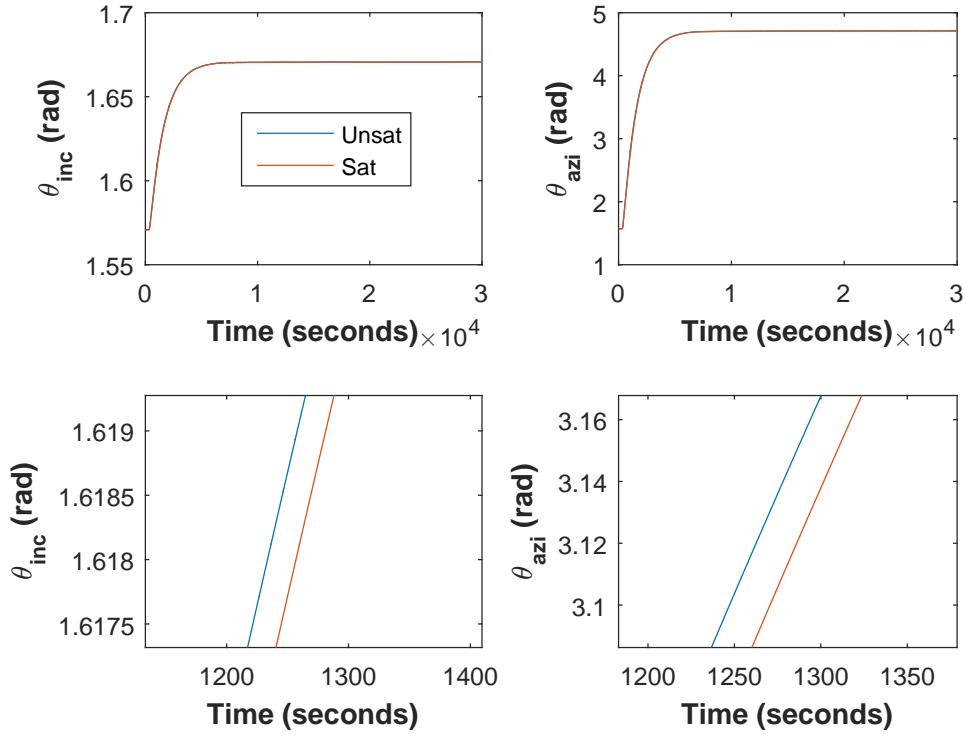
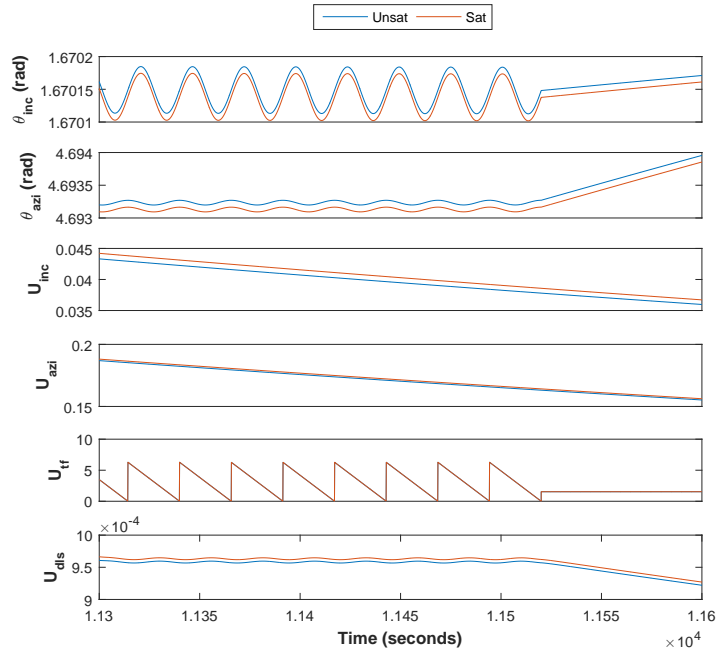


Figure 54: Effect of saturation on Controller Output- PI

Figure 55: Attitude-Tracking Transient Attitude Response, H_∞ Design, Zoomed View for Saturated and Unsaturated Signals

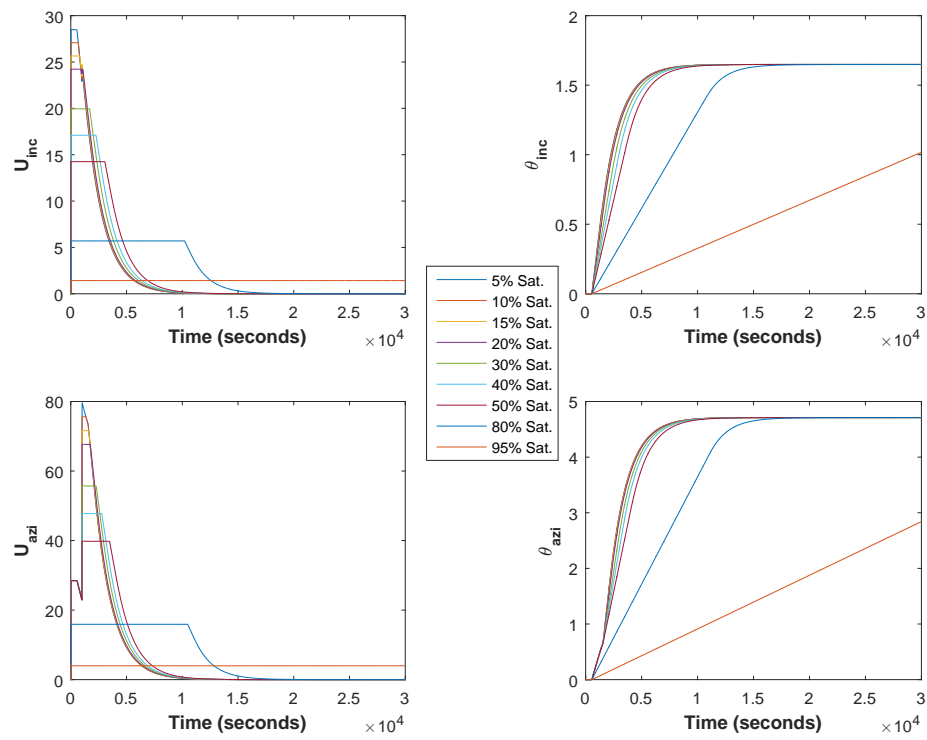


Figure 56: Different saturation level and their effect on performance

Chapter 10

Conclusion

10.1 Summary of contributions

This thesis studies robust controller design and analysis for attitude control of directional drilling tools. Inclination and azimuth angles govern the attitude dynamics of the directional drilling tool. A nonlinear multi-variable plant model is identified and linearized at the specified operating point. The un-modeled dynamics associated with the plant model are recognized and augmented into the open loop plant. The time delay is assumed to be a first order Pade approximant as it is the simplest to deal with. Higher order Pade approximants are better approximations of the delay but introduce oscillations in the system response and the system cannot be controlled. The eigenvalue analysis ascertains instability and the need for controller development. The controller design is achieved initially in two separate cases for the PI and H_∞ control techniques. .

PI and H_∞ controllers are designed for two separate cases. In the first case effect of the unmodelled dynamics are ignored for the controller design. The closed loop analysis for the preliminary designs suggests poor nominal performance for measurement delays greater than 100 seconds. The closed loop analysis is conducted on the plant model which includes the lag and delays and the parametric uncertainties. The eigenvalue analysis for the nominal and worst cases indicate that the designed controllers are not robust when the unmodelled dynamics and the parametric uncertainties are included.

To achieve better control over the plant model the second controller design includes the effects of the lag and delays. For the PI controller the uncertainties are included in the controller design and the controller is tuned using the Control System Tuner application in MATLAB. The uncertain closed loop analysis for both the robust PI controller and the H_∞ controller suggest both robust stability and robust performance considering the restrictions imposed by system weighting functions. The controller designs are confirmed to be robust subject to their closed loop analysis. The designed controllers successfully stabilize the dynamics however the presence of delay is found to be significant.

To counter the effect of this delay a Smith predictor inspired MIMO dead time compensator is designed. Two stabilizing controllers , PI and H_∞ are designed for the DTC predictor scheme and successfully ameliorate the effect of the delay associated with the plant. The effect of the delay is still present however significantly reduced. The PI-SP design is the

best design as it achieves the best combination between robustness and time response of closed loop. Both the SP designs are better than the previously designed controllers.

The developed controllers are subjected to a structure singular value analysis which powerfully demonstrates the robustness of the developed control schemes. The robust stability and performance of the closed loop system is partly indicated and partly confirmed in the closed analysis of the controllers. The designs for the plant model without delay and lag exhibit poor stability and performance as indicated earlier. The other controller meet the specified robust stability and robust performance criteria.

A comparative analysis of the system response and robustness criteria indicates better controller designs when the lag and delays are included. The transient response analysis confirms the application of the SP to reduce the effect of the time delay. The robustness comparison indicates that the PI-SP controllers achieves the best robust stability and robust performance margins. However, it is also noticed that the time response of the drills low frequency closed loop dynamics is sluggish and a trade off between the systems rise time and robust stability can be established.

Lastly, a high fidelity non linear simulation is made for each of the designed controllers and it is seen that the controllers exhibit similar control over the plant. The controller successfully track the attitude command for all the designs. The developed controllers can be successfully included in an trajectory control algorithm for directional drilling. The proposed controllers are robust and also successfully counter the presence of the delays. It is seen that when the lags and delays are included better control can be achieved.

10.2 Recommendations

The following recommendations are made which might help to enhance the scope of this work.

- The plant model can be studied further subjected to the systems practical application. The plant model studied in this work is restricted to its attitude control application and other variables governing borehole propagation are not included. Attitude control can be further explored keeping in mind the different typical directional well trajectories. Directional drilling can be made completely automated by using the developed controllers in trajectory controlled algorithms for predefined well geometries. Further study is suggested to include dynamics which are indirectly associated with the drills attitude.
- The drilling system dynamics are highly uncertain. The approach used in this work was to develop a robust controller. A linear parameter varying gain scheduled control technique can also be used instead. It can be assumed that the gain scheduled control is an alternative to robust control techniques at the expense of more complicated designs. The plant model can be linearized at various operating points and controllers can developed relevant to a specific pre-planned well geometry to check their practical applicability
- The pre-filter construction for the DTC is made only for the nominal plant. As the pre-filter is created in discrete time , all the discrete time domain uncertain

combinations would need to be included in the controller formulation. However, this is restricted because the use of the MATLAB command *d2c* which enables discrete time to continuous time conversion, is not defined for uncertain state space models. This can enable better control of the SP predictor model. Further work can be done in developing this control scheme.

- Structure singular value analysis which is used to prove the robust stability and robust performance goals of the designed controllers can be further used to develop mu-synthesis controllers, which directly affirm robustness.
- Knowledge about the engineering limitations of the actuators and sensors which are used in the system will help to design better controllers which will a more relevant industrial application. This will enable to design controllers which are more industrially acceptable and can be accommodated in Hardware-in-loop simulations.

Appendix A

MATLAB Code

A.1 Uncertain Parameters

```

1  clc
2  % close all
3  % clear all
4  %Nominal Values
5  Ts=3;
6  Vrop=100*0.3048/3600;
7  Kdls=5*pi/(100*180*0.3048);
8  alpha1=1;
9  alpha2=0;
10 t1=180;
11 t2=360;
12 td=10;
13 Vrop_un=ureal('Vrop_un',Vrop,'Percentage',50);
14 Kdls_un=ureal('Kdls_un',Kdls,'Percentage',10);
15 alpha1_un=ureal('alpha1_un',alpha1,'Range',[0.5 1.5]);
16 alpha2_un=ureal('alpha2_un',alpha2,'Range',[-0.0175 0.0175]);
17 t1_un=ureal('t1_un',t1,'Percentage',25);
18 t2_un=ureal('t2_un',t2,'Percentage',50);
19 td_un=ureal('td_un',td,'Percentage',25);
20 InputDelay=delay(t1_un);
21 OutputDelay=delay(t2_un);
22 Lag=tf([1],[td_un 1]);
23
24 save('UncertaintyParameters.mat','Vrop_un','Kdls_un','alpha1_un',...
25      'alpha2_un','t1_un','t2_un','td_un','Vrop','Kdls','alpha1','alpha2',...
26      't1','t2','td','InputDelay','OutputDelay','Lag')

```

A.2 H_∞ Controller

```

1  function [K,gamopt]=Hinfinity(Ps,W1,W2)
2  %% Hinfinity (Robust)
3
4  P=augw(Ps,W1,[],W2);

```

```

5 [K,Tzw,gamopt,Info]=hinfsvn(P,2,2);
6 K=hankelmr(K,4);
7
8
9
10 %%

```

```

1 clc
2 close all
3
4 %% Plant Construction(Uncertainty)
5 %Nominal Values
6
7 Vrop=100*0.3048/3600;
8 Kdls=5*pi/(100*180*0.3048);
9 alpha1=1;
10 alpha2=0;
11 t1=180;
12 t2=360;
13 td=10;
14 Vrop_un=ureal('Vrop_un',Vrop,'Percentage',50);
15 Kdls_un=ureal('Kdls_un',Kdls,'Percentage',10);
16 alpha1_un=ureal('alpha1_un',alpha1,'Range',[0.5 1.5]);
17 alpha2_un=ureal('alpha2_un',alpha2,'Range',[-0.0175 0.0175]);
18 t1_un=ureal('t1_un',t1,'Percentage',25);
19 t2_un=ureal('t2_un',t2,'Percentage',50);
20 td_un=ureal('td_un',td,'Percentage',25);
21
22 a=Vrop_un*Kdls_un;
23 b=a*alpha1_un;
24 c=-a*alpha1_un*alpha2_un;
25
26 InputDelay=delay(t1_un);
27 OutputDelay=delay(t2_un);
28 Lag=tf([1],[td_un 1]);
29
30 % Plant transfer function without delay neither lag
31
32 s=tf('s');
33 Gwd=[a/s 0; a*c/s^2 b/s];
34
35 % Linear Plant
36 ps=timeoptions;
37 ps.InputLabels.FontWeight='Bold';
38 ps.InputLabels.FontSize=12;
39 ps.OutputLabels.FontWeight='Bold';
40 ps.OutputLabels.FontSize=12;
41 ps.Title.FontWeight='Bold';
42 ps.Title.FontSize=12;
43 ps.Xlabel.FontWeight='Bold';
44 ps.Xlabel.FontSize=12;
45 ps.Ylabel.FontWeight='Bold';
46 ps.Ylabel.FontSize=12;
47 ps.Grid='on';
48
49
50
51 G=(OutputDelay*eye(2))*Gwd*(InputDelay*eye(2))*(Lag*eye(2));
52 G.InputName={'U_{inc}','U_{azi}'};

```

```

53 G.OutputName={'\theta_{inc}','\theta_{azi}'};
54
55 stepplot(G,ps)
56 ylabel('Attitude (Radians)')
57 title ' '
58
59
60 %% Hinfinity Construction Controller weights in the paper (Robust and Nominal with Delay and
61
62 M=[5 0.9];
63 A=[2.5e-3 0.3];
64 w=[2e-5 1e-4];
65 Gnom=G.NominalValue;
66 w1=tf([1/M(1) w(1)], [1 w(1)*A(1)]);
67 w2=tf([1 w(2)*A(2)], [1/M(2) w(2)]);
68 W1=append(w1,w1);
69 W2=append(w2,w2);
70 [K1,goptD1]=Hinfinity(Gwd,W1,W2);
71
72 %Robust Closed loop analysis
73 S1=feedback(eye(2), G*K1);
74 KS1=feedback(K1, G);
75 T1=feedback(G*K1, eye(2));
76
77 %Nominal Close Loop Analysis
78 Snom1=feedback(eye(2), Gnom*K1);
79 KSnom1=feedback(K1,Gnom);
80 Tnom1=feedback(Gnom*K1, eye(2));
81 FMIN=1e-6;
82 FMAX=0.01;
83
84 % Plot bounds robust and nominal
85 psig=sigmaoptions
86 psig.Title.FontWeight='Bold';
87 psig.Title.FontSize=12;
88 psig.Xlabel.FontWeight='Bold';
89 psig.Xlabel.FontSize=12;
90 psig.Ylabel.FontWeight='Bold';
91 psig.Ylabel.FontSize=12;
92 psig.Grid='on';
93
94 figure
95 h1=sigmaplot(S1,Snom1,'.-r'); hold on, sigma(inv(W1),psig),%hold off
96 sigma(T1,Tnom1,'.-k'); hold on, sigma(inv(W2),psig)
97 legend('\sigma(S)', '\sigma(Snom)', '\sigma(W1^{-1})', '\sigma(T)', ...
98         '\sigma(Tnom)', '\sigma(W2^{-1})', 'Location', 'SouthEast');hold off
99 p=getoptions(h1);
100 p.XLim=[FMIN FMAX];
101 setoptions(h1,p);
102 title ' '
103
104 %Close Loop Response
105
106 figure
107 T1.InputName={'R_{inc}','R_{azi}'};
108 T1.OutputName={'\theta_{inc}','\theta_{azi}'};
109 Tnom1.InputName={'R_{inc}','R_{azi}'};
110 Tnom1.OutputName={'\theta_{inc}','\theta_{azi}'};
111
112 h2=stepplot(T1,Tnom1,'.-r',ps);
113 title ' '

```

```

114 h=legend('T','Tnom');
115 set(h,'Position',[0.43 0.92 0.19 0.06],'Orientation','horizontal');
116 ylabel('Attitude (Radians)')
117
118 %% Mu Analysis
119 omega=logspace(-6,-2,100);
120 %Robust Stabiity
121 T1_frd=ufrd(T1,omega);
122 [stabmargD1,destabuncD1,stabReportD1,stabInfoD1]=robuststab(T1_frd);
123
124 %Robust Performance
125 systemnames = ' G K1 W1 ';
126 inputvar = '[ ref{2}]';
127 outputvar = '[ W1 ]';
128 input_to_G = '[ K1 ]';
129 input_to_K1 = '[ ref-G]';
130 input_to_W1 = '[ ref-G]';
131 clp = sysic;
132 clp_frd=ufrd(clp,omega);
133 [perfmargD1,perfabuncD1,perfReportD1,perfInfoD1]=robustperf(clp_frd);
134
135 % Nominal Performance
136
137 prf=clp(1:2,1:2);
138 sv=sigma(prf.NominalValue,omega);
139 prf_frdD1=frd(sv(1,:),omega);
140
141 %Plots
142
143 pbod= bodeoptions;
144 pbod.PhaseVisible = 'off';
145 pbod.XLim = [1e-6 1e-2];
146 pbod.MagUnits = 'abs';
147 pbod.Title.FontWeight='Bold';
148 pbod.Title.FontSize=12;
149 pbod.Xlabel.FontWeight='Bold';
150 pbod.Xlabel.FontSize=12;
151 pbod.Ylabel.FontWeight='Bold';
152 pbod.Ylabel.FontSize=12;
153 pbod.Grid='on';
154
155 figure
156 bodeplot(stabInfoD1.MussvBnds(1,1),perfInfoD1.MussvBnds(1,1),prf_frdD1,pbod)
157 xlabel('Frequency');
158 ylabel('\mu(M) and \mu(N) upper bounds (abs)');
159 legend('\mu(M) for RS','\mu(N) for RP','\mu(N) for NP','Location','North')
160 title ' '
161 %% Hinfinty Construction Controller our weights (Robusst and Nominal with Delay and Lag)
162
163 M=[5 0.9];
164 A=[2.5e-3 0.25];
165 w=[2e-5 8e-3];
166 Gnom=G.NominalValue;
167 w1=tf([1/M(1) w(1)],[1 w(1)*A(1)]);
168 w2=tf([1 w(2)*A(2)],[1/M(2) w(2)]);
169 W1=append(w1,w1);
170 W2=append(w2,w2);
171 [K2,goptD2]=Hinfinty(G,W1,W2);
172
173 %Robust Closed loop analysis
174

```

```

175 S2=feedback(eye(2), G*K2);
176 KS2=feedback(K2, G);
177 T2=feedback(G*K2, eye(2));
178
179 %Nominal Close Loop Analysis
180 Snom2=feedback(eye(2), Gnom*K2);
181 KSnom2=feedback(K2, Gnom);
182 Tnom2=feedback(Gnom*K2, eye(2));
183 FMIN=1e-6;
184 FMAX=0.01;
185 % Plot bounds robust and nominal
186 figure
187 h1=sigmaplot(S2,Snom2,'.-r'); hold on, sigma(inv(W1),psig),%hold off
188 sigma(T2,Tnom2,'.-k'); hold on, sigma(inv(W2))
189 legend('\sigma(S)', '\sigma(Snom)', '\sigma(W1^{-1})', '\sigma(T)', ...
190        '\sigma(Tnom)', '\sigma(W2^{-1})', 'Location', 'SouthEast');hold off
191 p=getoptions(h1);
192 p.XLim=[FMIN FMAX];
193 setoptions(h1,p);
194 title ' '
195
196 %Close Loop Response
197 T2.InputName={'R_{inc}', 'R_{azi}'};
198 T2.OutputName={'\theta_{inc}', '\theta_{azi}'};
199 Tnom2.InputName={'R_{inc}', 'R_{azi}'};
200 Tnom2.OutputName={'\theta_{inc}', '\theta_{azi}'};
201
202 figure
203 step(T2,Tnom2,'.-r',ps)
204 title ' '
205 h=legend('T', 'Tnom');
206 set(h, 'Position', [0.42 0.92 0.19 0.06], 'Orientation', 'horizontal');
207 ylabel('Attitude (Radians)')
208
209 %% Mu Analysis
210 omega=logspace(-6,-2,100);
211 %Robust Stabiity
212 T2_frd=ufrd(T2,omega);
213 [stabmargD2,destabuncD2,stabReportD2,stabInfoD2]=robuststab(T2_frd);
214
215 %Robust Stabiity
216 systemnames = ' G K2 W1 ';
217 inputvar = '[ ref{2}]';
218 outputvar = '[ W1 ]';
219 input_to_G = '[ K2 ]';
220 input_to_K2 = '[ ref-G]';
221 input_to_W1 = '[ ref-G]';
222 clp = sysic;
223 clp_frd=ufrd(clp,omega);
224 [perfmargD2,perfabuncD2,perfReportD2,perfInfoD2]=robustperf(clp_frd);
225
226 % Nominal Performance
227
228 prf=clp(1:2,1:2);
229 sv=sigma(prf.NominalValue,omega);
230 prf_frdD2=frd(sv(1,:),omega);
231
232 %Plots
233
234 figure
235 bodeplot(stabInfoD2.MussvBnds(1,1),perfInfoD2.MussvBnds(1,1),prf_frdD2,pbod)

```

```

236 xlabel('Frequency');
237 ylabel('\mu(M) and \mu(N) upper bounds (abs)');
238 legend('\mu(M) for RS', '\mu(N) for RP', '\mu(N) for NP', 'Location', 'North')
239 title ' '

```

A.3 Smith Predictor Controller

```

1 function d=delay(tdelay)
2 num=[-tdelay/2 1];
3 den=[ tdelay/2 1];
4 d=tf(num,den);

```

```

1 clc
2 clear H num
3
4 %%
5 %-----
6 %                               Discrete Time Plant
7 %-----
8 %
9 % % Plant Transfer function in discrete time without delay G(z)
10 Gwdtf=tf(Gwd);
11 Gp=[exp(-(t2)*s) 0; 0 exp(-(t2)*s)]*Gwdtf*[exp(-(t1)*s) 0; 0 exp(-(t1)*s)]
12 Pz=c2d(Gp,Ts);
13 Gz=c2d(Gwdtf,Ts)
14
15 %%
16 %-----
17 %                               Free delay Predictor Plant
18 %-----
19
20 % SS representation
21
22 [A,B,C,D]=ssdata(ss(Gz))
23
24 %%
25 % Prefilter Construction
26
27 % indexs delay matrix
28 Delay=[(t1+t2)/Ts 0; 0 (t1+t2)/Ts];
29 [I,J]=size(Gz);
30
31 for i=1:I
32     for j=1:J
33         d = Delay(1,1);
34         num=[];
35         if d==0
36             Y(i,j)=0;
37         else
38             for k=1:d
39                 H= A^(k-1)*B(:,j);
40                 num=[num C(i,:) *A^(-d)*H];
41             end
42             den=zeros(1,d+1);
43             den(1)=1;

```



```

44         Y(i,j)=tf(num,den,Ts);
45     end
46 end
47 end
48 Gtz=Y + Pz
49 Gtz=minreal(Gtz);
50 Gts=d2c(Gtz)
51 [Num,Den]=tfdata(Gts);
52 Y2=hankelmr(Y,32)
53 Yss=ss(Y2);
54 Yssc=d2c(Yss,'Tustin');
55 %%
56
57 save('ModifiedSmithMIMOPredictor.mat','G','G1','Gz','Gtz','Y','Pz','Gp','Yss','Yssc')

```

```

1  clc
2  close all
3
4  %% Plant Construction(Uncertainty)
5  %Nominal Values
6
7  Vrop=100*0.3048/3600;
8  Kdls=5*pi/(100*180*0.3048);
9  alpha1=1;
10 alpha2=0;
11 t1=180;
12 t2=360;
13 td=10;
14 Vrop_un=ureal('Vrop_un',Vrop,'Percentage',50);
15 Kdls_un=ureal('Kdls_un',Kdls,'Percentage',10);
16 alpha1_un=ureal('alpha1_un',alpha1,'Range',[0.5 1.5]);
17 alpha2_un=ureal('alpha2_un',alpha2,'Range',[-0.0175 0.0175]);
18 t1_un=ureal('t1_un',t1,'Percentage',25);
19 t2_un=ureal('t2_un',t2,'Percentage',50);
20 td_un=ureal('td_un',td,'Percentage',25);
21
22 a=Vrop_un*Kdls_un;
23 b=a*alpha1_un;
24 c=-a*alpha1_un*alpha2_un;
25
26 InputDelay=delay(t1_un);
27 OutputDelay=delay(t2_un);
28 Lag=tf([1],[td_un 1]);
29
30 % Plant transfer function without delay neither lag
31
32 s=tf('s');
33 Gwd=[a/s 0; a*c/s^2 b/s];
34
35 % Linear Plant
36 ps=timeoptions;
37 ps.InputLabels.FontWeight='Bold';
38 ps.InputLabels.FontSize=12;
39 ps.OutputLabels.FontWeight='Bold';
40 ps.OutputLabels.FontSize=12;
41 ps.Title.FontWeight='Bold';
42 ps.Title.FontSize=12;
43 ps.Xlabel.FontWeight='Bold';
44 ps.Xlabel.FontSize=12;

```

```

45 ps.Ylabel.FontWeight='Bold';
46 ps.Ylabel.FontSize=12;
47 ps.Grid='on';
48
49
50
51 G=(OutputDelay*eye(2))*Gwd*(InputDelay*eye(2))*(Lag*eye(2));
52 G.InputName={'U-{inc}','U-{azi}'};
53 G.OutputName={'\theta-{inc}','\theta-{azi}'};
54
55 stepplot(G,ps)
56 ylabel('Attitude (Radians)')
57 title ' '
58
59
60 %% Hinfinity Construction Controller new weights using SP (Robust and Nominal with Delay and
61
62 M=[5 0.9];
63 A=[2.5e-3 0.25];
64 w=[2e-5 8e-3];
65 Gnom=G.NominalValue;
66 w1=tf([1/M(1) w(1)], [1 w(1)*A(1)]);
67 w2=tf([1 w(2)*A(2)], [1/M(2) w(2)]);
68 W1=append(w1,w1);
69 W2=append(w2,w2);
70 [K5,goptD5]=Hinfinity(Gts,W1,W2);
71
72 %Close Loop Creation
73
74 systemnames = ' G K5 Yssc ';
75 inputvar = '[ ref{2}]';
76 outputvar = '[ G ]';
77 input_to_G = '[ K5 ]';
78 input_to_K5 = '[ ref-G-Yssc]';
79 input_to_Yssc = '[ K5 ]';
80 T5 = sysic;
81
82 %Close Loop Response
83
84 figure
85 T5.InputName={'R-{inc}','R-{azi}'};
86 T5.OutputName={'\theta-{inc}','\theta-{azi}'};
87
88 h2=stepplot(T5,T5.NominalValue,'.-r',ps);
89 title ' '
90 h=legend('T','Tnom');
91 set(h,'Position',[0.43 0.92 0.19 0.06],'Orientation','horizontal');
92 ylabel('Attitude (Radians)')
93
94 %% Mu Analysis
95 omega=logspace(-6,-2,100);
96 %Robust Stabiity
97 T5_frd=ufrd(T5,omega);
98 [stabmargD5,destabuncD5,stabReportD5,stabInfoD5]=robuststab(T5_frd);
99
100 %Robust Performance
101 systemnames = ' G K5 W1 Yssc ';
102 inputvar = '[ ref{2}]';
103 outputvar = '[ W1 ]';
104 input_to_G = '[ K5 ]';
105 input_to_K5 = '[ ref-G-Yssc]';

```

```

106 input_to_W1 = '[ ref-G-Yssc]';
107 input_to_Yssc='[ K5 ]';
108 clp = sysic;
109
110 clp_frd=ufrd(clp,omega);
111 [perf margD5,perf abuncD5,perfReportD5,perfInfoD5]=robustperf(clp_frd);
112
113 % Nominal Performance
114
115 prf=clp(1:2,1:2);
116 sv=sigma(prf.NominalValue,omega);
117 prf_frdD5=frd(sv(1,:),omega);
118
119 %Plots
120
121 pbod= bodeoptions;
122 pbod.PhaseVisible = 'off';
123 pbod.XLim = [1e-6 1e-2];
124 pbod.MagUnits = 'abs';
125 pbod.Title.FontWeight='Bold';
126 pbod.Title.FontSize=12;
127 pbod.Xlabel.FontWeight='Bold';
128 pbod.Xlabel.FontSize=12;
129 pbod.Ylabel.FontWeight='Bold';
130 pbod.Ylabel.FontSize=12;
131 pbod.Grid='on';
132
133 figure
134 bodeplot(stabInfoD5.MussvBnds(1,1),perfInfoD5.MussvBnds(1,1),prf_frdD5,pbod)
135 xlabel('Frequency ');
136 ylabel('\mu(M) and \mu(N) upper bounds (abs)');
137 legend('\mu(M) for RS','\mu(N) for RP','\mu(N) for NP','Location','North')
138 title ' '
139 %% PI Construction Controller new weights using SP (Robusst and Nominal with Delay and Lag)
140
141 load_system('MIMOPredictorTuned')
142 BP=find_system('MIMOPredictorTuned','Type','Block');
143 PID3=getSimulinkBlockHandle(BP(2),true);
144 PID4=getSimulinkBlockHandle(BP(1),true);
145
146 Kpi=eval(get_param(PID3,'P'));
147 Kpa=eval(get_param(PID4,'P'));
148 Kii=eval(get_param(PID3,'I'));
149 Kia=eval(get_param(PID4,'I'));
150 Ki=pid(Kpi,Kii);
151 Ka=pid(Kpa,Kia);
152 K6=[Ki 0;0 Ka];
153
154 M=[5 0.9];
155 A=[2.5e-3 0.25];
156 w=[2e-5 8e-3];
157 Gnom=G.NominalValue;
158 w1=tf([1/M(1) w(1)], [1 w(1)*A(1)]);
159 w2=tf([1 w(2)*A(2)], [1/M(2) w(2)]);
160 W1=append(w1,w1);
161 W2=append(w2,w2);
162
163
164 %Closed loop Creation
165
166 systemnames = ' G K6 Yssc ';

```

```

167 inputvar = '[ ref{2}]';
168 outputvar = '[ G ]';
169 input_to_G = '[ K6 ]';
170 input_to_K6 = '[ ref-G-Yssc]';
171 input_to_Yssc = '[ K6 ]';
172 T6 = sysic;
173
174
175 %Close Loop Response
176 T6.InputName={'R_{inc}','R_{azi}'};
177 T6.OutputName={'\theta_{inc}','\theta_{azi}'};
178
179
180 figure
181 step(T6,T6.NominalValue,'.-r',ps)
182 title ' '
183 h=legend('T','Tnom');
184 set(h,'Position',[0.42 0.92 0.19 0.06],'Orientation','horizontal');
185 ylabel('Attitude (Radians)')
186
187 %% Mu Analysis
188 omega=logspace(-6,-2,100);
189 %Robust Stabiity
190 T6_frd=ufrd(T6,omega);
191 [stabmargD6,destabuncD6,stabReportD6,stabInfoD6]=robuststab(T6_frd);
192
193 %Robust Stabiity
194 systemnames = ' G K6 W1 Yssc ';
195 inputvar = '[ ref{2}]';
196 outputvar = '[ W1 ]';
197 input_to_G = '[ K6 ]';
198 input_to_K6 = '[ ref-G-Yssc]';
199 input_to_W1 = '[ ref-G-Yssc]';
200 input_to_Yssc='[ K6 ]';
201 clp = sysic;
202 clp_frd=ufrd(clp,omega);
203 [perfmargD6,perfabuncD6,perfReportD6,perfInfoD6]=robustperf(clp_frd);
204
205 % Nominal Performance
206
207 prf=clp(1:2,1:2);
208 sv=sigma(prf.NominalValue,omega);
209 prf_frdD6=frd(sv(1,:),omega);
210
211 %Plots
212
213 figure
214 bodeplot(stabInfoD6.MussvBnds(1,1),perfInfoD6.MussvBnds(1,1),prf_frdD6,pbod)
215 xlabel('Frequency');
216 ylabel('\mu(M) and \mu(N) upper bounds (abs)');
217 legend('\mu(M) for RS','\mu(N) for RP','\mu(N) for NP','Location','North')
218 title ' '

```

A.4 PI controller

```

1 clc

```

```

2 close all
3
4 %% Plant Construction(Uncertainty)
5 %Nominal Values
6
7 Vrop=100*0.3048/3600;
8 Kdls=5*pi/(100*180*0.3048);
9 alpha1=1;
10 alpha2=0;
11 t1=180;
12 t2=360;
13 td=10;
14 Vrop_un=ureal('Vrop_un',Vrop,'Percentage',50);
15 Kdls_un=ureal('Kdls_un',Kdls,'Percentage',10);
16 alpha1_un=ureal('alpha1_un',alpha1,'Range',[0.5 1.5]);
17 alpha2_un=ureal('alpha2_un',alpha2,'Range',[-0.0175 0.0175]);
18 t1_un=ureal('t1_un',t1,'Percentage',25);
19 t2_un=ureal('t2_un',t2,'Percentage',50);
20 td_un=ureal('td_un',td,'Percentage',25);
21
22 a=Vrop_un*Kdls_un;
23 b=a*alpha1_un;
24 c=-a*alpha1_un*alpha2_un;
25
26 InputDelay=delay(t1_un);
27 OutputDelay=delay(t2_un);
28 Lag=tf([1],[td_un 1]);
29
30 % Plant transfer function without delay neither lag
31
32 A=[0 0;c 0];
33 B=[a 0;0 b];
34 C=eye(2);
35 D=0;
36 G_0=uss(A,B,C,D);
37
38 % Linear Plant
39 ps=timeoptions;
40 ps.InputLabels.FontWeight='Bold';
41 ps.InputLabels.FontSize=12;
42 ps.OutputLabels.FontWeight='Bold';
43 ps.OutputLabels.FontSize=12;
44 ps.Title.FontWeight='Bold';
45 ps.Title.FontSize=12;
46 ps.Xlabel.FontWeight='Bold';
47 ps.Xlabel.FontSize=12;
48 ps.Ylabel.FontWeight='Bold';
49 ps.Ylabel.FontSize=12;
50 ps.Grid='on';
51
52
53
54 G=(OutputDelay*eye(2))*G_0*(InputDelay*eye(2))*(Lag*eye(2));
55 G.InputName={'U_{inc}','U_{azi}'};
56 G.OutputName={'\theta_{inc}','\theta_{azi}'};
57
58 stepplot(G,ps)
59 ylabel('Attitude (Radians)')
60 title ' '
61
62

```

```

63 %% PI Construction Controller gains in the paper
64
65 wi=5.24e-4;
66 wa=1.3e-3;
67 Kpi=(sqrt(2)*wi)/a.NominalValue;
68 Kpa=(sqrt(2)*wa)/b.NominalValue;
69 Kii=(wi^2)/a.NominalValue;
70 Kia=(wa^2)/b.NominalValue;
71 Ki=pid(Kpi,Kii);
72 Ka=pid(Kpa,Kia);
73 K3=[Ki 0;0 Ka];
74
75 M=[5 0.9];
76 A=[2.5e-3 0.25];
77 w=[2e-5 8e-3];
78 Gnom=G.NominalValue;
79 w1=tf([1/M(1) w(1)], [1 w(1)*A(1)]);
80 w2=tf([1 w(2)*A(2)], [1/M(2) w(2)]);
81 W1=append(w1,w1);
82 W2=append(w2,w2);
83
84
85 %Robust Closed loop analysis
86 S3=feedback(eye(2), G*K3);
87 KS3=feedback(K3, G);
88 T3=feedback(G*K3, eye(2));
89
90 %Nominal Close Loop Analysis
91 Snom3=feedback(eye(2), Gnom*K3);
92 KSnom3=feedback(K3,Gnom);
93 Tnom3=feedback(Gnom*K3, eye(2));
94 FMIN=1e-6;
95 FMAX=0.01;
96
97 % Plot bounds robust and nominal
98 psig=sigmaoptions
99 psig.Title.FontWeight='Bold';
100 psig.Title.FontSize=12;
101 psig.Xlabel.FontWeight='Bold';
102 psig.Xlabel.FontSize=12;
103 psig.Ylabel.FontWeight='Bold';
104 psig.Ylabel.FontSize=12;
105 psig.Grid='on';
106
107 figure
108 h1=sigmaplot(S3,Snom3,'.-r'); hold on, sigma(inv(W1),psig),%hold off
109 sigma(T3,Tnom3,'-k'); hold on, sigma(inv(W2),psig)
110 legend('\sigma(S)', '\sigma(Snom)', '\sigma(W1^{-1})', '\sigma(T)', ...
111        '\sigma(Tnom)', '\sigma(W2^{-1})', 'Location', 'SouthEast');hold off
112 p=getoptions(h1);
113 p.XLim=[FMIN FMAX];
114 setoptions(h1,p);
115 title ' '
116
117 %Close Loop Response
118
119 figure
120 T3.InputName={'R_{inc}', 'R_{azi}'};
121 T3.OutputName={'\theta_{inc}', '\theta_{azi}'};
122 Tnom3.InputName={'R_{inc}', 'R_{azi}'};
123 Tnom3.OutputName={'\theta_{inc}', '\theta_{azi}'};

```

```

124 h2=stepplot(T3,Tnom3,'.-r',ps);
125 title ' '
126 h=legend('T','Tnom');
127 set(h,'Position',[0.43 0.92 0.19 0.06],'Orientation','horizontal');
128 ylabel('Attitude (Radians)')
129
130 %% Mu Analysis
131 omega=logspace(-6,-2,100);
132 %Robust Stabiity
133 T3_frd=ufrd(T3,omega);
134 [stabmargD3,destabuncD3,stabReportD3,stabInfoD3]=robuststab(T3_frd);
135
136 %Robust Performance
137 systemnames = ' G K3 W1 ';
138 inputvar = '[ ref{2}]';
139 outputvar = '[ W1 ]';
140 input_to_G = '[ K3 ]';
141 input_to_K3 = '[ ref-G]';
142 input_to_W1 = '[ ref-G]';
143 clp = sysic;
144 clp_frd=ufrd(clp,omega);
145 [perf margD3,perf abuncD3,perf ReportD3,perf InfoD3]=robustperf(clp_frd);
146
147 % Nominal Performance
148
149 prf=clp(1:2,1:2);
150 sv=sigma(prf.NominalValue,omega);
151 prf_frdD3=frd(sv(1,:),omega);
152
153 %Plots
154
155 pbod= bodeoptions;
156 pbod.PhaseVisible = 'off';
157 pbod.XLim = [1e-6 1e-2];
158 pbod.MagUnits = 'abs';
159 pbod.Title.FontWeight='Bold';
160 pbod.Title.FontSize=12;
161 pbod.Xlabel.FontWeight='Bold';
162 pbod.Xlabel.FontSize=12;
163 pbod.Ylabel.FontWeight='Bold';
164 pbod.Ylabel.FontSize=12;
165 pbod.Grid='on';
166
167 figure
168 bodeplot(stabInfoD3.MussvBnds(1,1),perfInfoD3.MussvBnds(1,1),prf_frdD3,pbod)
169 xlabel('Frequency ');
170 ylabel('\mu(M) and \mu(N) upper bounds (abs)');
171 legend('\mu(M) for RS','\mu(N) for RP','\mu(N) for NP','Location','North')
172 title ' '
173 %% PI Construction Controller gains to the tune
174 load.system('MIMOPIONly')
175 BP=find.system('MIMOPIONly','Type','Block');
176 PID1=getSimulinkBlockHandle(BP(2),true);
177 PID2=getSimulinkBlockHandle(BP(1),true);
178
179 Kpi=eval(get_param(PID1,'P'));
180 Kpa=eval(get_param(PID2,'P'));
181 Kii=eval(get_param(PID1,'I'));
182 Kia=eval(get_param(PID2,'I'));
183 Ki=pid(Kpi,Kii);
184 Ka=pid(Kpa,Kia);

```

```

185 K4=[Ki 0;0 Ka];
186
187 M=[5 0.9];
188 A=[2.5e-3 0.25];
189 w=[2e-5 8e-3];
190 Gnom=G.NominalValue;
191 w1=tf([1/M(1) w(1)], [1 w(1)*A(1)]);
192 w2=tf([1 w(2)*A(2)], [1/M(2) w(2)]);
193 W1=append(w1,w1);
194 W2=append(w2,w2);
195
196
197 %Robust Closed loop analysis
198
199 S4=feedback(eye(2), G*K4);
200 KS4=feedback(K4, G);
201 T4=feedback(G*K4, eye(2));
202
203 %Nominal Close Loop Analysis
204 Snom4=feedback(eye(2), Gnom*K4);
205 KSnom4=feedback(K4, Gnom);
206 Tnom4=feedback(Gnom*K4, eye(2));
207 FMIN=1e-6;
208 FMAX=0.01;
209 % Plot bounds robust and nominal
210 figure
211 h1=sigmaplot(S4,Snom4,'.-r'); hold on, sigma(inv(W1),psig),%hold off
212 sigma(T4,Tnom4,'.-k'); hold on, sigma(inv(W2))
213 legend('\sigma(S)', '\sigma(Snom)', '\sigma(W1^{-1})', '\sigma(T)', ...
214        '\sigma(Tnom)', '\sigma(W2^{-1})', 'Location', 'SouthEast');hold off
215 p=getoptions(h1);
216 p.XLim=[FMIN FMAX];
217 setoptions(h1,p);
218 title ' '
219
220 %Close Loop Response
221 T4.InputName={'R_{inc}', 'R_{azi}'};
222 T4.OutputName={'\theta_{inc}', '\theta_{azi}'};
223 Tnom4.InputName={'R_{inc}', 'R_{azi}'};
224 Tnom4.OutputName={'\theta_{inc}', '\theta_{azi}'};
225 figure
226 step(T4,Tnom4,'.-r',ps)
227 title ' '
228 h=legend('T', 'Tnom');
229 set(h, 'Position', [0.42 0.92 0.19 0.06], 'Orientation', 'horizontal');
230 ylabel('Attitude (Radians)')
231
232 %% Mu Analysis
233 omega=logspace(-6,-2,100);
234 %Robust Stabiity
235 T4_frd=ufrd(T4,omega);
236 [stabmargD4,destabuncD4,stabReportD4,stabInfoD4]=robuststab(T4_frd);
237
238 %Robust Stabiity
239 systemnames = ' G K4 W1 ';
240 inputvar = '[ ref{2}]';
241 outputvar = '[ W1 ]';
242 input_to_G = '[ K4 ]';
243 input_to_K4 = '[ ref-G]';
244 input_to_W1 = '[ ref-G]';
245 clp = sysic;

```



```

246 clp_frd=ufrd(clp,omega);
247 [perfmargD4,perfabuncD4,perfReportD4,perfInfoD4]=robustperf(clp_frd);
248
249 % Nominal Performance
250
251 prf=clp(1:2,1:2);
252 sv=sigma(prf.NominalValue,omega);
253 prf_frdD4=frd(sv(1,:),omega);
254
255 %Plots
256
257 figure
258 bodeplot(stabInfoD4.MussvBnds(1,1),perfInfoD4.MussvBnds(1,1),prf_frdD4,pbod)
259 xlabel('Frequency ');
260 ylabel('\mu(M) and \mu(N) upper bounds (abs)');
261 legend('\mu(M) for RS','\mu(N) for RP','\mu(N) for NP','Location','North')
262 title ' '

```

A.5 Comparisons

```

1 close all
2 clc
3 T1nom=T1.NominalValue;
4 T2nom=T2.NominalValue;
5 T3nom=T3.NominalValue;
6 T4nom=T4.NominalValue;
7 T5nom=T5.NominalValue;
8 T6nom=T6.NominalValue;
9 [a1,b1]=wcgain(T1,omega);
10 T1w=usubs(T1,b1);
11 [a2,b2]=wcgain(T2,omega);
12 T2w=usubs(T2,b2);
13 [a3,b3]=wcgain(T3,omega);
14 T3w=usubs(T3,b3);
15 [a4,b4]=wcgain(T4,omega);
16 T4w=usubs(T4,b4);
17 [a5,b5]=wcgain(T5,omega);
18 T5w=usubs(T5,b5);
19 [a6,b6]=wcgain(T6,omega);
20 T6w=usubs(T6,b6);
21
22 figure
23 stepplot(T2nom,T2w,T4nom,T4w,ps)
24 title ' '
25 ylabel('Attitude (Radians)')
26 legend('H_{\infty} Design 2 Nominal','H_{\infty} Design 2 Worst case',...
27        'Robust PI Nominal','Robust PI Worst case')
28
29 figure
30 stepplot(T5nom,T5w,T6nom,T6w,ps)
31 title ' '
32 ylabel('Attitude (Radians)')
33 legend('H_{\infty} with SP Nominal','H_{\infty} with SP Worst Gain',...
34        'Robust PI with SP Nominal','Robust PI with SP Worst Gain')
35
36 figure

```

```

37 stepplot(T2nom,T2w,T5nom,T5w,ps)
38 title ' '
39 ylabel('Attitude (Radians)')
40 legend('H-{\infty} Design 2 Nominal','H-{\infty} Design 2 Worst case',...
41        'H-{\infty} with SP Nominal','H-{\infty} with SP Worst case')
42
43 figure
44 stepplot(T4nom,T4w,T6nom,T6w,ps)
45 title ' '
46 ylabel('Attitude(Radians)')
47 legend('Robust PI Nominal','Robust PI Worst case',...
48        'Robust PI with SP Nominal','Robust PI with SP Worst case')
49
50 figure
51 bodeplot(perfInfoD1.MussvBnds(1,1),perfInfoD2.MussvBnds(1,1),...
52          perfInfoD3.MussvBnds(1,1),perfInfoD4.MussvBnds(1,1),...
53          perfInfoD5.MussvBnds(1,1),perfInfoD6.MussvBnds(1,1),pbod)
54 title ' '
55 xlabel('Frequency');
56 ylabel('\mu(N) upper bounds ');
57 legend('H-{\infty} Design 1','H-{\infty} Design 2',...
58        'PI Pole Placement','Robust PI','H-{\infty} with SP',...
59        'Robust PI with SP')
60
61 figure
62 bodeplot(stabInfoD1.MussvBnds(1,1),stabInfoD2.MussvBnds(1,1),...
63          stabInfoD3.MussvBnds(1,1),stabInfoD4.MussvBnds(1,1),...
64          stabInfoD5.MussvBnds(1,1),stabInfoD6.MussvBnds(1,1),pbod)
65 title ' '
66 xlabel('Frequency');
67 ylabel('\mu(M) upper bounds ');
68 legend('H-{\infty} Design 1','H-{\infty} Design 2',...
69        'PI Pole Placement','Robust PI','H-{\infty} with SP',...
70        'Robust PI with SP')
71
72 figure
73 bodeplot(prf_frdD1,prf_frdD2,prf_frdD3,prf_frdD4,prf_frdD5,prf_frdD6,pbod)
74 title ' '
75 xlabel('Frequency');
76 ylabel('\mu(N) upper bounds ');
77 legend('H-{\infty} Design 1','H-{\infty} Design 2',...
78        'PI Pole Placement','Robust PI','H-{\infty} with SP',...
79        'Robust PI with SP')

```

Appendix B

Control System Tuner Graphical Representation

The chapter gives a graphical representation of the tuning steps to achieve the controller design. The figure titles indicate the step undertaken.

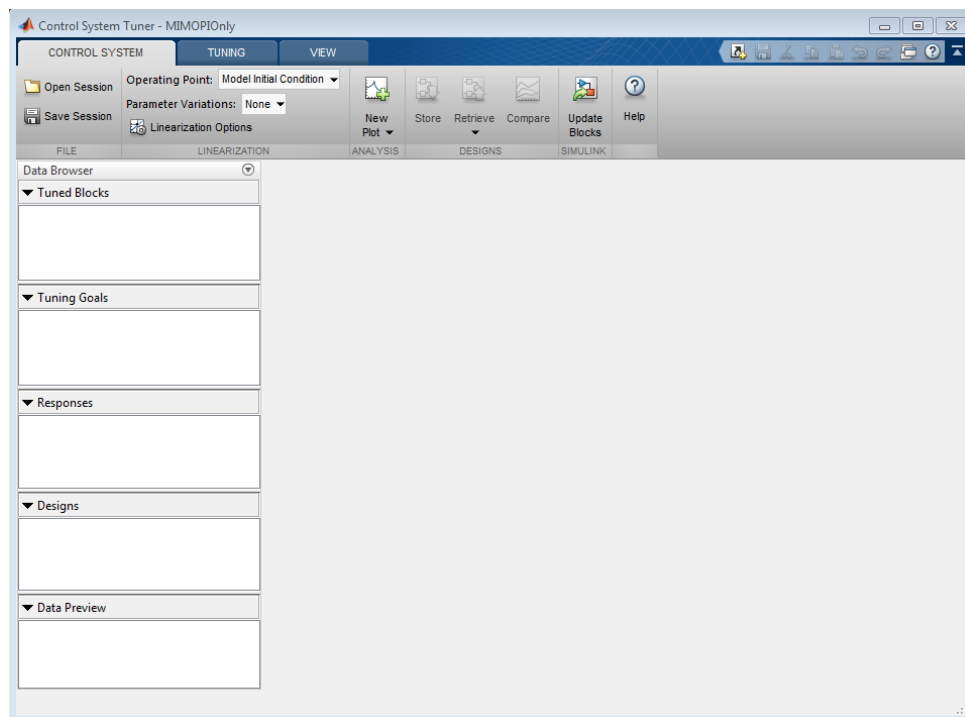


Figure 57: Control System Tuner Application

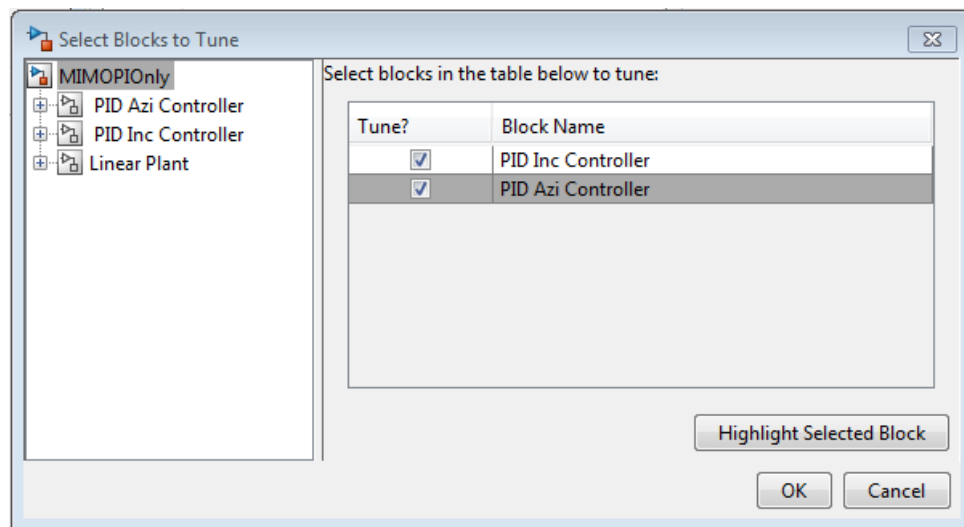
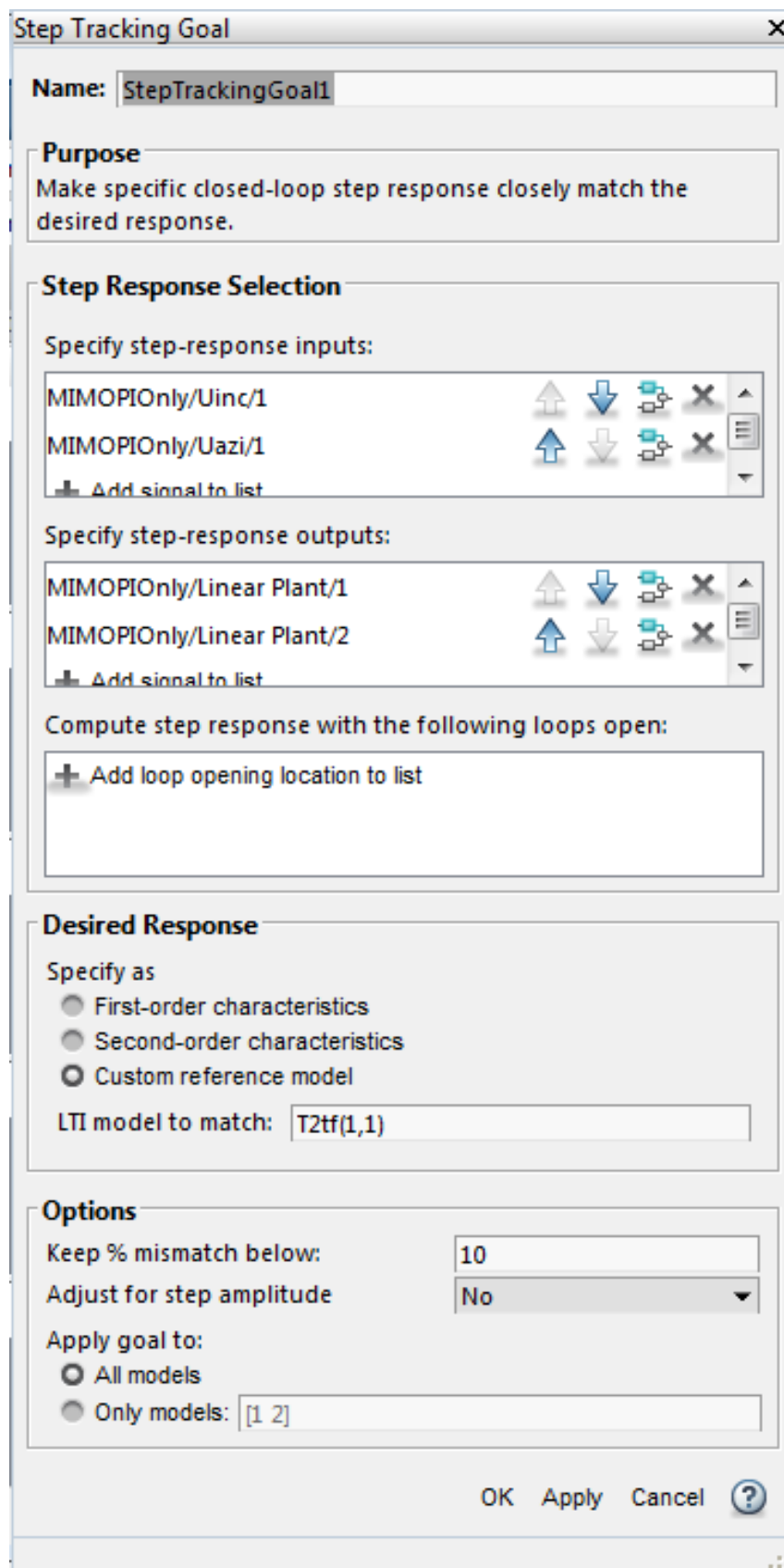


Figure 58: Select Blocks to Tune



The image shows a 'Step Tracking Goal' dialog box with a title bar and a close button. It is divided into several sections: 'Name' with a text field containing 'StepTrackingGoal1'; 'Purpose' with a description; 'Step Response Selection' with two lists of inputs and outputs, each with move and delete icons and an 'Add signal to list' button; a section for 'Compute step response with the following loops open:' with an 'Add loop opening location to list' button; 'Desired Response' with radio buttons for 'First-order characteristics', 'Second-order characteristics', and 'Custom reference model' (which is selected), and an 'LTI model to match' text field containing 'T2tf(1,1)'; and 'Options' with a 'Keep % mismatch below' text field (10), an 'Adjust for step amplitude' dropdown (No), and 'Apply goal to:' radio buttons for 'All models' and 'Only models:' (selected) with a corresponding text field containing '[1 2]'. At the bottom are 'OK', 'Apply', 'Cancel' buttons and a help icon.

Step Tracking Goal

Name: StepTrackingGoal1

Purpose
Make specific closed-loop step response closely match the desired response.

Step Response Selection

Specify step-response inputs:

- MIMOPIOnly/Uinc/1
- MIMOPIOnly/Uazi/1
- + Add signal to list

Specify step-response outputs:

- MIMOPIOnly/Linear Plant/1
- MIMOPIOnly/Linear Plant/2
- + Add signal to list

Compute step response with the following loops open:

- + Add loop opening location to list

Desired Response

Specify as

- ☐ First-order characteristics
- ☐ Second-order characteristics
- ☒ Custom reference model

LTI model to match: T2tf(1,1)

Options

Keep % mismatch below: 10

Adjust for step amplitude: No

Apply goal to:

- ☐ All models
- ☒ Only models: [1 2]

OK Apply Cancel ?

Figure 59: Step Tracking Goal

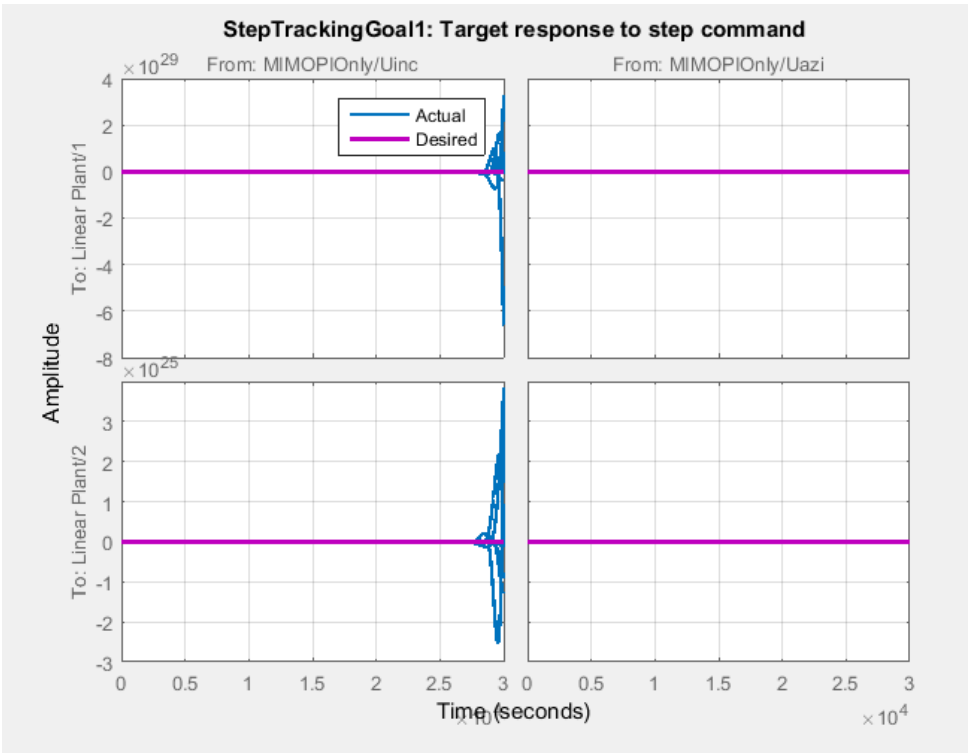


Figure 60: Step Tracking Goal Graphical Illustration

Sensitivity Goal [X]

Name:

Purpose
Limit the sensitivity of feedback loops to disturbances.

Sensitivity Evaluation

Measure sensitivity at the following locations:

MIMOPIOnly/Sum2/1	↑	↓	↻	✕	⋮
MIMOPIOnly/Sum3/1	↑	↓	↻	✕	⋮

+ Add signal to list

Measure sensitivity with the following loops open:

+ Add loop opening location to list

Sensitivity Bound

Max sensitivity as a function of frequency (LTI model):

Options

Enforce goal in frequency range

Equalize cross-channel effects

Apply goal to

☒ All models

☐ Only models:

OK Apply Cancel ?

Figure 61: Sensitivity Goal

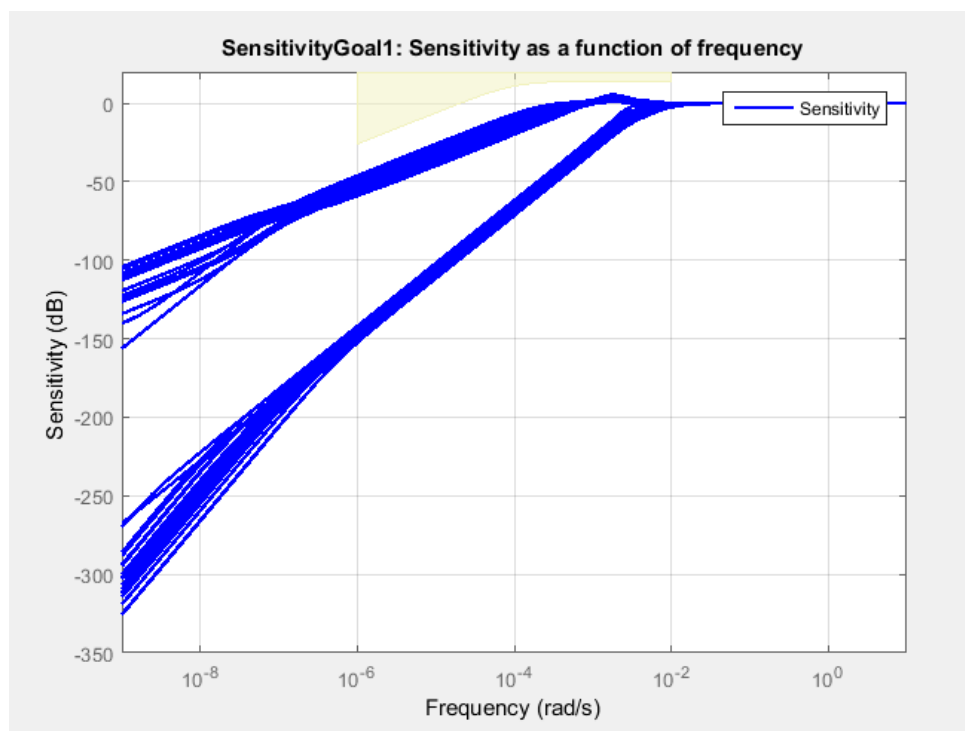
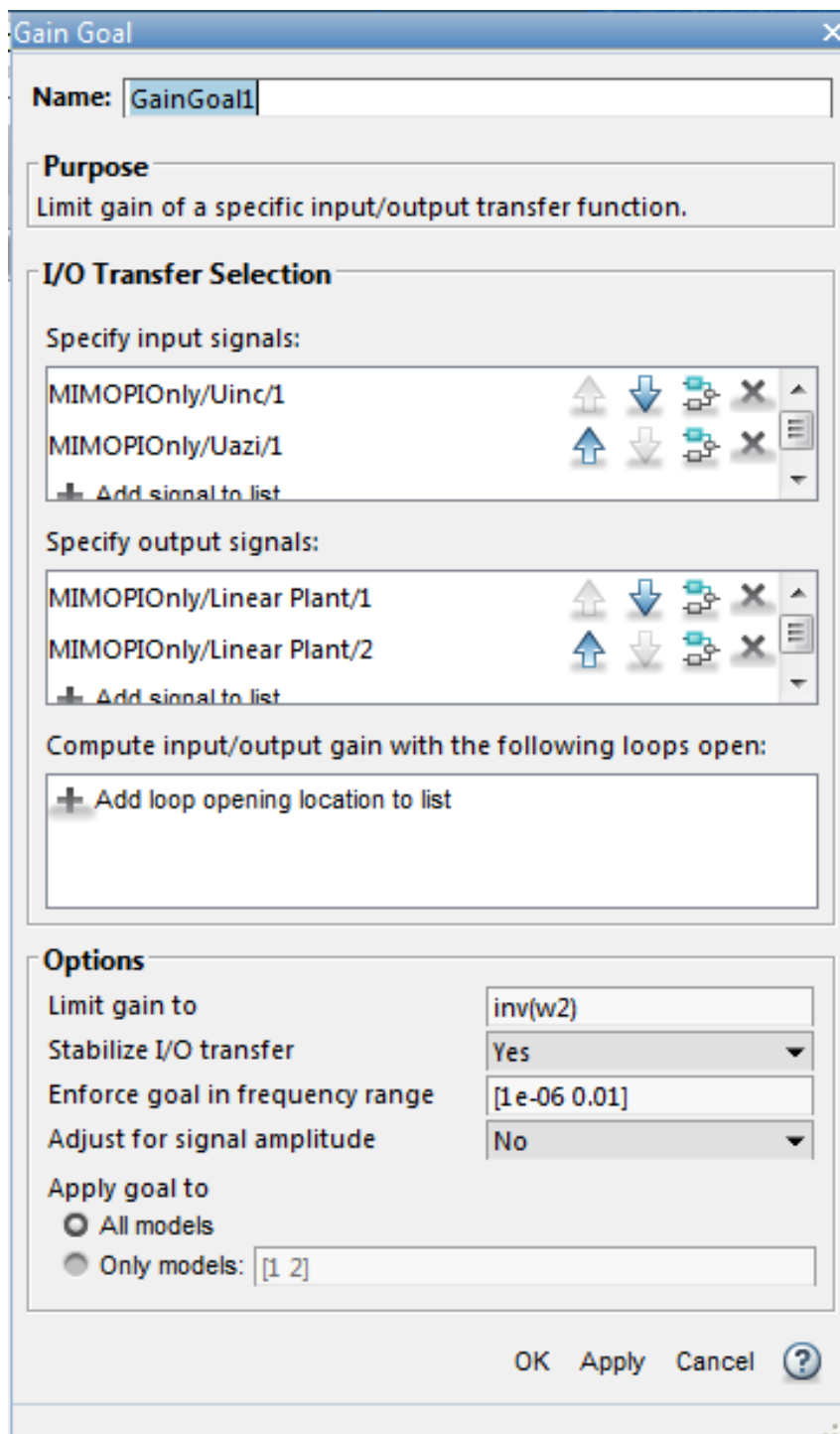


Figure 62: Sensitivity Goal Graphical Illustration



The image shows a 'Gain Goal' dialog box with a blue title bar and a close button. It contains several sections: 'Name' with a text field 'GainGoal1'; 'Purpose' with a text area 'Limit gain of a specific input/output transfer function.'; 'I/O Transfer Selection' with two lists of signals and their associated icons; 'Compute input/output gain with the following loops open:' with an empty list; and 'Options' with various settings like 'Limit gain to', 'Stabilize I/O transfer', 'Enforce goal in frequency range', 'Adjust for signal amplitude', and 'Apply goal to'. At the bottom are 'OK', 'Apply', 'Cancel', and a help button.

Name: GainGoal1

Purpose
Limit gain of a specific input/output transfer function.

I/O Transfer Selection

Specify input signals:

MIMOPIOnly/Uinc/1	↑	↓	↻	✕	⌵
MIMOPIOnly/Uazi/1	↑	↓	↻	✕	⌵

+ Add signal to list

Specify output signals:

MIMOPIOnly/Linear Plant/1	↑	↓	↻	✕	⌵
MIMOPIOnly/Linear Plant/2	↑	↓	↻	✕	⌵

+ Add signal to list

Compute input/output gain with the following loops open:

+ Add loop opening location to list

Options

Limit gain to:

Stabilize I/O transfer:

Enforce goal in frequency range:

Adjust for signal amplitude:

Apply goal to:

☒ All models

☐ Only models:

OK Apply Cancel ?

Figure 63: Robustness goal

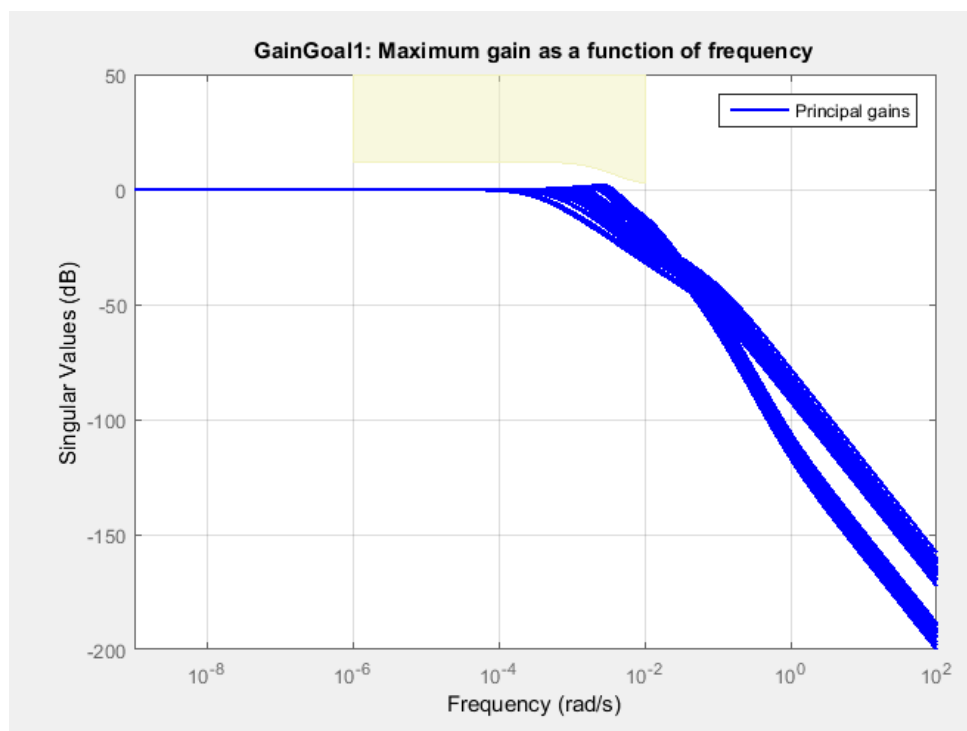


Figure 64: Robustness Goal Graphical Illustration

Overshoot Goal

Name:

Purpose
Limit overshoot in step response (approximate only, see [Overshoot Goal](#)).

Response Selection

Specify step-response inputs:

MIMOPIOnly/Uinc/1	↑	↓	↻	✕	⌵
MIMOPIOnly/Uazi/1	↑	↓	↻	✕	⌵

+ Add signal to list

Specify step-response outputs:

MIMOPIOnly/Linear Plant/1	↑	↓	↻	✕	⌵
MIMOPIOnly/Linear Plant/2	↑	↓	↻	✕	⌵

+ Add signal to list

Evaluate overshoot with the following loops open:

+ Add loop opening location to list

Options

Limit % overshoot to

Adjust for step amplitude

Apply goal to

☒ All models

☐ Only models:

OK Apply Cancel ?

Figure 65: Overshoot Goal

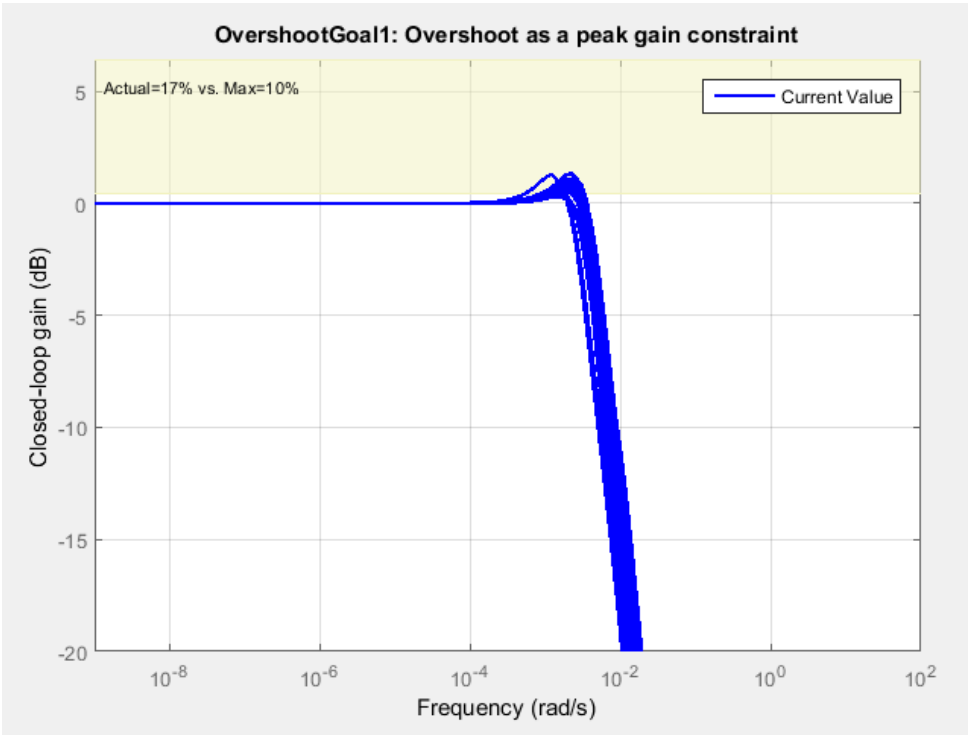


Figure 66: Overshoot Goal Graphical Illustration

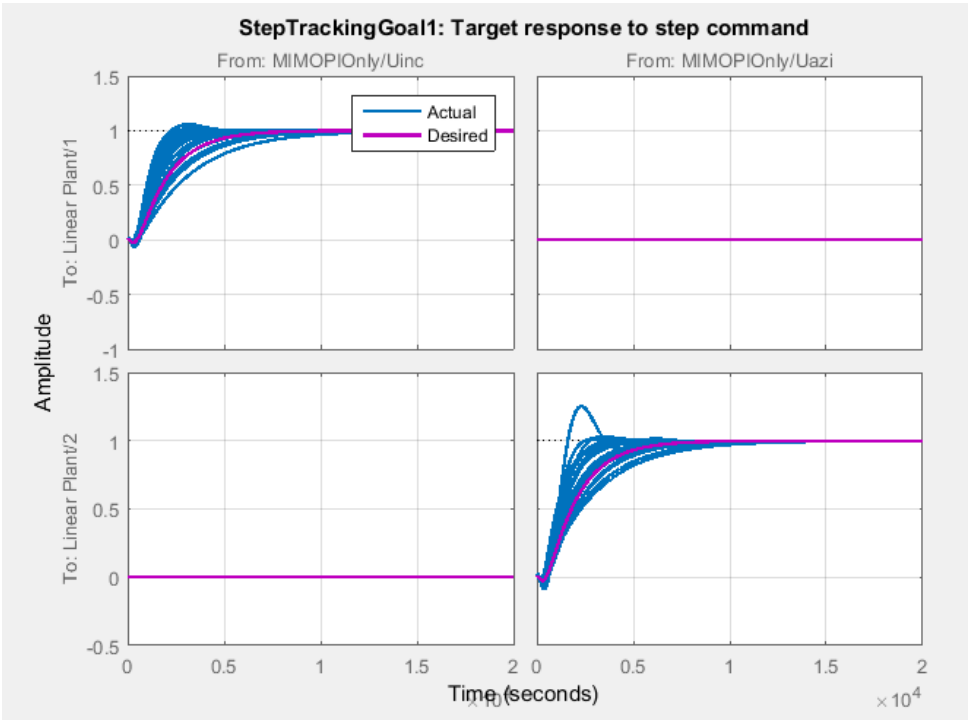


Figure 67: Achieved Step Tracking Goal

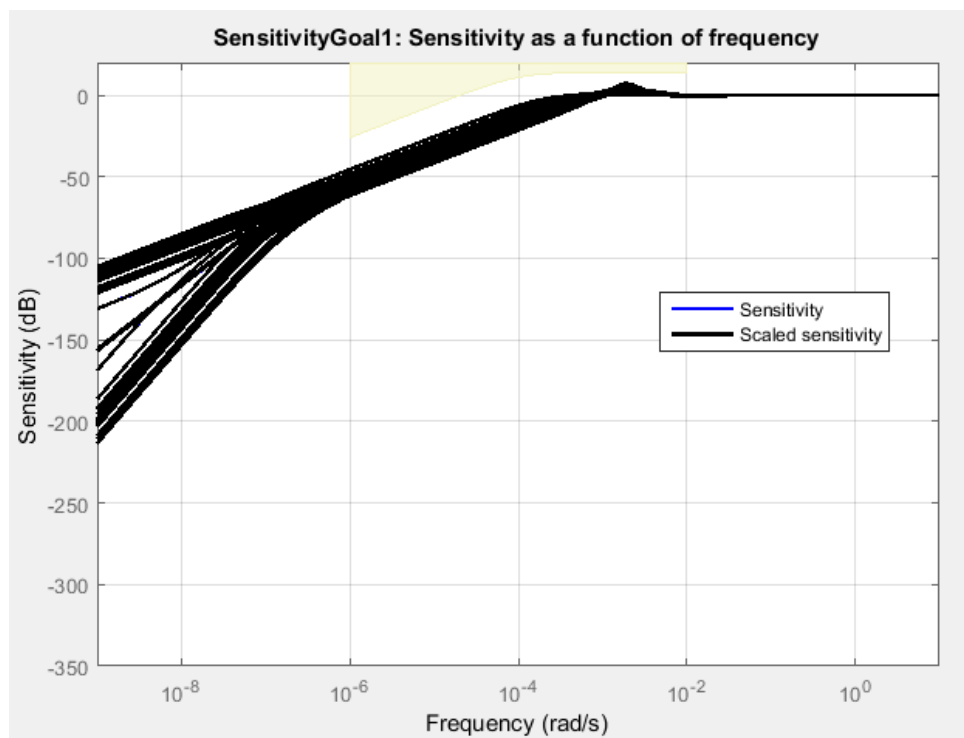


Figure 68: Achieved Sensitivity Tracking Goal

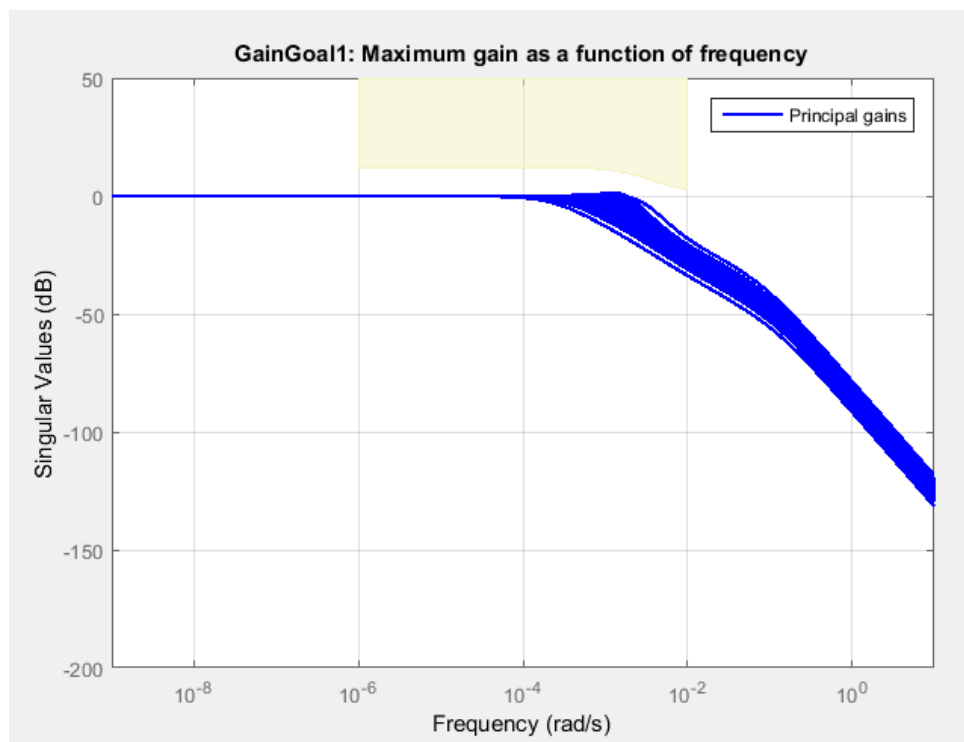


Figure 69: Achieved Robustness Goal

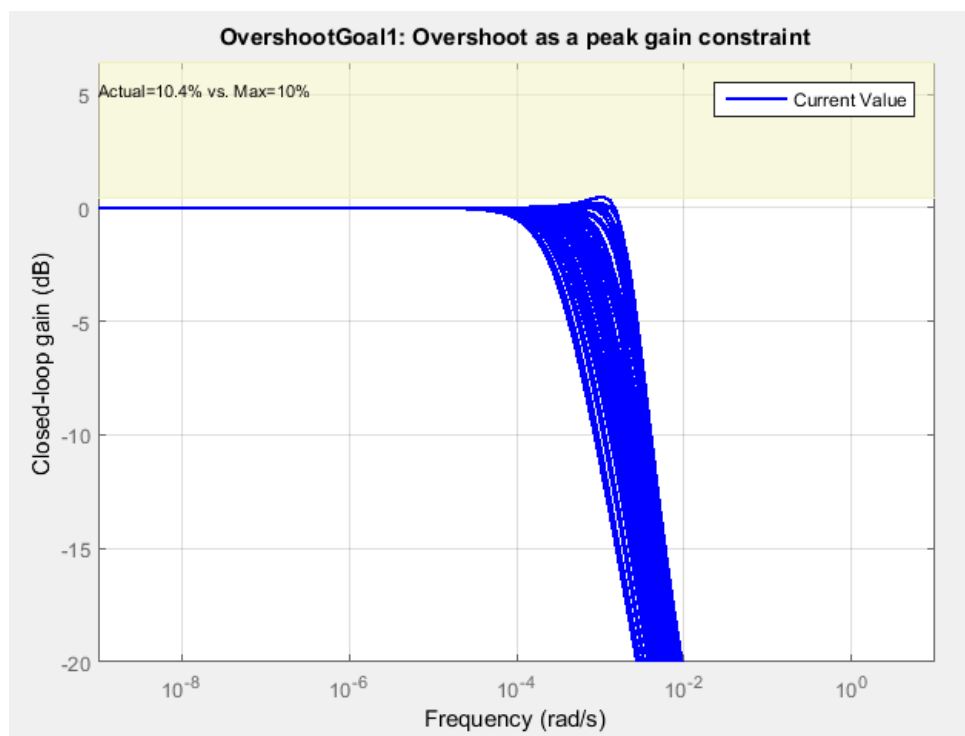


Figure 70: Overshoot Goal

Appendix C

Reports

```

perfReportD1 =
Uncertain system does not achieve performance robustness to modeled uncertainty.
-- The tradeoff of model uncertainty and system gain is balanced at a level of 17.7% of the modeled uncertainty.
-- A model uncertainty of 20.1% can lead to input/output gain of 4.96 at 0.00628 rad/seconds.
-- Sensitivity with respect to the uncertain elements are:
  'Kdls_un' is 5%. Increasing 'Kdls_un' by 25% leads to a 1% decrease in the margin.
  'Vrop_un' is 5%. Increasing 'Vrop_un' by 25% leads to a 1% decrease in the margin.
  'alpha1_un' is 1%. Increasing 'alpha1_un' by 25% leads to a 0% decrease in the margin.
  'alpha2_un' is 1%. Increasing 'alpha2_un' by 25% leads to a 0% decrease in the margin.
  't1_un' is 4%. Increasing 't1_un' by 25% leads to a 1% decrease in the margin.
  't2_un' is 1%. Increasing 't2_un' by 25% leads to a 0% decrease in the margin.
  'td_un' is 1%. Increasing 'td_un' by 25% leads to a 0% decrease in the margin.

```

Figure 71: Report Performance PI pole placement

```

perfReportD2 =
Assuming nominal UFRD system is stable...
Uncertain system achieves performance robustness to modeled uncertainty.
-- The tradeoff of model uncertainty and system gain is balanced at a level of 127% of the modeled uncertainty.
-- A model uncertainty of 132% can lead to input/output gain of 0.758 at 0.00171 rad/seconds.
-- Sensitivity with respect to the uncertain elements are:
  'Kdls_un' is 13%. Increasing 'Kdls_un' by 25% leads to a 3% decrease in the margin.
  'Vrop_un' is 38%. Increasing 'Vrop_un' by 25% leads to a 10% decrease in the margin.
  'alpha1_un' is 41%. Increasing 'alpha1_un' by 25% leads to a 10% decrease in the margin.
  'alpha2_un' is 45%. Increasing 'alpha2_un' by 25% leads to a 11% decrease in the margin.
  't1_un' is 15%. Increasing 't1_un' by 25% leads to a 4% decrease in the margin.
  't2_un' is 36%. Increasing 't2_un' by 25% leads to a 9% decrease in the margin.
  'td_un' is 36%. Increasing 'td_un' by 25% leads to a 9% decrease in the margin.

```

Figure 72: Report Performance Robust PI

```

perfReportD3 =
Uncertain system does not achieve performance robustness to modeled uncertainty.
-- The tradeoff of model uncertainty and system gain is balanced at a level of 7.57% of the modeled uncertainty.
-- A model uncertainty of 10.1% can lead to input/output gain of 9.93 at 0.00226 rad/seconds.
-- Sensitivity with respect to the uncertain elements are:
  'Kdls_un' is 4%. Increasing 'Kdls_un' by 25% leads to a 1% decrease in the margin.
  'Vrop_un' is 2%. Increasing 'Vrop_un' by 25% leads to a 1% decrease in the margin.
  'alpha1_un' is 1%. Increasing 'alpha1_un' by 25% leads to a 0% decrease in the margin.
  'alpha2_un' is 2%. Increasing 'alpha2_un' by 25% leads to a 1% decrease in the margin.
  't1_un' is 5%. Increasing 't1_un' by 25% leads to a 1% decrease in the margin.
  't2_un' is 1%. Increasing 't2_un' by 25% leads to a 0% decrease in the margin.
  'td_un' is 2%. Increasing 'td_un' by 25% leads to a 1% decrease in the margin.

```

Figure 73: Report Performance H_∞ Design 1

```

perfReportD4 =
Assuming nominal UFRD system is stable...
Uncertain system achieves performance robustness to modeled uncertainty.
-- The tradeoff of model uncertainty and system gain is balanced at a level of 105% of the modeled uncertainty.
-- A model uncertainty of 108% can lead to input/output gain of 0.927 at 0.00187 rad/seconds.
-- Sensitivity with respect to the uncertain elements are:
  'Kdls_un' is 11%. Increasing 'Kdls_un' by 25% leads to a 3% decrease in the margin.
  'Vrop_un' is 20%. Increasing 'Vrop_un' by 25% leads to a 5% decrease in the margin.
  'alpha1_un' is 2%. Increasing 'alpha1_un' by 25% leads to a 1% decrease in the margin.
  'alpha2_un' is 55%. Increasing 'alpha2_un' by 25% leads to a 14% decrease in the margin.
  't1_un' is 11%. Increasing 't1_un' by 25% leads to a 3% decrease in the margin.
  't2_un' is 19%. Increasing 't2_un' by 25% leads to a 5% decrease in the margin.
  'td_un' is 25%. Increasing 'td_un' by 25% leads to a 6% decrease in the margin.

```

Figure 74: Report Performance H_∞ Design 2

```

perfReportD5 =
Assuming nominal UFRD system is stable...
Uncertain system achieves performance robustness to modeled uncertainty.
-- The tradeoff of model uncertainty and system gain is balanced at a level of 117% of the modeled uncertainty.
-- A model uncertainty of 123% can lead to input/output gain of 0.814 at 0.00226 rad/seconds.
-- Sensitivity with respect to the uncertain elements are:
  'Kdls_un' is 13%. Increasing 'Kdls_un' by 25% leads to a 3% decrease in the margin.
  'Vrop_un' is 3%. Increasing 'Vrop_un' by 25% leads to a 1% decrease in the margin.
  'alpha1_un' is 9%. Increasing 'alpha1_un' by 25% leads to a 2% decrease in the margin.
  'alpha2_un' is 8%. Increasing 'alpha2_un' by 25% leads to a 2% decrease in the margin.
  't1_un' is 6%. Increasing 't1_un' by 25% leads to a 2% decrease in the margin.
  't2_un' is 8%. Increasing 't2_un' by 25% leads to a 2% decrease in the margin.
  'td_un' is 10%. Increasing 'td_un' by 25% leads to a 3% decrease in the margin.

```

Figure 75: Report Performance PI-SP

```

perfReportD6 =
Assuming nominal UFRD system is stable...
Uncertain system achieves performance robustness to modeled uncertainty.
-- The tradeoff of model uncertainty and system gain is balanced at a level of 105% of the modeled uncertainty.
-- A model uncertainty of 111% can lead to input/output gain of 0.903 at 0.00226 rad/seconds.
-- Sensitivity with respect to the uncertain elements are:
  'Kdls_un' is 43%. Increasing 'Kdls_un' by 25% leads to a 11% decrease in the margin.
  'Vrop_un' is 63%. Increasing 'Vrop_un' by 25% leads to a 16% decrease in the margin.
  'alpha1_un' is 13%. Increasing 'alpha1_un' by 25% leads to a 3% decrease in the margin.
  'alpha2_un' is 60%. Increasing 'alpha2_un' by 25% leads to a 15% decrease in the margin.
  't1_un' is 54%. Increasing 't1_un' by 25% leads to a 14% decrease in the margin.
  't2_un' is 19%. Increasing 't2_un' by 25% leads to a 5% decrease in the margin.
  'td_un' is 12%. Increasing 'td_un' by 25% leads to a 3% decrease in the margin.

```

Figure 76: Report Performance H_∞ SP

```

stabReportD1 =
Uncertain system is not robustly stable to modeled uncertainty.
-- It can tolerate up to 20.7% of the modeled uncertainty.
-- A destabilizing combination of 24.1% of the modeled uncertainty was found.
-- This combination causes an instability at 0.00628 rad/seconds.
-- Sensitivity with respect to the uncertain elements are:
  'Kdls_un' is 2%. Increasing 'Kdls_un' by 25% leads to a 1% decrease in the margin.
  'Vrop_un' is 3%. Increasing 'Vrop_un' by 25% leads to a 1% decrease in the margin.
  'alpha1_un' is 0%. Increasing 'alpha1_un' by 25% leads to a 0% decrease in the margin.
  'alpha2_un' is 1%. Increasing 'alpha2_un' by 25% leads to a 0% decrease in the margin.
  't1_un' is 7%. Increasing 't1_un' by 25% leads to a 2% decrease in the margin.
  't2_un' is 2%. Increasing 't2_un' by 25% leads to a 1% decrease in the margin.
  'td_un' is 1%. Increasing 'td_un' by 25% leads to a 0% decrease in the margin.

```

Figure 77: Report stability PI Pole placement

```

stabReportD2 =
Assuming nominal UFRD system is stable...
Uncertain system is robustly stable to modeled uncertainty.
-- It can tolerate up to 167% of the modeled uncertainty.
-- A destabilizing combination of 180% of the modeled uncertainty was found.
-- This combination causes an instability at 0.00187 rad/seconds.
-- Sensitivity with respect to the uncertain elements are:
  'Kdls_un' is 16%. Increasing 'Kdls_un' by 25% leads to a 4% decrease in the margin.
  'Vrop_un' is 92%. Increasing 'Vrop_un' by 25% leads to a 23% decrease in the margin.
  'alpha1_un' is 18%. Increasing 'alpha1_un' by 25% leads to a 5% decrease in the margin.
  'alpha2_un' is 16%. Increasing 'alpha2_un' by 25% leads to a 4% decrease in the margin.
  't1_un' is 18%. Increasing 't1_un' by 25% leads to a 5% decrease in the margin.
  't2_un' is 15%. Increasing 't2_un' by 25% leads to a 4% decrease in the margin.
  'td_un' is 13%. Increasing 'td_un' by 25% leads to a 3% decrease in the margin.

```

Figure 78: Report stability Robust PI


```

stabReportD3 =
Uncertain system is not robustly stable to modeled uncertainty.
-- It can tolerate up to 10.7% of the modeled uncertainty.
-- A destabilizing combination of 12% of the modeled uncertainty was found.
-- This combination causes an instability at 0.00226 rad/seconds.
-- Sensitivity with respect to the uncertain elements are:
  'Kdls_un' is 3%. Increasing 'Kdls_un' by 25% leads to a 1% decrease in the margin.
  'Vrop_un' is 0%. Increasing 'Vrop_un' by 25% leads to a 0% decrease in the margin.
  'alpha1_un' is 4%. Increasing 'alpha1_un' by 25% leads to a 1% decrease in the margin.
  'alpha2_un' is 4%. Increasing 'alpha2_un' by 25% leads to a 1% decrease in the margin.
  't1_un' is 0%. Increasing 't1_un' by 25% leads to a 0% decrease in the margin.
  't2_un' is 1%. Increasing 't2_un' by 25% leads to a 0% decrease in the margin.
  'td_un' is 0%. Increasing 'td_un' by 25% leads to a 0% decrease in the margin.

```

Figure 79: Report stability H_∞ Design 1

```

stabReportD4 =
Assuming nominal UFRD system is stable...
Uncertain system is robustly stable to modeled uncertainty.
-- It can tolerate up to 133% of the modeled uncertainty.
-- A destabilizing combination of 148% of the modeled uncertainty was found.
-- This combination causes an instability at 0.00206 rad/seconds.
-- Sensitivity with respect to the uncertain elements are:
  'Kdls_un' is 9%. Increasing 'Kdls_un' by 25% leads to a 2% decrease in the margin.
  'Vrop_un' is 16%. Increasing 'Vrop_un' by 25% leads to a 4% decrease in the margin.
  'alpha1_un' is 7%. Increasing 'alpha1_un' by 25% leads to a 2% decrease in the margin.
  'alpha2_un' is 11%. Increasing 'alpha2_un' by 25% leads to a 3% decrease in the margin.
  't1_un' is 9%. Increasing 't1_un' by 25% leads to a 2% decrease in the margin.
  't2_un' is 8%. Increasing 't2_un' by 25% leads to a 2% decrease in the margin.
  'td_un' is 6%. Increasing 'td_un' by 25% leads to a 2% decrease in the margin.

```

Figure 80: Report stability H_∞ Design 2

```

stabReportD5 =
Assuming nominal UFRD system is stable...
Uncertain system is robustly stable to modeled uncertainty.
-- It can tolerate up to 138% of the modeled uncertainty.
-- A destabilizing combination of 151% of the modeled uncertainty was found.
-- This combination causes an instability at 0.00226 rad/seconds.
-- Sensitivity with respect to the uncertain elements are:
  'Kdls_un' is 10%. Increasing 'Kdls_un' by 25% leads to a 3% decrease in the margin.
  'Vrop_un' is 11%. Increasing 'Vrop_un' by 25% leads to a 3% decrease in the margin.
  'alpha1_un' is 14%. Increasing 'alpha1_un' by 25% leads to a 4% decrease in the margin.
  'alpha2_un' is 20%. Increasing 'alpha2_un' by 25% leads to a 5% decrease in the margin.
  't1_un' is 19%. Increasing 't1_un' by 25% leads to a 5% decrease in the margin.
  't2_un' is 11%. Increasing 't2_un' by 25% leads to a 3% decrease in the margin.
  'td_un' is 9%. Increasing 'td_un' by 25% leads to a 2% decrease in the margin.
..

```

Figure 81: Report stability PI-SP

```

stabReportD6 =
Assuming nominal UFRD system is stable...
Uncertain system is robustly stable to modeled uncertainty.
-- It can tolerate up to 122% of the modeled uncertainty.
-- A destabilizing combination of 133% of the modeled uncertainty was found.
-- This combination causes an instability at 0.00248 rad/seconds.
-- Sensitivity with respect to the uncertain elements are:
  'Kdls_un' is 19%. Increasing 'Kdls_un' by 25% leads to a 5% decrease in the margin.
  'Vrop_un' is 25%. Increasing 'Vrop_un' by 25% leads to a 6% decrease in the margin.
  'alpha1_un' is 6%. Increasing 'alpha1_un' by 25% leads to a 2% decrease in the margin.
  'alpha2_un' is 7%. Increasing 'alpha2_un' by 25% leads to a 2% decrease in the margin.
  't1_un' is 12%. Increasing 't1_un' by 25% leads to a 3% decrease in the margin.
  't2_un' is 14%. Increasing 't2_un' by 25% leads to a 4% decrease in the margin.
  'td_un' is 4%. Increasing 'td_un' by 25% leads to a 1% decrease in the margin.

```

Figure 82: Report stability H_∞ -SP

Appendix D

Transient simulations results

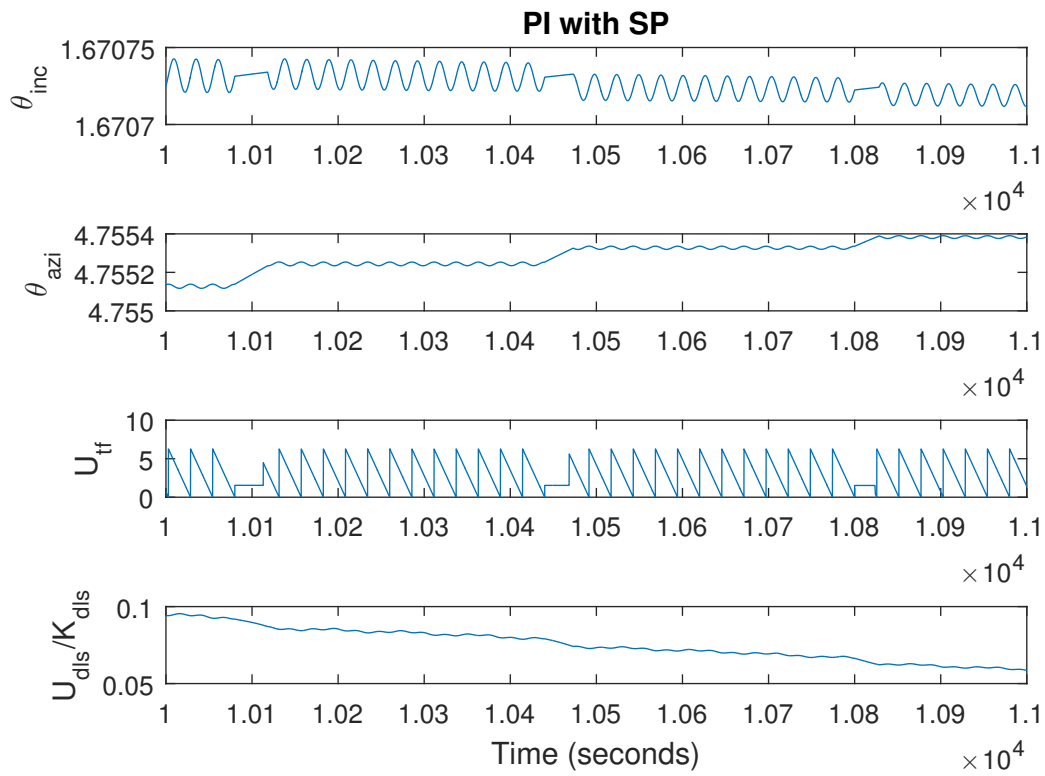


Figure 83: Attitude-tracking Transient Attitude Response, PI-SP design, Zoomed View

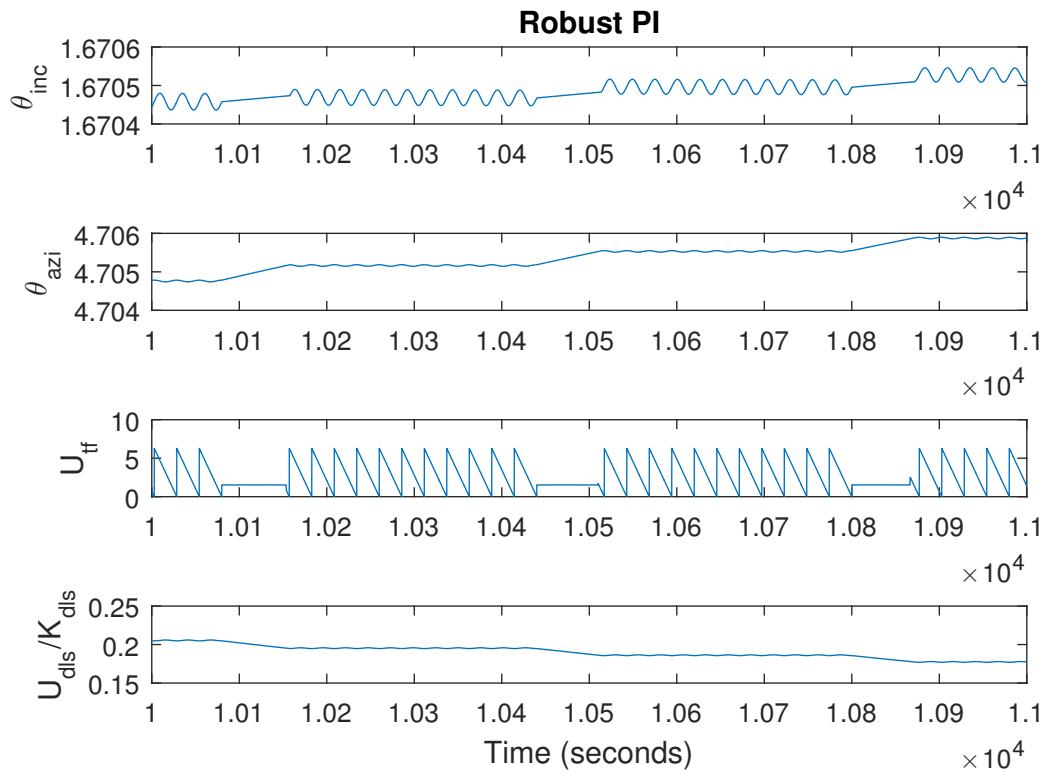


Figure 84: Attitude-tracking Transient Attitude Response, Robust PI design, Zoomed View

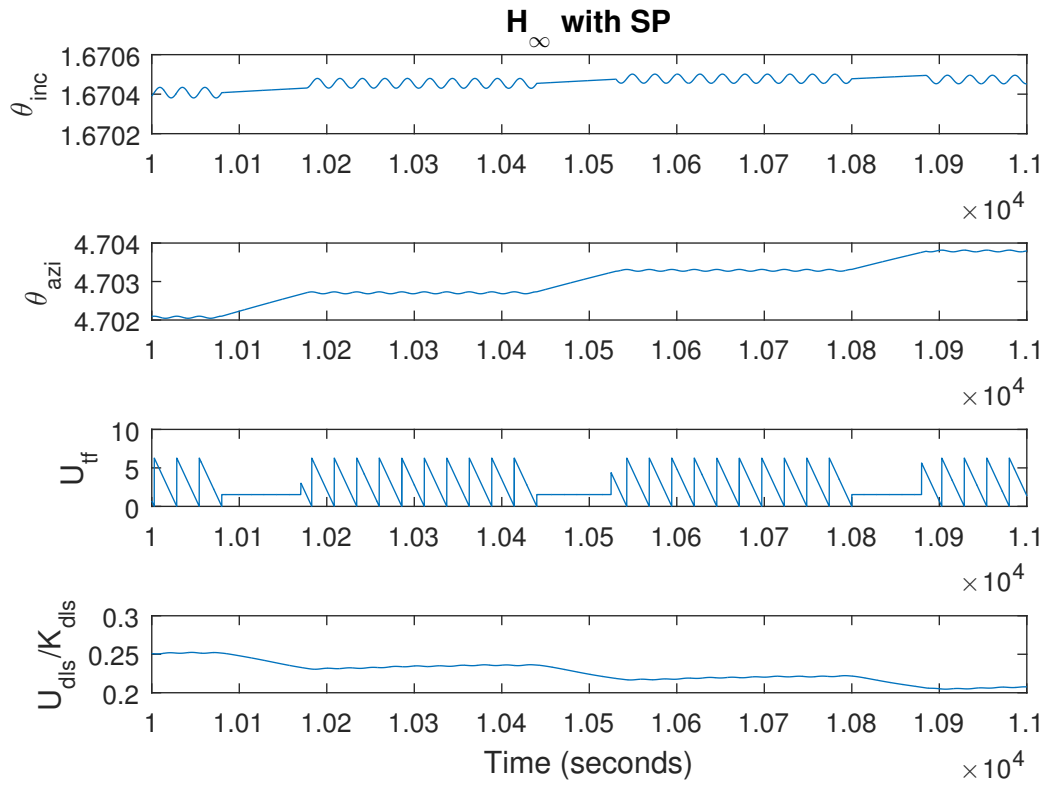


Figure 85: Attitude-tracking Transient Attitude Response, H_{∞} -SP Design, Zoomed View

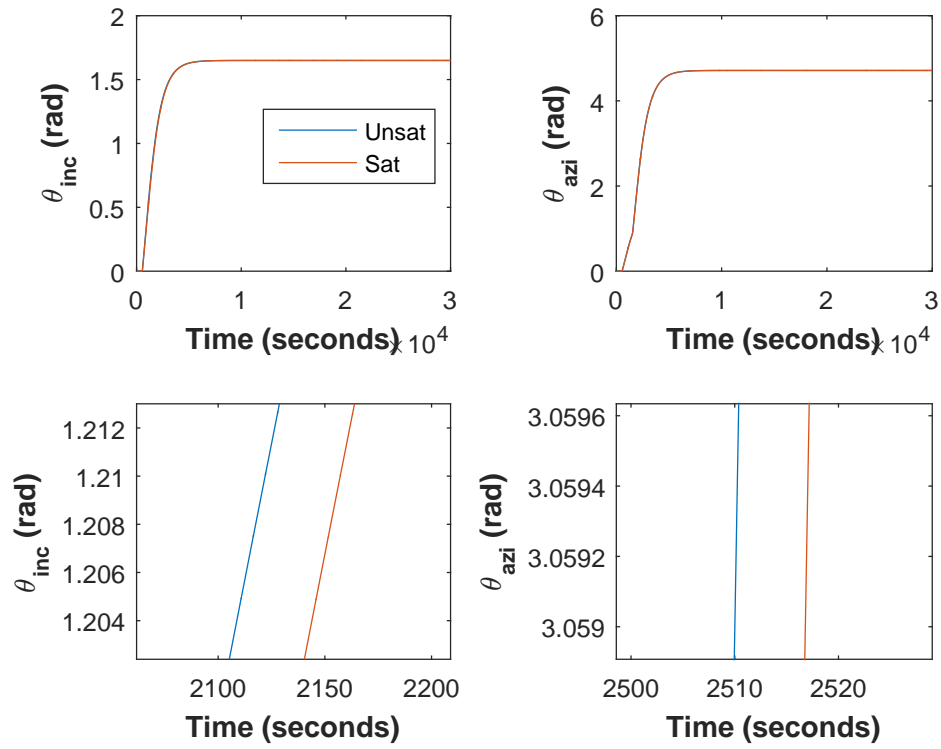


Figure 86: Effect of saturation on Controller Output- PI

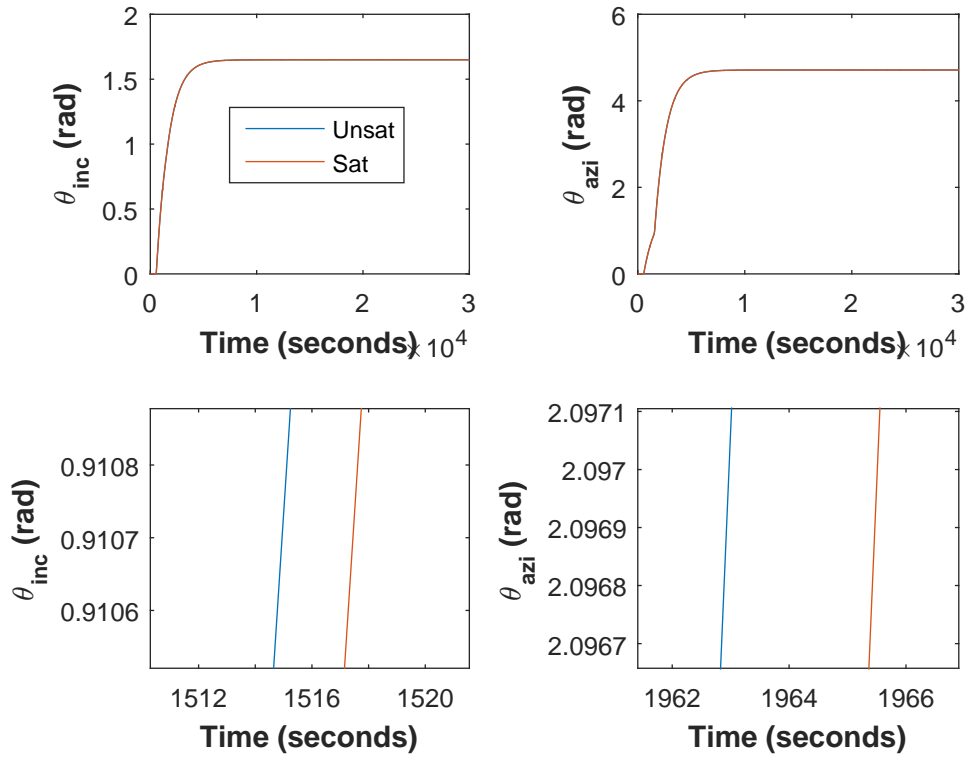


Figure 87: Effect of saturation on Controller Output- H_{∞} -SP

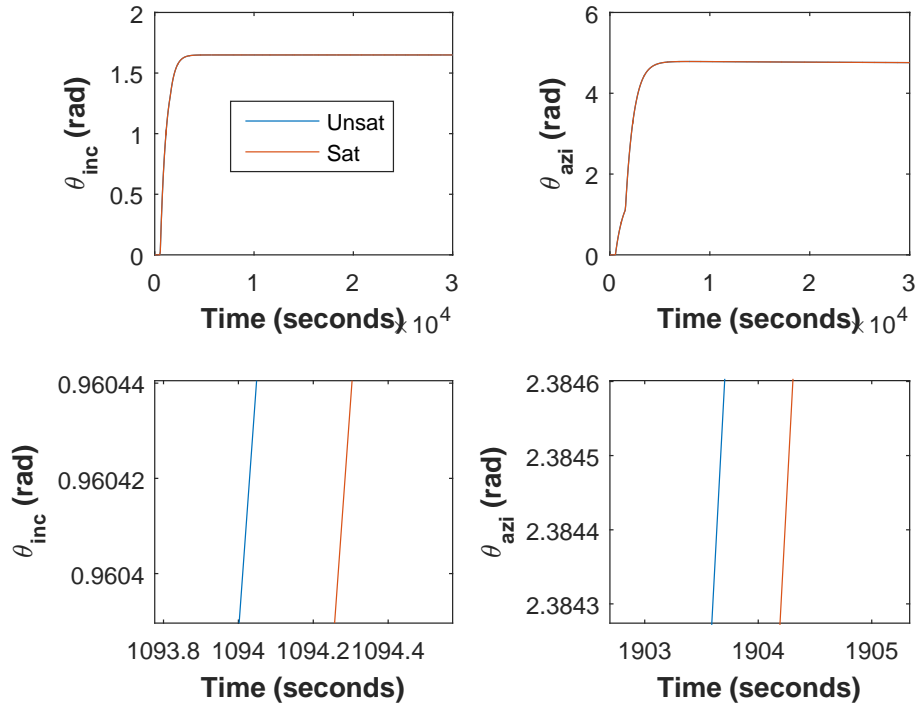


Figure 88: Effect of saturation on Controller Output- PISP

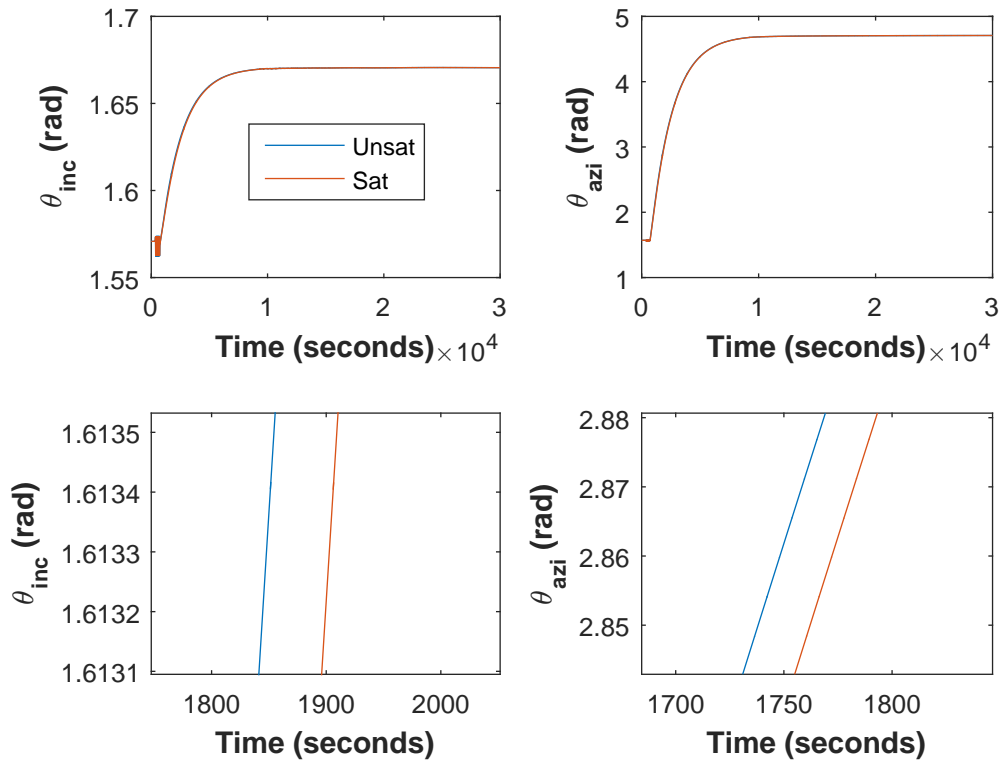


Figure 89: Effect of saturation on Controller Output- Nonlinear PI simulation

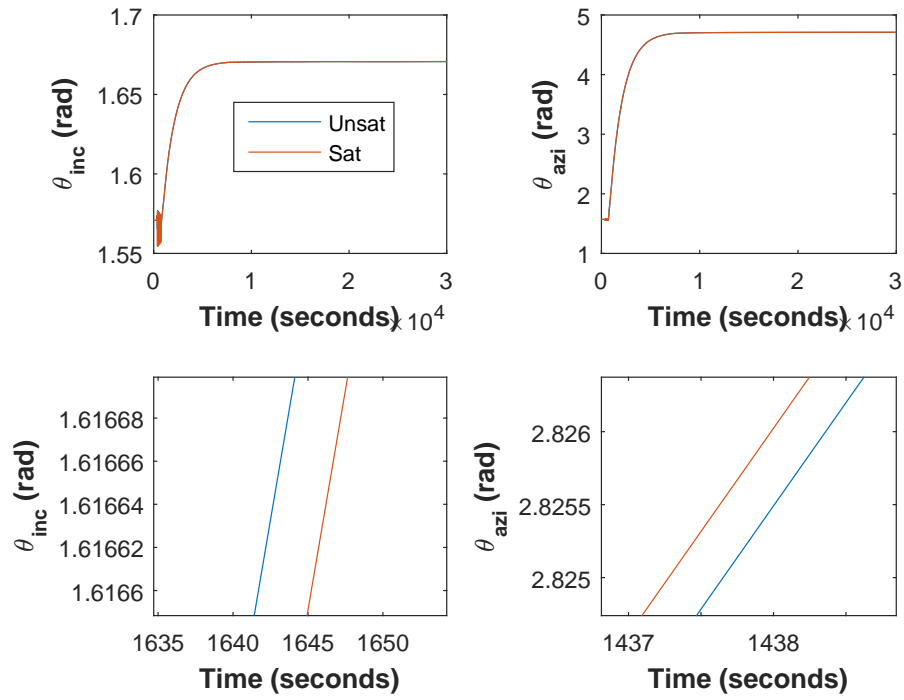


Figure 90: Effect of saturation on Controller Output- Nonlinear H_{∞} SP Simulation

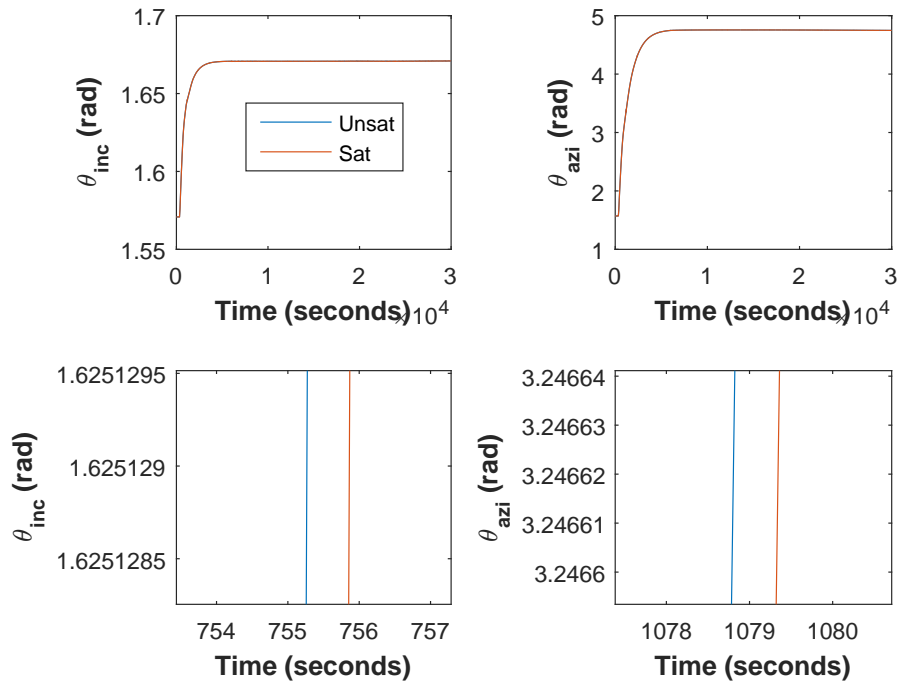


Figure 91: Effect of saturation on Controller Output- Nonlinear PISP simulation

Appendix E

Simulink

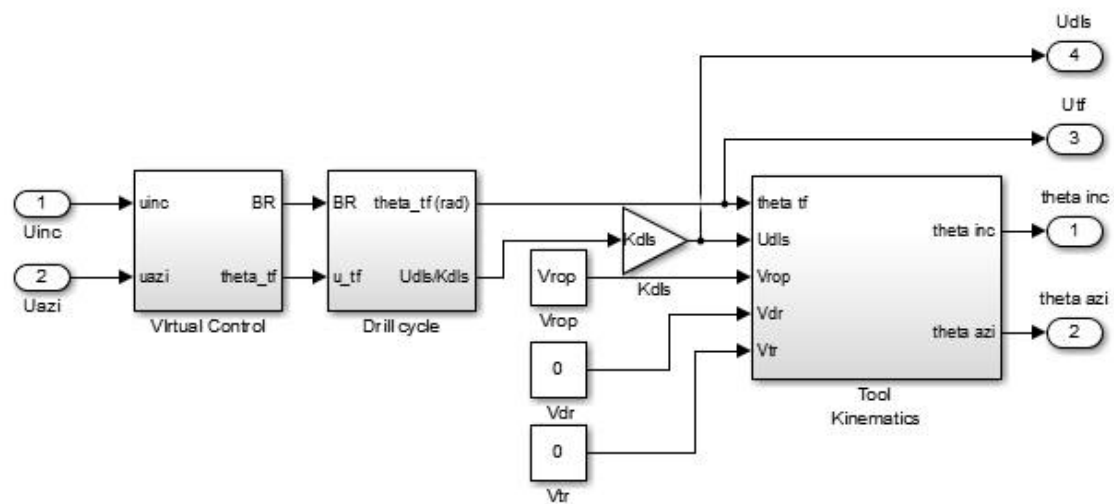


Figure 92: Sub-system Directional Drilling Plant

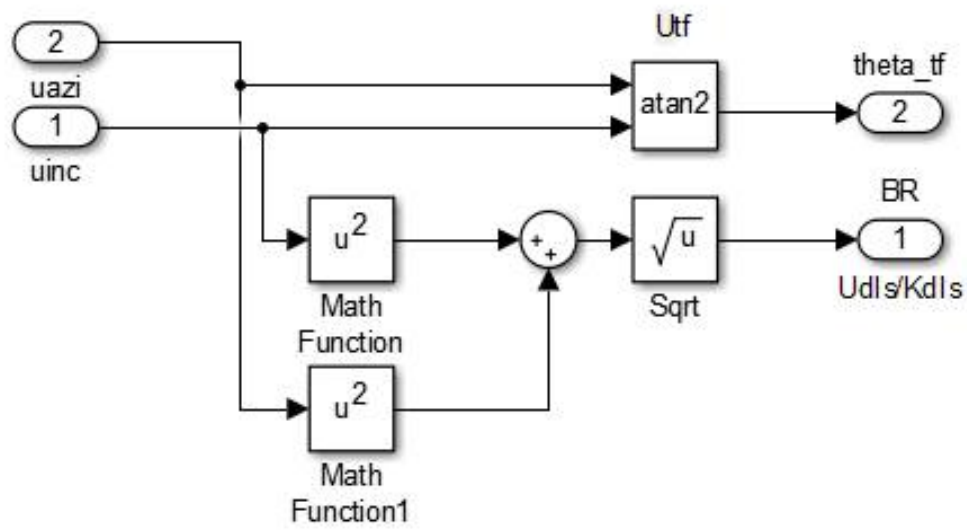


Figure 93: Sub-system Virtual Control Transformation

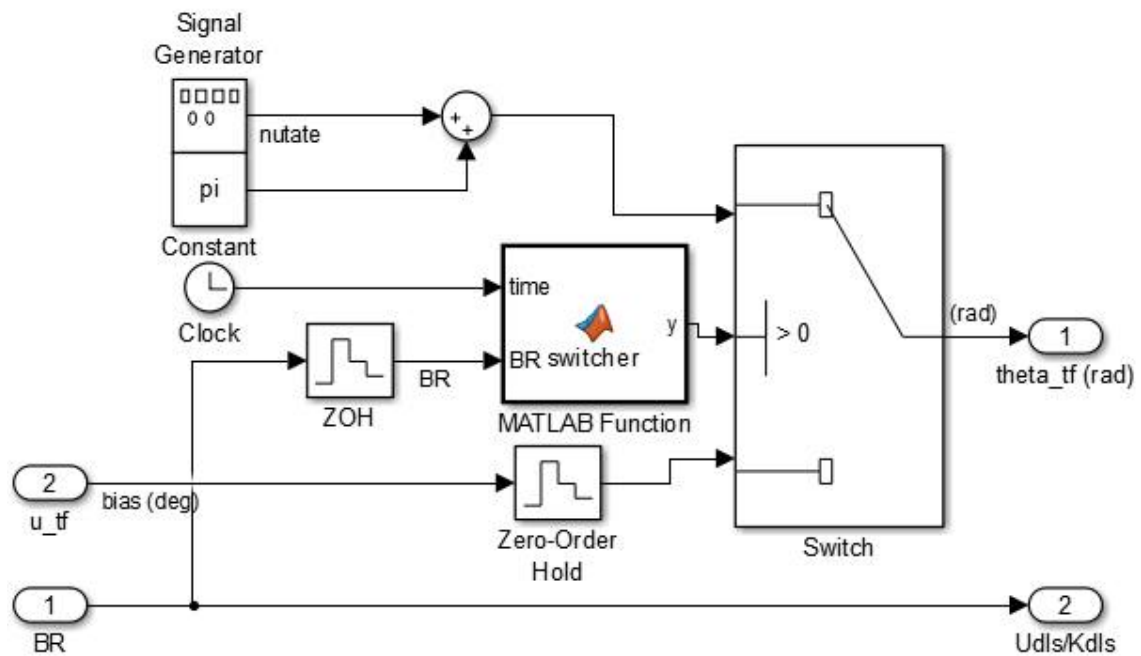


Figure 94: Sub-system Drill Cycle

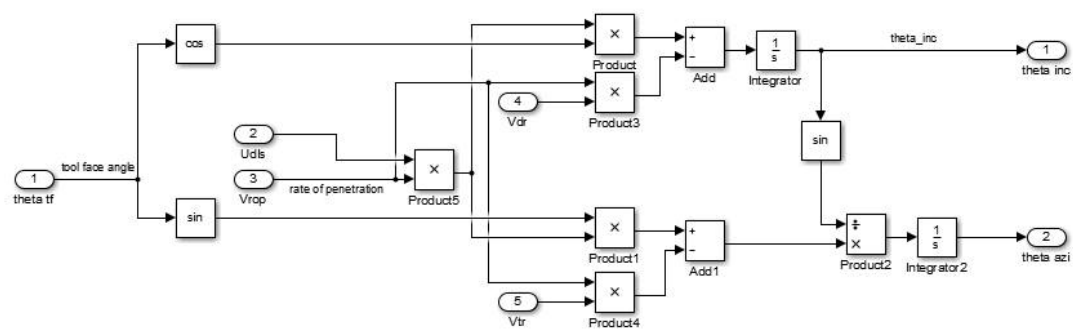


Figure 95: Sub-system Drill Kinematics

References

- Albertos, P., Garcia, P. and Sanz, R. (2015). Control of Input/Output Delayed and Disturbed Unstable Plants, *20th International Conference on Methods and Models in Automation and Robotics*, Miedzydroje, pp. 1–10.
- B. Ogunnaike and W. Ray (1979). Multivariable Controller Design for Linear Systems Having Multiple Time Delays, *AIChE Journal* **25**(6): 1043–1057.
- Balas, G. J., Doyle, J. C., Glover, K., Packard, A. and Smith, R. (1991). *-Analysis and Synthesis Toolbox: For Use with MATLAB*, The MathWorks, Inc., Natick.
- Bansal, A. and Sharma, V. (2013). Design and Analysis of Robust H-infinity Controller, *Control Theory and Informatics* **3**(2): 7–14.
- Barr, J. D., Clegg, J. M. and Russell, M. K. (1995). Steerable Rotary Drilling With an Experimental System, *1995 SPE/IADC Drilling Conference*, Amsterdam, pp. 435–450.
- Bayliss, M. T. and Whidborne, J. F. (2015). Mixed Uncertainty Analysis of Pole Placement and H Controllers for Directional Drilling Attitude Tracking, *Journal of Dynamic Systems, Measurement, and Control* **137**(12): 1–8.
- Bayliss, M. T., Whidborne, J. F. and Panchal, N. (2014). Structured Uncertainty Analysis of Pole Placement and H Controllers for Directional Drilling Attitude Tracking, *19th IFAC World Congress*, Cape Town, pp. 9283–9288.
- Bommer, P. (2008). *A Primer of Oilwell Drilling: A Basic Text of Oil and Gas Drilling*, 7th edn, The University of Texas, Austin.
- Brakel, J. and Azar, J. (1989). Prediction of Wellbore Trajectory Considering Bottomhole Assembly and Drill-Bit Dynamics, *SPE Drilling Engineering* **4**(2): 109–118.
- Downton, G. C. (2007). Directional Drilling System Response and Stability, *16th IEEE International Conference on Control Applications*, Singapore, pp. 1543–1550.
- Downton, G. C. (2012). Challenges of Modeling Drilling Systems for the Purposes of Automation and Control, *2012 IFAC Workshop on Automatic Control in Offshore Oil and Gas Production*, Vol. 1, Trondheim, pp. 201–210.
- Downton, G. C. and Ignova, M. (2011). Stability and Response of Closed Loop Directional Drilling System using Linear Delay Differential Equations, *2011 IEEE International Conference on Control Applications*, Denver, pp. 893–898.
- Downton, G., Klausen, T. S., Hendricks, A. and Pafitis, D. (2000). New Directions in Rotary Steerable Drilling, *Oilfield Review* pp. 18–29.

- Felczak, E., Godwin, N. D., Hawkins, R., Jones, S. and Slayden, F. (2012). The Best of Both Worlds A Hybrid Rotary Steerable System, *Oilfield Review* pp. 36–44.
- Gaynor, T., Chen, D. C. K., Darren, S. and Blaine, C. (2001). Tortuosity Versus Micro-Tortuosity - Why Little Things Mean a Lot, *SPE/IADC Drilling Conference*, Amsterdam, pp. 1–12.
- Genevois, J.-M., Boulet, J., Christophe, S. and Christophe, R. (2003). Gyrostab Project: The Missing Link Azimuth And Inclination Mastered With New Principles For Standard Rotary BHAs, *SPE/IADC Drilling Conference*, Amsterdam, pp. 1–11.
- Glover, K. (1984). All Optimal Hankel-Norm Approximations of Linear Multivariable Systems and Their L-error Bounds, *International Journal of Control* **39**(6): 1115–1193.
- Gruenhagen, H., Hahne, U. and Alvord, G. (2002). Application of New Generation Rotary Steerable System for Reservoir Drilling in Remote Areas, *IADC/SPE Drilling Conference*, Dallas, pp. 1–7.
- Gu, D. W., Petkov, P. H. and Konstantinov, M. M. (2005). *Advanced Textbooks in Control and Signal Processing*, Springer-Verlag London Limited, London.
- Hahne, U., Risdal, G., Ruzska, J. and Wahlen, L. S. (2004). Integrated BHA Concept of the Latest Generation Rotary Closed-Loop System for Hole Sizes from 5 7/8 to 18 , *IADC/SPE Drilling Conference*, Dallas, pp. 1–9.
- Ho, H.-S. (1987). Prediction of Drilling Trajectory in Directional Wells Via a New Rock-Bit Interaction Model, *62nd Annual Technical Conference and Exhibition of the Society of Petroleum Engineers*, Dallas, pp. 83–95.
- Jerome, N. and Ray, W. (1986). High-Performance Multivariable Control Strategies for Systems Having Time Delays, *AIChE Journal* **32**(6): 914–931.
- Johnstone, J. A. and Stevenson, P. (2001). The Value of Rotary Closed - Loop Drilling Technology on Chevron Alba's North Sea Horizontal Field Development, *SPE/IADC Drilling Conference*, Amsterdam, pp. 1–11.
- Kim, J., Park, B., Shin, J.-U., Jung, S. and Myung, H. (2014). A Novel Steering Sections of Hybrid Rotary Steerable System for Directional Drilling, *14th International Conference on Control, Automation and Systems*, Gyeonggi-do, pp. 1617–1619.
- Li, A., Feng, E. and Gong, Z. (2008). An Optimal Control Model and Algorithm for the Deviated Well's Trajectory Planning, *Applied Mathematical Modelling* **33**(7): 3068–3075.
- Lin, C.-a. and Gundes, A. N. (2000). Multi-input Multi-output PI Controller Design, *IEEE Conference on Decision and Control*, Sydney, pp. 0–5.
- Maciejowski, J. (1994). Robustness of Multivariable Smith Predictor, *Journal of Process Control* **4**(1): 29–32.
- Maidla, E. and Haci, M. (2004). Understanding Torque: The Key to Slide-Drilling Directional Wells, *IADC/SPE Drilling Conference*, Dallas, pp. 1–7.
- Matheus, J., Ignova, M. and Hornblower, P. (2014). A Hybrid Approach to Closed-Loop Directional Drilling Control using Rotary Steerable Systems, *SPE Latin American and Caribbean Petroleum Engineering Conference*, Maracaibo, pp. 1–10.

- MATLAB (2015). Robust Control Toolbox Release 2015a.
URL: <http://uk.mathworks.com/products/robust/>
- Millheim, K., Jordan, S. and Ritter, C. (1978). Bottom-Hole Assembly Analysis Using the Finite-Element Method, *Journal of Petroleum Technology* **30**(2): 265–274.
- Niculescu, S. and Gu, K. (2004). *Advances in Time-Delay Systems*, Vol. 38, Springer-Verlag London Limited, London.
- Ogata, K. (2005). *Modern Control Engineering*.
- O.J.Smith (1959). A Controller to Overcome Deadtime, *ISA Journal* **6**(2): 28–33.
- Panchal, N., Bayliss, M. T. and Whidborne, J. F. (2010). Robust Linear Feedback Control of Attitude for Directional Drilling Tools, *13th IFAC Symposium on Automation in Mining, Mineral and Metal Processing*, Cape Town, pp. 92–97.
- Panchal, N., Bayliss, M. T. and Whidborne, J. F. (2011). Minimum Strain Energy Waypoint-Following Controller for Directional Drilling using OGH Curves, *2011 IEEE International Conference on Control Applications*, Denver, pp. 887–892.
- Panchal, N., Bayliss, M. and Whidborne, J. F. (2012). Attitude Control System for Directional Drilling Bottom Hole Assemblies, *IET Control Theory and Applications* **6**(6): 884–892.
- Perdikaris, G. (1991). *Computed Control System Theory and Applications*.
- Pirovolou, D., Chapman, C. D., Chau, M. T., Arismendi, H., Ahorukomeye, M. and Penaranda, J. (2011). Drilling Automation: An Automatic Trajectory Control System, *SPE Digital Energy Conference and Exhibition*, The Woodlands, pp. 1–8.
- Ranger Survey Systems (2016). Directional Drill Hole Surveying The Earth’s Gravitational Field.
URL: http://rangersurveys.com/docs/Technical_Presentation_V1.pdf
- Scherer, C. W. and Weiland, S. (2005). Linear Matrix Inequalities in Control, *Technical report*, Delft Center for Systems and Control.
- Shengzong, J., Xilu, W., Limin, C. and Kunfang, L. (1999). A New Method for Designing 3D Trajectory in Sidetracking Horizontal Wells Under Multi-constraints, *1999 SPE Asia Pacific Improved Oil Recovery Conference*, Kuala Lumpur, pp. 1–8.
- Skogestad, S. and Postlethwaite, I. (2001). *Multivariable Feedback Control: Analysis and Design*, 2nd edn, John Wiley & Sons.
- Smith, O. (1957). Closer Control of Loops with Dead Time, *Chemical Engineering Progress* **53**(5): 217–219.
- Sourdille, P. and Dwyer, A. (2003). A New Modified Smith Predictor Designs, *4th IFAC Workshop on Time Delay Systems*, Rocquencourt, pp. 1–7.
- Sugiura, J., Bowler, A. and Lowdon, R. (2014). Improved Continuous Azimuth and Inclination Measurement by Use of a Rotary-Steerable System Enhances Downhole-Steering Automation and Kickoff Capabilities Near Vertical, *SPE Annual Technical Conference and Exhibition*, New Orleans, pp. 226–235.

- Sun, H., Li, Z., Hovakimyan, N., Basar, T. and Dowton, G. (2012). L1 Adaptive Control for Directional Drilling Systems, *I2012 FAC Workshop on Automatic Control in Offshore Oil and Gas Production*, Trondheim, pp. 72–77.
- Thorogood, J., Aldred, W., Florence, F. and Iversen, F. (2010). Drilling Automation: Technologies, Terminology and Parallels With Other Industries, *SPE/IADC Drilling Conference*, Amsterdam, pp. 419–425.
- Urayama, T., Yonezawa, T., Nakahara, A., Ikeda, A., Nakayama, T. and Gleitman, D. (1999). Development of Remote-Controlled Dynamic Orientating System, *1999 SPE Annual Technical Conference and Exhibition*, Houston, pp. 1–14.
- Wang, Q., Zou, B. and Zhang, Y. (2000). Decoupling Smith Predictor Design for Multivariable Systems with Multiple Time Delays, *Chemical Engineering Research and Design Transactions* **78**(4): 565–572.
- Wen, J.-Y. and Kreutz-Delgado, K. (1991). The Attitude Control Problem, *IEEE Transactions on Automatic Control* **36**(10): 1148–1162.
- Yiyong, Y., Baolin, L., Kai, Z., Dianfeng, Z. and Jian, C. (2009). Control Unit of the Directional Drilling System, *2009 Chinese Control and Decision Conference*, Guilin, pp. 1000–1004.
- Yonezawa, T., Cargill, E. J., Gaynor, T. M., Hardin Jr., J. R., Hay, R. T., Ikeda, A. and Kiyosawa, Y. (2002). Robotic Controlled Drilling: A New Rotary Steerable Drilling System for the Oil and Gas Industry, *IADC/SPE Drilling Conference*, Dallas, pp. 1–15.
- Zhou, K. and Doyle, J. C. (1998). *Essentials Of Robust Control*, Prentice-Hall, Inc., New Jersey.